Harnessing Nonlinearities: Behavior Generation from Natural Dynamics

---

Disseration

zur

Erlangung der naturwissenschaftlichen Doktorwürde
(Dr. sc. nat.)

vorgelegt der

Mathematisch-naturwissenschaftlichen Fakultät

der

Universität Zürich

von

Juan Pablo Carbajal

aus

Argentinien

Promotionskomitee

Prof. Dr. Rolf Pfeifer (Vorsitz und Leitung der Dissertation)

Prof. Dr. Andre Seyfarth

Prof. Dr. Renato Pajarola

Prof. Dr. Camillo De Lellis

Zürich, 2012

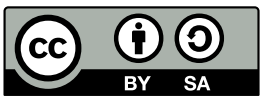

Abstract

This thesis studies the relation between the morphology of a physical platform and the behavior observed under defined actuation. The task is tackled with two complementary approaches: numerical simulations and experiments. The latter are carried out using experimental platforms termed *parametric robots*, i.e. robot-like setups whose parameters can be varied systematically over a relevant range. Simulations are performed using simple mathematical models tailored to recover the main aspects of the behavior under consideration. In the context of locomotion, the ultimate and ambitious aim of the work, is to found a bridge between the thorough and systematic methodologies used in mature experimental disciplines, and the more *ad hoc* approaches currently used in embodied artificial intelligence and some subfields of robotics. This is pursued by reviewing relevant methods for the analysis of experimental results, as well as key physical concepts related to them; e.g. resonance analysis, normal modes, etcetera. Discussions are kept to a technical level that should be accessible to a multidisciplinary audience and with the hope that they would be of broad interest. The thesis also deals with the generation of reaching behaviors with the introduction of a novel method that explicitly makes use of the natural dynamics of the platform: the dynamic response decomposition method (DRD). To my knowledge, this is the first publication of a methodology with this characteristic and represents the major contribution of this thesis. The evaluation of the proposed algorithm is performed in numerical simulations, using different models of varied complexity.

The first chapter presents a succinct introduction to the topics most pertinent to the exposition of the results. It is provided with the hope that the reader without intense training in physics or mathematical physics, can assimilate the concepts in the studies reported herein.

Locomotion is discussed in the subsequent two chapters. The concepts of resonance, resonant frequencies and normal modes are introduced and discussed, highlighting the contrast of these linear concepts with their nonlinear counterparts. Two current methods for the identification of resonances and nonlinear normal modes are briefly introduced, followed by three case studies of parametric robots: Zürihopper, WandaX and MagE. Zürihopper is a platform designed to study the role of leg parameters in hopping, the results obtained provide a strategy to cope with grounds of varying stiffness without changes in the controlled inputs. WandaX and MagE are innovative platforms that were used to comprehend the advantages of flexible bodies for underwater locomotion. WandaX, in direct analogy with Zürihopper, provides a mechanical strategy to keep behavior performance under periodic forcing caused by external vortices. Though utterly simplified scenarios are presented, the analysis should be applicable in more general interactions with the environment. Closing the thematic bundle, a simple mathematical model is presented in order to demonstrate the nonlinear nature and complexity of one dimensional hopping, even with the utilization of linear legs. The presentation is complemented with the optimization of hopping with emphasis on the mechanical properties of the leg. The optimization aims to maximize the height of the first hop; this differs from the usual approach where long term behaviors are optimized, e.g. overcoming a fence with a single jump and not bouncing until the jumping height is enough. The optimization is attained through the variation of the parameters of the force function of the leg.

The final chapters introduce the dynamic response decomposition method (DRD). This method directly uses the motion when inputs are absent, i.e. the natural behavior of the platform, to generate the actuation needed to solve a given reaching task. Natural behavior and reaching tasks are formally defined and the treatment aspires to be rigorous. Additionally, the method is shown to be strongly related to current methodologies for the analysis of biomechanical data: synergies and motor primitives. The demonstration is accompanied

with a numerical scheme that produces a mixture of given motor primitives to solve reaching tasks. These simulations are performed on spring-mass systems and planar kinematic chains.

The document finishes with a summary of the whole thesis and a succinct enumeration of the scientific contributions contained in it.

Zusammenfassung

Diese Dissertation untersucht die Beziehung zwischen der Morphologie einer mechanischen Vorrichtung und dem beobachteten Verhalten, wenn diese in einer bestimmten Art und Weise gesteuert ist.Dies geschieht mit Hilfe zweier komplementärer Methoden: numerische Simulationen und Experimente. Die Experimente werden mit Hilfe von experimentellen Plattformen, sogenannten *parametrischen Robotern* durchgeführt. Das sind Geräte deren physikalische Parameter systematisch über ein Intervall, das von Interesse ist, verändert werden können. Numerische Simulationen werden mit Hilfe einfacher mathematischer Modelle durchgeführt, die entwickelt wurden, um die wichtigsten Aspekte des untersuchten Verhaltens zu reproduzieren. Zusätzlich behandelt diese Dissertation die Kontrolle mechanischer Arme. Deshalb wird über einen neuen Algorithmus berichtet, der auf dem natürlichen Verhalten dieser Geräte basiert: die Methode der Zerlegung in dynamischen Reaktionen (DRD). Die Auswertung des Algorithmus wird durch numerische Simulationen anhand von Modellen unterschiedlicher Komplexität durchgeführt.

Im Zusammenhang mit Fortbewegung hat diese Arbeit das ehrgeizige Ziel, eine Brücke zwischen den Methoden aus ausgereiften Disziplinen und den Methoden aus verkörperter Künstlicher Intelligenz (embodied artificial intelligence) zu bauen. Mit diesem Ziel soll eine kurze Zusammenstellung von Methoden zur Analyse der experimentellen Ergebnisse gegeben werden sowie ein Überblick über die physikalischen Konzepte, die für das Thema relevant sind: Resonanzfrequenzen, Normalschwingungen und so weiter. Die meisten Diskussionen sind auf einem zugänglichen technischen Niveau für ein breites interdisziplinäres Publikum gehalten.

Das erste Kapitel dieser Arbeit ist eine kurze Einführung in die Konzepte für das Verständnis der berichteten Ergebnisse.

Kapitel 2 untersucht Fortbewegung zu Lande und im Wasser. Experimente mit drei parametrischen Robotern und ihren numerischen Modellen werden vorgestellt: Zürihopper, WandaX und MagE. Die drei Plattformen werden verwendet, um die Rolle zu evaluieren, die die mechanischen Eigenschaften für die Qualität des beobachteten Verhaltens haben. Die Nichtlinearitäten des WandaX und des Zürihoppers erlauben, dass die Eigenschaften des Körpers angepasst werden können, um Energie aus der Umgebung zu extrahieren und Verhalten zu generieren: Springen im Fall vom Zürihopper und Schwimmen durch Turbulenzen im Fall von WandaX. Die entdeckten Strategien, um diese Anpassungen zu machen, haben wichtige Ähnlichkeiten, welche die gemeinsame Natur der beiden Verhaltensweisen betonen. MagE wird verwendet um zu demonstrieren, wie magneto-mechanische Kopplung als alternativer Mechanismus für einen Unterwasserantrieb verwendet werden kann.

In Kapitel 3 wird das Studium der physikalischen Parameter, welche am Springen beteiligt sind, aus der Perspektive der numerischen Simulation wiederaufgenommen. Das Bein eines einbeinigen Roboters wird optimiert, um die Sprunghöhe zu maximieren. Nichtlineare Beine haben bessere Leistungen als lineare Beine für eine Vielzahl von Situationen. Die Optimierung wird durch eine Interpretation der Ergebnisse in Bezug auf die Physik begleitet.

Kapitel 4 und 5 bieten eine theoretische und numerische Präsentation der DRD-Methode. Dieser Algorithmus wird verwendet, um die Kontrollprobleme, welche mit dem biomechanischen Modell des oberen Torso zusammenhängen, zu lösen. Die Methode beinhaltet die Verwendung des natürlichen Verhaltens des Systems für die Zusammensetzung der gewünschter Trajektorie. Gleichzeitig ist DRD eines der ersten Modelle, das die Entwicklung von Muskel-Synergien (Hypothese der Biomechanik) erklärt.

Die Arbeit schließt mit einer Zusammenfassung aller wissenschaftlichen Beiträge, die während ihrer Entwicklung erzeugt wurden (Kapitel 6).

Resumen

En esta tesis se estudia la relación entre la morfología de un dispositivo mecánico y el comportamiento observado al actuarlo de manera determinada. Esta tarea se realiza utilizando dos metodologías complementarias: simulaciones numéricas y experimentos. Estos últimos se llevan acabo con la ayuda de plataformas experimentales denominadas *robots paramétricos*, i.e. dispositivos semejantes a robots cuyos parámetros físicos pueden ser variados de forma sistemática en un intervalo de interés. Las simulaciones numéricas se realizan utilizando modelos matemáticos sencillos desarrollados para reproducir los aspectos más importantes del comportamiento a estudiar. Adicionalmente, este documento trata sobre el control de brazos mecánicos. Por lo tanto se reporta un nuevo algoritmo de generación de movimiento basado en el comportamiento natural de estos dispositivos: el método de descomposición en respuestas dinámicas (DRD). La evaluación del algoritmo se realiza mediante simulaciones numéricas usando modelos de complejidad variada.

En el contexto de locomoción, esta tesis tiene el ambicioso objetivo de fundar un puente entre las metodologías de estudio de disciplinas maduras y las metodologías de carácter *ad hoc* actualmente utilizadas en inteligencia artificial corporeizada (embodied artificial intelligence) y algunas sub-disciplinas de la robótica. Con este objetivo se brinda una breve recopilación de métodos para el análisis de resultados experimentales, como así también se repasan los conceptos físicos relevantes a la temática: frecuencias de resonancia, modos normales, etcétera. La mayoría de las discusiones se mantienen en un nivel técnico accesible a una amplia audiencia interdisciplinaria.

El primer capítulo de este documento constituye una breve introducción a los conceptos necesarios para la comprensión de los resultados reportados.

El capítulo 2 estudia la locomoción en tierra y agua. Se reportan experimentos realizados con tres robots paramétricos y sus modelos numéricos: Zürihopper, WandaX y MagE. Las tres plataformas se utilizan para evaluar el rol que las propiedades mecánicas tienen en la calidad del comportamiento observado. Las características no lineales de Zürihopper y WandaX permiten ajustar las propiedades del cuerpo para extraer energía del medio y generar comportamiento: saltar en el caso del Zürihopper y nadar a través de turbulencias en el caso de WandaX. Las estrategias encontradas para realizar estos ajustes presentan una similitud importante que resaltan la naturaleza en común de ambos comportamientos. MagE se utiliza para demostrar un mecanismo alternativo para la propulsión sub-acuatica basada en acoples magneto-mecánicos.

En el capítulo 3 se retoma el estudio de parámetros físicos involucrados en la actividad de saltar (Zürihopper) desde la perspectiva de la simulación numérica. Se optimiza la pierna de un robot unípede con el fin de maximizar la altura de salto. Piernas no lineales presentan mejores desempeños que piernas lineales para una amplia gama de situaciones. La optimización se acompañan con una interpretación de los resultados en términos de la física involucrada.

Los capítulos 4 y 5 presentan el método DRD de forma teórica y numérica. Este algoritmo se utiliza para resolver problemas de control en cadenas cinemáticas asociadas a modelos biomecánicos de la parte superior del torso humano. El método se basa en la utilización del movimiento natural del sistema para la composición de las trayectorias deseadas. Al mismo tiempo, DRD representa uno de los primeros modelos capaces de explicar el desarrollo de sinergias musculares (hipótesis proveniente de la biomecánica).

La tesis finaliza con una recapitulación de todas las contribuciones científicas generadas durante su desarrollo (capítulo 6).

Preface

In my view, this thesis represents a small step forward in the understanding of the role of nonlinear physical substrates (the body, the machine) in the production of behavior. The presentation is quantitative and inspired by the ideas present in the scientific milieu where I did my research. These ideas emanate from the field of embodied artificial intelligence, nonlinear control, under-actuated robotics and biomechanics.

In these fields of study, the used terminology has different (sometimes conflicting) meanings. On one hand I think this is due to still insufficient interdisciplinary collaboration (good is that there is real support for interdisciplinary activities). On the other hand this may be the symptoms of a incoming shift of scientific paradigm. Society has already gone to such confounding periods, pumped by a ramming insertion of new technologies in everyday life. A quote from Harper's New Monthly Magazine 1873[1], during the onset of the telegraph, describes the situation clearly,

> The difficulty of forming a clear conception of the subject is increased by the fact that while we have to deal with novel and strange facts, we have also to use old words in novel and inconsistent senses.

With this in mind, I made special effort to highlight the words that we (scientists) are overloading with different meanings, many times without proper definition.

The results and discussions I present, focus on physical models of real devices. Hence, in an attempt to establish the basic context, the document begins with a review of the concepts related to physical modeling. Inevitably, several issues from the philosophy of science will be mentioned. However, since those are not the object of this work only references are provided. I must point out that there is a difference in approach between the philosopher on the one hand and the scientist and the engineer on the other. The latter face the reality of having to obtain numerical measures out of concepts and thus, they face the need to derive an objective definition of the nature of the concept on which they define quantitative measures of analysis. This alone represents a challenging task and therefore it seems to ambitious to try to cover, in addition, its philosophical implications.

The thesis is aimed at a wide public with extremely different and not necessarily overlapping background knowledge. Therefore, the thesis contains sections that are succinct in technical details, aimed to the ones who prefer to read the concepts. Notwithstanding my attempt to reach a broad audience, the document is populated with technicalities aiming to present a quantitative description of the ideas. Formal descriptions are pursued but kept to a reasonable level, having in mind that "One man's rigor, is another man's mortis"[2]. I tried to keep the conceptual reading of this thesis independent of the technical details. However, the work can be appreciated better if the conceptual and technical content are conjointly understood.

The document is organized in two main thematic axes: locomotion and reaching. Chapters 2 and 3 cover my work in the context of the SNSF project "From locomotion to cognition". The results there are mainly related to locomotion and the notion of resonance in nonlinear systems. Several robot platforms and their mathematical models are presented. The research is focused on the use of the dynamical properties of these robots for the generation of efficient locomotion on land and in water. The second thematic axis is reaching, it is covered in Chapters 4 and 5. This work was inspired by the research of Andrea d'Avella (in the context of the European project AMARSi) and his quest for the understanding how the central nervous

[1] As cited in James Gleick (2011), "The information: A History, A Theory, A Flood", Knopf Doubleday Publishing Group

[2] Quote from the preface of Bohren and Huffman, John Wiley & Sons, first edition, 1983.

system controls the motion of the human body. In this second part, I present a method to control arm-like devices for reaching in different directions. Additionally, the methodology is linked to the synergy hypothesis and may provide a tool for further understanding of their development.

Finally, I have marked some chapters and sections with an asterisk ($*$). These parts present technically more advanced topics. They are important elements of the thesis but could be postponed until a thorough read is needed.

I hope you enjoy the ride!

Juan Pablo Carbajal, March 15, 2012, Winterthur, Switzerland.

Acknowledgements

> What one man does is something done, in some measure, by all men.
>
> "Ficciones" by Jorge Luis Borges (1944)(Translated by Anthony Kerrigan)

This thesis was only possible thanks to the support (direct and indirect) of many, many people. Probably so many, that I will fail to thank everybody properly.

I am grateful to the supervision «beyond the call of duty» I enjoyed from Andrea d'Avella, Gustavo Buscaglia, Alejandro Kolton and Tobi Delbrück who where always present providing suggestions, criticism and support, emotional and academic. I would like to recognize the help of researchers at the Department of Mathematics of the University of Zürich: Prof. Dr. Camillo De Lellis and Prof. Dr. Thomas Kappeler; who spent some of their mornings trying to understand my mathematical rant. The Swiss National Science Foundation and the European Project AMARSi were the source of the needed financial support and of great opportunities for my career. I thank the anonymous writers of the proposals of the projects in which I participated.

I am also grateful to the reviewers of the document for they comments and corrections: Rolf Pfeifer, Veljko Potkonjak and Andre Seyfarth. Without a doubt, I owe much to my colleagues at the AILab. Massimiliano "Max" Lungarella who was a distant but constant supervisor. Cristiano Alessandro, fought by my side the many questions that rose from my research, it was a pleasure to work together with him. Naveen Suresh Kuppuswamy and Konstantinos "Costas" Dermitzakis were always ready for academic discussions (and not so academic ones also). I enjoyed working with Harold Roberto Martinez Salazar, sadly, the outputs from the collaboration could not fit this thesis. I extend my thanks to Daniel Germann who had the patience to proofread the German version of the abstract. Thanks to Hugo Gravato Marquez, Matej Hoffman, Marc Ziegler and Dandolo Flumini. Finally, to Thierry Bücheler for his «game days», that gave us unlimited fun.

Several Bachelor and Master students at our laboratory deserve mention, in particular Emanuel Benker for his priceless aid with machine building. With some help from my side, Emanuel Benker designed the Zürihopper. The robot was brought to life solely thanks to Emanuel's building prowess and his ability to make the best of outdated machinery. Mathias Weyland, who joined us by the end of my thesis work, but nevertheless provided loads of interesting and fruitful discussions. I should not continue without mentioning the support from the kind Rudolf "Ruedi" Füchslin who always supported me and knew how to handle my «edges» with patience. Ruedi and Peter Biller kept open the doors of the Physics department of the ZHAW, and provided me with a tranquil place to finish the writing of this thesis, I am deeply thankful. Peter's death was a shock to all of us, I treasure the memory of his joyful personality and his commitment to the quality of his work.

The people from the consortium of the European Project AMARSi played an important role for my motivation. I thank Bejamin Schrauwen and his amazing minions: Tim Waegeman, Francis Wyffels, Ken Caluwaerts and Pieter-Jan Kindermans. Albert Mukovskiy was always an excellent source for mathematical references that enriched this document. Thanks go also for people at the the CoR-Lab: Andrea Soltoggio, Arne Nordmann, Sebastian Wrede and Andre Lemme, for all the «unofficial» chatting. Last but not least, Auke Ijspeert and his students: Alexander Sproewitz, Mostafa Ajallooeian and all the participants of the AMARSi Workshops in Zürich.

I owe Physics to my first mentor Daniel Córdoba: there are not enough words to thank

him properly. In the same vein, the ones who showed me the way at early stages deserve (and have) my gratitude: Elvio Alanis and the Asociación Salteña de Astronomía, Nicolás von Ellerienderand Victor Passamai. I express my deep and sincere appreciation for the quality of the knowledge provided by teachers at the National University of La Plata: Jorge "Toto" A. Martinez, Graciela María Punte, José Luis Alessandrini (I owe you the lost Physics Teachers), Nicolás Grandi (the first person to ever show me a Lagrangian) and Ezequiel Albano. From the same institution I keep a special place in my heart for the ones who love, and taught me how to love mathematics: Adriana Galli, Oscar Barraza and Gerardo Rossini. To the teacher assistants of Algebra, Mathematical analysis and Complex analysis: Thanks for your patience! Thanks to Daniel “Mingo” Domínguez, who introduced me to the field of dynamical systems in the classrooms of the beautiful Instituto Balseiro; and to Gabriel Mindlin who completed the formal introduction to that amazing field. Also, thanks to the ones who suffered my grumpiness at very early stages Jorge Daniel Czajkowski and Gustavo Montero.

The online community deserves my gratitude as well. Thanks to David Pritchard, for his blog column “Better Know a theorem”. Thanks to the blog posts by Michael Nielsen, always providing excellent reads of intriguing and relevant topics. Thanks to Jordi Gutiérrez Hermoso, for his help improving the wording of my math. The whole GNU Octave community was there when I need them, thanks to jwe and carandraug.

I reckon the help of my good old friends Ezequiel Pozzo, Federico Späth, Tomás Guozden and Cesar Chialvo, for what is a man without a past? While in La Plata, I enjoyed the support of many friends who deserve my attention: Laura, Antonella, Nico D., Nico M. (you will never understand coca-leafs), Nippur, Caro, Vicente, Mariana, Tere, Miguel, Facu ... so many more!

Finally, my family. I owe them all, all my achievements are theirs. My parents, Sergio y Ana Rosa, who gave me all that I needed to develop, to survive and to learn. I thank my brother Ignacio and my sister Ana and their offspring, since they were always a «cable to Earth». To my beloved partner Jeannette, thanks for your love and patience!

To all the ones that I have undoubtedly forgotten to mention: Sorry, and thank you!

Contents

Chapter 1

Introduction

> In physical science a first essential step in the direction of learning any subject, is to find principles of numerical reckoning, and methods for practicably measuring, some quality connected with it. I often say that when you can measure what you are speaking about, and express it in numbers, you know something about it; but when you cannot measure it, when you cannot express it in numbers, your knowledge is of a meagre and unsatisfactory kind: it may be the beginning of knowledge, but you have scarcely, in your thought, advanced to the stage of science, whatever the matter may be.
>
> William Thompson 1883 (Lord Kelvin)

Whenever an inquiring person spends some time observing the behavior of any non-human living creature, they end up puzzled. The low intelligence that is usually attributed to the creature, appears not to match the performance on its whereabouts. We can hardly understand how the richness, quality and elegance of motion is generated. This is even true when we observe ourselves, since we move without understanding how the motion of our limbs is generated. We have got considerable knowledge, from the basic sciences, about the processes and mechanisms that are used to generate motion; nevertheless, many questions remain unanswered and hypotheses untested. From a applied science perspective, we have a solid set of methodologies to build machines and to program them for a prescribed task (generally referenced as control theory), but we are still missing the design principles that, we believe, underlie the motion of biological machines.

During the last four decades, *bioinspiration*, the use of our insights into biology to solve technological problems, became a main trend in almost all scientific activities. However, we should not take for granted that nature is the ultimate source of perfection in design. As we understand it, natural selection is a trial-and-error process solving an ever changing problem. Among other constraints, there are fundamentally inferior designs that remain for very long time, it deals with unavoidably multi-functional devices and resources are locally accessible in time and space (geographical segregation)(Vogel, 2003). Hence, we have to learn how to apply nature's lessons while understanding the constraints of these lessons. Additionally, the idealized model of natural selection as an optimization of fitness, though practical, is source of scientific controversy (Toffoli, 2004; Thurner et al., 2010).

On the bright side, the *biomimetic* hubbub had a serendipitous effect. It refueled the efforts to solve problems that involve nonlinear systems, which had been somehow relegated,

mainly due to the lack of methods to tackle these problems and the astonishing success of solutions based on linear methodologies. For example, most fundamental control theoretic tools deal solely with linear systems. However, engineers have been always very aware of the difficulties involved when nonlinearities come into play. In a technical report by Brilliant (1958) we read:

> *Sometimes nonlinearity is avoided, not because it would have an undesired effect in practice, but simply because its effect cannot be computed.*

In view of this, the preference for linear systems in control theory or classical engineering methods should not be fenced as criticism, but highlights the need of extending them to embrace nonlinear phenomena. More powerful computers, new simulation methods and some novel uses of classical tools promise help to cruise the mangrove forest of nonlinear systems that waits ahead.

This thesis is about the body of animals, robots, machines, or generally *agents*. Particularly, we study the role that physical properties have in the generation of behavior. These physical properties, termed *morphology*, appear as numerical parameters in the mathematical models that we use to describe the agent. The dependency that the behavior exhibits on these parameters is a reflection of the agent's morphology. However, this reflection is blurred when strong external purposeful influences are exerted upon the system; they override the characteristics of the agent. Therefore, the role of the morphology is highlighted in situations where the system behaves under little or no external purposeful influence. Colloquially, what was just said seems intelligible. Nevertheless the notions used for that explanation, when quantified, become relative to what we understand by *system* and to the meaning of *little or no influence*.

The objective of the subsequent sections is to briefly discuss these notions, the concept of *physical system* and of *model*. Models based on our experience are fundamental in our life; they allow us to predict events before they happen. In particular, mathematical models are the cornerstone of scientific research and several paragraphs are devoted to their description. Additionally, concepts of dynamical systems that are necessary to understand the results presented in this thesis are shortly reviewed.

1.1 Physical systems

We will use the word *system* in a technical sense. A system is the portion of the physical universe chosen for analysis. The systems considered herein will mainly be mechanical systems, formed by rigid or elastic bodies in interaction. These interactions will be described in the context of mechanics[1]. Everything that is not described as the system is known as the *environment* or the exterior of the system. The analysis of the environment is ignored except for its influence on the system, i.e. the interaction with the system. Following a quantitative spirit, the influences we care about are those that can be measured[2] and we call them *signals*. The set of external signals that can be manipulated are called *inputs*. This definition of input plays a fundamental role throughout the document and it should be kept in mind.

It should be noted that the definition of the boundary between system and environment is arbitrary; thus, the notions of external and internal are also arbitrary. A cut between what is internal and what external is made solely to simplify the analysis in a convenient way.

[1] systems whose kinetic energy takes the form $\frac{1}{2}\dot{\boldsymbol{q}}^T M(\boldsymbol{q})\dot{\boldsymbol{q}}$

[2] This is another word with a technical definition and more about it can be read in (Youden, 1998; Joint Committee for Guides in Metrology, 2008; J. C. Gibbings, 2011). According to the quote at the beginning of the chapter, measure is a synonym of expressing in numbers and I will stick to that idea.

The interactions among the components of a system (sometimes referred to as subsystems) and the environment can be classified as information driven interactions and force-field driven interactions (Roederer, 2003, 2010) depending on their nature. Information driven interactions are those, generally speaking, for which the (physical) energy of the causes are not related to the energy content of the consequences. An example is the call of the master to their dog; the physical energy associated with the call is clearly not enough to fuel the unfold of forces and torques in the body of the animal. Herein, we will be concerned with force-field driven interactions, which encompasses the usual physical interactions we are so used to talk about, such as forces and torques.

The *intensity* of a signal is another concept that deserves some clarification. We cannot talk of the intensity of interactions in absolute terms. This means that phrases like "small input" or "little influence" make sense only relative to the system under study. Lets illustrate this with an example. If we try to bend a slab of concrete with our own hands, it is clear that it will behave like a rigid body; there will be no observable deformations when we apply the maximum force a human could apply. If instead of our bare hands we used a powerful tool, the slab would behave like a piece of rubber (the Tacoma Narrows bridge collapse being an extreme example). In contrast, our hands are more than enough to bend a leaf of grass at will. These two situations try to intuitively show that it only makes sense to talk about the "intensity" of the input, in relation to a given system.

Similarly, the concepts of *fast* and *slow* are also relative to the properties of the system under study. Lets take a real life example of a misconception in this regard. Several people like to spread the idea that "plants do not move". Leaving aside the issue that these promoters do not provide a concrete definition of "to move", the belief is sustained by the difference of time scales between the life of humans and that of plants. The life of plants occurs at rates that are much slower than that of humans, and we can hardly perceive it without the help of instruments. When video recordings of plants are played at high speed, several instances of motion become evident: not only growing, but also rearrangement of body parts to improve feeding, support and the dispersal of seeds. Plants do embody several instances of the notion of motion.

There are systems that naturally define a time scale and others that do not. A book example of the former is the mass-spring system with its characteristic period of oscillation; another one is the pendulum: the fundamental piece in mechanical clocks[3].

1.2 System models

To quantify and practice logic when forming an analytical description of an observed physical phenomenon we use mathematics. We will describe our system with variables and establish relations between these variables using mathematical expressions. This description of a system, is known as an analytical or *mathematical model*. These models can be characterized by properties like discrete, continuous, linear, nonlinear, etc; depending on the nature of the expressions used. Most of the models used in this thesis are differential equations, which belong to the continuous realm, but are discretized when numerical simulations are performed. When dealing with locomotion mostly hybrid dynamical system will be used (see Section 1.4.4).

The mathematical model of a physical system and the physical system itself are of a different nature. We can compare certain aspects of the physical system with its mathematical representation, but we can never establish any exact connection between them. This has some deep philosophical aspects that we want to avoid, thus the acceptance of models is guided by their usability. This criterion can be extended to the internal models believed to be present in animals and used for the generation of their behavior (Kawato, 1999). These internal models do not need to be physically real or meaningful, but rather they have to be

[3] An excellent and fun class on this topic can be watched at http://academicearth.org/lectures/hookes-law-and-simple-harmonic-motion

useful to reliably predict future events. It is not uncommon to find published results that draw a straight connection between the model and the physical system under study (the title of Burdet et al., 2001, provides an ideal example), this is a dangerous path to follow. Though the model can indeed reproduce the observed behavior, this does not imply that the physical entity is itself built in the way that the model describes. We can illustrate this with a computational example: two different machines can implement the same function between a set of given inputs and outputs, nevertheless their physical implementation may be quite different: think of your laptop running an algorithm to solve a differential equation and Vannevar Bush's Differential Analyzer (a metal platform of rotating shafts and gears weighing hundred tons, Bush (1931)) doing the same thing. Do you think they are built in the same way? Consequently, if we develop a model (mathematical or physical) that produces the outputs of an agent (of which we are oblivious to its internal mechanisms), we cannot state anything but that mere fact: we built a model that simulates the behavior of the agent, little else can be said about the internals of the machine based on that evidence. Once more, this discussion has some deep philosophical implications that we will not cover, the interested reader could start by looking into the Church-Turing-Deutsch principle[4] (Deutsch, 1985) .

Models are built from observation and experience, i.e. measurements, experimental data. On one hand, if there are validated models available (i.e. models that are proven to reproduce the behavior of the system they model), some new models can be built by their aggregation. This way of proceeding is known as system modeling or dynamic modeling. On the other hand, models can directly be inferred from experimental data. This can be done by estimating the values of certain physically meaningful parameters (as the elasticity of a spring), or by finding the values of parameters of a general enough model (like the weights of a neural network). This general way of proceeding is known as *system identification*, a crucial field that should not go unnoticed by roboticists and researchers in embodied artificial intelligence (an essential reference is the book of Ljung (1999), source of most part of the preceding digression).

1.3 Nonlinear systems

An mathematical relation is called nonlinear when it does not fulfill the properties of linearity; therefore we need to define linearity. To do that we need the following ingredients:

- Three sets S,V and W that can be all the same or not.
- Two binary operations (addition): $+$ defined between elements of V, and $\oplus$ defined in W. The operations take two elements of the given set and return a third one, also in that set (closure).
- Two binary operations (multiplication by scalars): $\otimes$ defined between elements of V and S, and $\times$ defined in W and S. Each operation takes a scalar from S and an element from the set V (or W) and returns an element in that same set.
- The mathematical relation in question, f, taking an element of V and returning an element of W.

We say that f is linear if

$$f(\alpha \otimes x + \beta \otimes y) = \alpha \times f(x) \oplus \beta \times f(y) \quad \textbf{for all} \quad x, y \in V \quad \alpha, \beta \in S. \tag{1.3.1}$$

[4]The essay "Interesting problems: The Church-Turing-Deutsch Principle" by Micheal Nielsen, is definitely a good starting point for the conceptual reader. www.michaelnielsen.org/blog/interesting-problems-the-church-turing-deutsch-principle/

whenever the equality is not true, the relation f is called nonlinear.

Example 1 (Real functions)**.** Take $S = V = W = \mathbb{R}$, i.e. the real numbers. The addition and multiplications are the usual operations in the reals. Take $f(x) = 3x$, then f is linear. If we take $g(x) = x^2$, g is not linear because $g(ax + y) = a^2x^2 + 2axy + y^2 \neq ax^2 + y^2$ for at least one value of the triplet a, x, y. ◀

Example 2 (Derivatives)**.** Take $S = \mathbb{R}$ and $V, W \in C^\infty(\mathbb{R})$, i.e. real functions with continuous derivative of any order. We take the addition of two functions as the point-wise operation $(f + g)(x) = f(x) + g(x)$. The multiplication is defined as $(\alpha f)(x) = \alpha f(x)$. Take as our relation the derivative with respect to the argument, then it is a linear relation since $(\alpha f + g)'(x) = (\alpha f' + g')(x)$. ◀

The definition of linearity can be made more general, but the important property is that linearity implies that superposition holds, i.e. the relation applied on the joint elements is the superposition of the relation applied to each element separately.

1.4 Differential equations

In this section we give a brief and shallow overview of this branch of mathematics, thus to have a proper introduction to the topic, the reader should resort to any introductory book of differential calculus.

Differential equations, as the name indicates, are equalities expressed in terms of derivatives of a function with respect to one or more variables. Since their introduction, (in the hands of Leibniz and Newton) they have become the basic tool for the creation of models in physical sciences. In particular classical Mechanics is a theory that has its roots in the differential calculus. For example, Newton's second law is a second order differential equation which belong to a very important class: Ordinary Differential Equations (ODEs). A N-th order linear ODE takes the form,

$$\sum_{n=0}^{N} a_n(t) \frac{\mathrm{d}^n x}{\mathrm{d}t^n} = 0, \tag{1.4.1}$$

where $a(t)$ are functions of the independent variable and $x(t)$ is the incognita function. When the order of the equation is low, typically no more than 3, then the derivative notation can be replaced by dots on top of x, e.g. $\dot{x}, \ddot{x}$ stand for the first and second derivative with respect to t. We can think of the previous equation as an abstract operator acting on the variable x,

$$L(t)x := \left(\sum_{n=0}^{N} a(t)_n \frac{\mathrm{d}^n}{\mathrm{d}t^n} \right) x = 0, \tag{1.4.2}$$

which in turn is a combination of simpler operators (i.e. the derivatives themselves)[5]. Note that the operator can be autonomous, i.e. it does not depend on time explicitly, which is not the case for the one shown above. We will use the name differential operator when we refer to these entities (autonomous or not). Linear differential equations follow the superposition principle characteristic of linear entities. That is, a linear combination of solutions of a linear ODE are solutions of the same ODE.

[5]We use the symbol := to denote assignation, i.e. when we store an expression inside a symbol. The symbol = represents numerical equality, e.g. two different expression can take the same value. The symbol $\doteq$ is used with the purpose of highlighting definition but is essentially the same as numerical equality.

Example 3 (Superposition of solutions)**.** Assume $x(t), y(t)$ are solutions of eq. (1.4.2). Apply the operator to the linear combination $\alpha x(t) + y(t)$ to get

$$\sum a_n(t)\frac{\mathrm{d}^n(\alpha x + y)}{\mathrm{d}t^n} = \alpha \sum a_n(t)\frac{\mathrm{d}^n x}{\mathrm{d}t^n} + \sum a_n(t)\frac{\mathrm{d}^n y}{\mathrm{d}t^n}, \tag{1.4.3}$$

by using the linearity of the derivative. ◀

ODEs can be linear, as the one shown in eq. (1.4.2), or they can be nonlinear. For example,

$$\mathcal{D}_1(x) := \dot{x} - ax^2, \tag{1.4.4}$$

$$\mathcal{D}_2(x) := \ddot{x} + \dot{x}^2, \tag{1.4.5}$$

$$\tag{1.4.6}$$

are nonlinear differential operators, albeit different. Operator (1.4.4) has algebraic nonlinearities since they do not involve derivatives. Operator (1.4.5), in contrast, has nonlinear terms that involve derivatives. This classification is not crucial but it has relevance in the discussions presented in the thesis. Note that the incognita can be a vector function, and the solution $\boldsymbol{x}(t)$ represents a curve parametrized by t, in the corresponding vector space.

There are many solutions to these equations and to pick one out of the many, values of the function or its derivatives (or combinations of these) must be provided at certain points, these values are called *point conditions* or *point constraints*. When initial conditions are given an ODE defines an *initial value problem* (IVP). If conditions are defined at the extrema of the time interval $t \in [0, T]$, the problem is known as a *boundary value problem* (BVP). Conditions given at intermediate values are not officially named since the problem can be formally broken into several BVPs, nevertheless point constraints at intermediate points are not uncommon in some fields of research (e.g. in biomechanics: via-point reaching).

Many control problems of ODEs are stated as BVPs. In general we can write all these problems in the form

$$\begin{aligned} \mathcal{D}(\boldsymbol{q}) &= \boldsymbol{u}(t), \\ g_i(\boldsymbol{q}, \dot{\boldsymbol{q}}, \ldots, t_i) &= 0. \end{aligned} \tag{1.4.7}$$

Where $\mathcal{D}$ is a differential operator modeling the agent in question and $\boldsymbol{u}(t)$ is associated with the inputs to the system (discussed in Sec. 1.1). If the input vector is zero for all time, the problem is *homogeneous*. The vector functions g_i describe point constraints for the system at given time values t_i. For example, a boundary value problem can be defined by setting

$$g_0(\boldsymbol{q}, \dot{\boldsymbol{q}}, t_0 = 0) \doteq \begin{bmatrix} \boldsymbol{q}(0) - \boldsymbol{q}_0 \\ \dot{\boldsymbol{q}}(0) - \dot{\boldsymbol{q}}_0 \end{bmatrix} \tag{1.4.8}$$

$$g_1(\boldsymbol{q}, \dot{\boldsymbol{q}}, t_1 = T) \doteq \begin{bmatrix} \boldsymbol{q}(T) - \boldsymbol{q}_T \\ \dot{\boldsymbol{q}}(T) - \dot{\boldsymbol{q}}_T \end{bmatrix} \tag{1.4.9}$$

where $\boldsymbol{s}_i := [\boldsymbol{q}_i, \dot{\boldsymbol{q}}_i]$ with $i \in \{0, T\}$, are given configurations and velocities, respectively. In the context of robot manipulators, these problems (taking $\dot{\boldsymbol{q}}_i = 0$) are known as *reaching*, since the manipulator starts in a motionless posture and goes to a different one, also motionless. However, equation (1.4.7) can accommodate a more general class of problems, as we will see in Chapter 5. We associate the functions g_k to the *task* or *goals* that the system has to solve or achieve.

For "sufficiently smooth" operators $\mathcal{D}$ [6], when initial conditions $\boldsymbol{s}_0$ and input $\boldsymbol{u}(t)$ are given, Eq. (1.4.7) has a unique solution $\boldsymbol{q}(t, \boldsymbol{s}_0, \boldsymbol{u})$, called *forward dynamics*. The mathematical properties of these trajectories are thus defined by the properties of $\mathcal{D}$ and of $\boldsymbol{u}$.

[6] A simple characterization of smoothness is given in Strogatz (1994) and references therein.

Conversely, by applying $\mathcal{D}$ to a given trajectory (satisfying the goals g_i) we can calculate the inputs that generate it, called *inverse dynamics*. In this case, the properties of $\boldsymbol{u}$ are defined by the properties of the given trajectory and the operator $\mathcal{D}$.

In this document we will reiteratively use the fact that a differential operator $\mathcal{D}$ can be split into its linear and its nonlinear part,

$$\mathcal{D}(\boldsymbol{q}) := L(\boldsymbol{q}) + f(\boldsymbol{q}), \tag{1.4.10}$$

where L and f stand for the linear and nonlinear part, respectively.

1.4.1 Inputs and actuations

A final mention must be made of the vector of inputs $\boldsymbol{u}(t)$, and it involves the term "actuation". Equation (1.4.7) can be rewritten into,

$$\mathcal{D}(\boldsymbol{q}) = K\boldsymbol{m}(t), \tag{1.4.11}$$

by replacing $\boldsymbol{u}(t)$ with $K\boldsymbol{m}(t)$. In this form, $\boldsymbol{m}(t)$ corresponds to the inputs, since those are the functions we can arbitrarily control and $\boldsymbol{u}(t)$ could be called *actuations*. The matrix K (sometimes called input matrix) mixes and scales the inputs to conform the net actuation applied to the system. A system is called *under-actuated* if $\operatorname{rank}(K) < \dim(q)$, i.e. the row rank of K is smaller than the dimension of the configuration space. This means that we are not able to arbitrarily modify as many actuations as inputs; rendering the distinction between input and actuations useful. When the actuations are generated via a nonlinear function (that is, when K is not a constant matrix but a non-constant vector valued function) the definition is trickier, but the idea holds: if the components of the actuation do not span all the space of actuation, then the system is under-actuated. When the rank of K equals the dimension of the configuration space the system is called *fully-actuated*. Clearly, the rank of K cannot by bigger than the dimension of $\boldsymbol{q}$ and therefore the (commonly used) word "over-actuated" is a misnomer. Usually, what is meant by over-actuation is that $\dim(\boldsymbol{m}) > \dim(\boldsymbol{q})$ (more inputs than dimensions) **and** that $\operatorname{rank}(K) = \dim(q)$. If the second condition is not met, regardless of how big $\boldsymbol{m}$ is, the system is still under-actuated. Even in this case the relation between $\boldsymbol{m}$ and $\boldsymbol{u}$ need not be simple, nor even one-to-one, rendering some problems very difficult to solve. A system with $\dim(\boldsymbol{m}) \geq \dim(\boldsymbol{q}) = \operatorname{rank}(K)$ should probably be called "overadic"[7], but the more commonly used term *redundant* already prevents confusion[8].

1.4.2 Kinematic chains

There is a family of ODEs that will appear repetitively throughout this document: kinematic chains. This equations model the dynamics of a group of rigid bodies (called segments) connected by joints that allow each rigid body to rotate independently while keeping them attached, e.g. a Byōbu (or folding screen) is a kinematic chain. Kinematic chains is a synonym of mechanical linkage which can be traced at least back to 1876, in the book "The Kinematics of Machinery" by the German scientist Franz Reuleaux.

For a kinematic chains to model a device accurately, several conditions must be satisfied. First, the different segments must behave as rigid bodies, i.e. they should not show considerable deformations during their motion. Second, the joints must be fixed with respect

[7] In reference to arity, i.e. the number of arguments that a function takes; e.g. ternary, n-ary, polyadic.

[8] Almost! classical roboticists call redundant to robot manipulators with more than six revolute joints. The issue is solved by understanding that, for them, a revolute joint is always an active joint (it has a motor on it) and that most of the time they describe the kinematics of the end effector position an orientation (3 spatial coordinates and 3 angular).

to the center of mass of the segments or, if they move, the motion has to be defined by a predefined smooth surface. That is, the motion of the joints should not depend on the motion of the segments in a way that is unknown a priori, i.e. the motion of the joint cannot be un-prescribed.

There are many borderline situations in which kinematic chains models are used, but the correctness is justified by the quality of the results. In biomechanics, kinematic chains are used to model the limbs of animals. The results obtained with these models are, in many situations, correct. Nevertheless, there are many cases in which kinematic chains must be generalized to more complex situations. For example, when you bend your knee, the muscles pulling your limbs change the lever arm along the motion in a discrete way (e.g. muscles that span more than one joint change the bone of support during motion). Consequently, the torques from these muscles present discrete jumps during the motion, and these jumps depend on the particular motion. The software package simtk-OpenSim[9] contains many models with this an other generalizations.

If we denote the degrees of freedom of the system with the symbol $\boldsymbol{q}$ (e.g. the relative angles of the joints) and with $\boldsymbol{u}(t)$ the net torques applied to them, a modern mathematical description of the equations of motion of kinematic chains is a follows

$$M(\boldsymbol{q})\ddot{\boldsymbol{q}} + C(\boldsymbol{q}, \dot{\boldsymbol{q}})\dot{\boldsymbol{q}} + N(\boldsymbol{q}) = \boldsymbol{u}(t). \tag{1.4.12}$$

These equations can be obtained using the Langrange-Euler equation. The particular shape of these equations is not unique, the one used here is in accordance with the practice of the robotics community. Refer to Westervelt et al. (2007, appendix B.4) for a modern quick reference of the planar case and to Ortega et al. (1998) for a general approach. Note the similarity of the structure of the equations with that of the equation of motion of a point-mass obtained by Newton's laws

$$m\ddot{\boldsymbol{x}} + c\dot{\boldsymbol{x}} + N(\boldsymbol{x}) = \boldsymbol{u}(t). \tag{1.4.13}$$

where m is the mass of the point-mass, c a damping coefficient and $N(\boldsymbol{x})$ are all the forces generated by potential fields (gravity, springs, etc. The meaning of this term is exactly the same in the case of Eq. (1.4.12)). Here $\boldsymbol{u}(t)$ stands for the net force applied to the point-mass. Following this association, we can interpret the coefficients in the equation of the kinematic chain.

The vector-valued function $M(\boldsymbol{q})$ is called the mass matrix (or mass-inertia matrix) and represents the inertia of the different degrees of freedom. Since the degrees of freedom can be represented by any generalized coordinate by a change of variable, the particular shape of $M(\boldsymbol{q})$ might not be simple, but it always has the property of being positive definite and bounded (i.e invertible)[10].

$C(\boldsymbol{q}, \dot{\boldsymbol{q}})$ is called Coriolis matrix (Coriolis and centripetal coupling matrix, Coriolis-centrifugal matrix, etc.), this matrix is not unique for a given system, however the product $C(\boldsymbol{q}, \dot{\boldsymbol{q}})\dot{\boldsymbol{q}}$ is. Intuitively, what is important for the motion of the system is the torques generated by this product, not the particular shape of the product. The equations of motion (1.4.12) are obtained using the Lagrangian of the system and the Coriolis term takes the form

$$C(\boldsymbol{q}, \dot{\boldsymbol{q}})\dot{\boldsymbol{q}} = \frac{\partial}{\partial \boldsymbol{q}} \left[M(\boldsymbol{q})\dot{\boldsymbol{q}}\right] \dot{\boldsymbol{q}} - \frac{1}{2} \left\{ \frac{\partial}{\partial \boldsymbol{q}} \left[M(\boldsymbol{q})\dot{\boldsymbol{q}}\right] \right\}^T \dot{\boldsymbol{q}}, \tag{1.4.14}$$

where the exponent T indicates the transpose of a matrix.

The numerical simulation of kinematic chains with many segments can be carried out efficiently using freely available software packages. The Robotics Toolbox by Peter Corke[11]

[9] https://simtk.org/home/opensim

[10] Except maybe in a set of isolated points.

[11] http://petercorke.com/Robotics_Toolbox.html

is particularly easy to use.

1.4.3 *State space representation

When the differential equations (1.4.7) allow us to solve for the first time derivative of $\boldsymbol{q}$, we can write the equations in an equivalent form, called the state representation. Define the state of the system as $\boldsymbol{s} := [\boldsymbol{q}\ \dot{\boldsymbol{q}}]^T$ and write the equations

$$\dot{\boldsymbol{s}} = F(\boldsymbol{s}) + B\boldsymbol{u}(t) \tag{1.4.15}$$

Where $F(s)$ is obtained from $\mathcal{D}$ and B is a matrix used to match dimensions. For example, in mechanics, passing from Euler-Lagrange equations to Hamilton equations, is such a transformation. This is not always possible (due to the inverse/implicit function theorem), and there are very useful models that prevent such transformation, in particular when using massless variables. Examples and technical treatment of the latter can be found in Agrawal (1991); Bhat and Bernstein (1996); Zhechev (2007); Schutte and Udwadia (2011).

Since Eq. (1.4.15) puts all explicit time dependency on the input term, when $\boldsymbol{u}(t) \equiv \boldsymbol{0}$ the system does not depend explicitly on time, i.e. it is autonomous. The set of all solutions of such a system, $\boldsymbol{X}$, is parametrizable with the initial condition, i.e. $\boldsymbol{X}(t, \boldsymbol{s}_0)$, with $\boldsymbol{s}_0 := [\boldsymbol{q}_0, \dot{\boldsymbol{q}}_0]$. In the dynamical system jargon, $\boldsymbol{X}(t, \boldsymbol{s}_0)$ is called the *evolution function* of the dynamical system. If we fix the argument $\boldsymbol{s}_0$, associated with the initial conditions, the evolution function produces the state of a system that started at $\boldsymbol{s}_0$, at any time t; i.e. it produces the orbit of the system through $\boldsymbol{s}_0$. If we fix the time argument $t = T$, the function describes the state at $t = T$ of all possible initial conditions (or system *ensemble*).

1.4.4 Hybrid dynamical systems

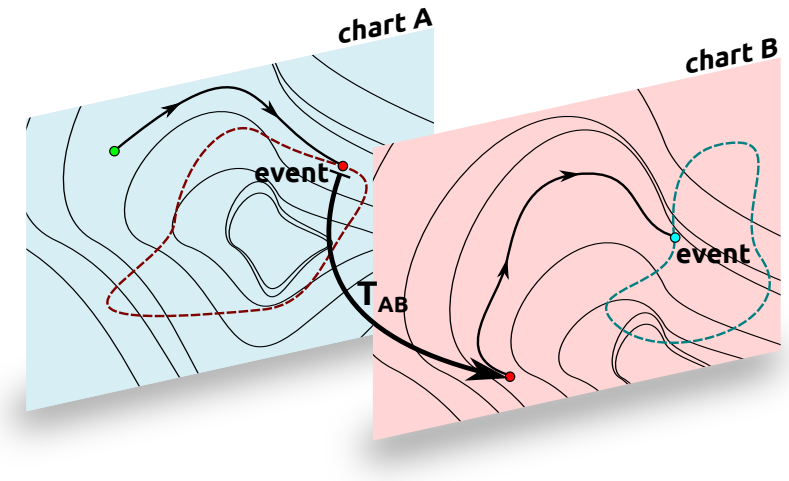

Figure 1.1: Hybrid systems. The system evolves continuously while it remains in a chart. When the event function achieves a given value (the event) the state of the system is mapped to another chart by means of the transition function.

Of importance for robotics are *hybrid systems* (Guckenheimer and Johnson, 1995), also known as Fillipov systems (Piiroinen and Kuznetsov, 2008). These systems are described by

differential equations connected by discrete maps and are used for the modeling of systems with impacts such as robots and running agents (Ghigliazza and Holmes, 2005); or discontinuous forces as dry friction, solenoid switches, etc. Figure 1.1 illustrates the structure of these systems. The time evolution is described by a set of continuous differential equations (the *chart*) until a function of the state of the system (called *event function*) reaches a given value. At this point the state of the system is mapped into a new chart (i.e. a new set of differential equations) and the evolution continues until a new event occurs. The mapping between the charts is called *transition function*, *switching function* or *reset map*. The charts can be very different from each other; for example, they not need to share the number of dimensions, in which case the transition map must resolve the induced ambiguity when going from the chart with fewer dimensions to the other.

The Spring Loaded Inverted Pendulum (SLIP) model is a typical example of hybrid system and is commonly used to study locomotion. To illustrate this lets consider the running gate of bipeds: we can identify a support phase and a flight phase. During support, the motion is influenced by the ground reaction force mediated by the limbs. During the flight phase, inertial motion of the body parts take place without any other external influence but that of gravity[12]. Figure 1.2 depicts some gaits and the transitions involved during a gait cycle.

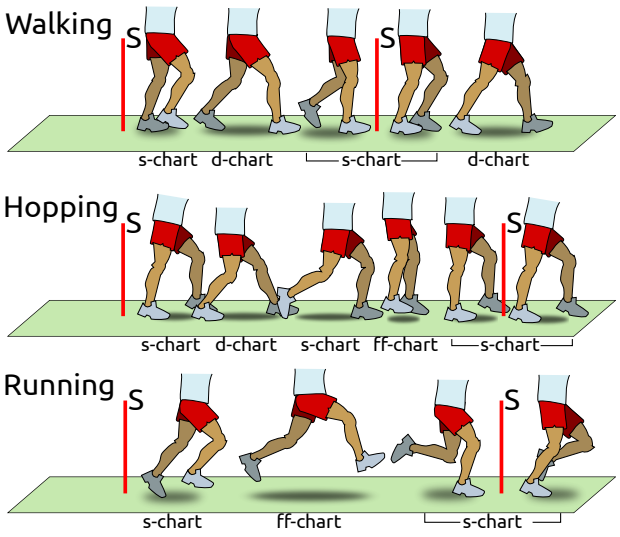

Figure 1.2: Different gaits described as hybrid systems (Martinez Salazar and Carbajal, 2011b). The charts during walking are single stance (s-chart) and double stance (d-chart). During Running we have the s-chart and free-fall (ff-chart). Hopping is a playful gait mostly used by kids, it comprises the three charts mentioned.

1.4.5 Characteristic time and scaling properties

Some systems have a time scaling property, i.e. the same path in configuration space can be performed at different time scales by just scaling the input. Systems that store energy in springs or gravitational fields do not have this property in general, on the contrary, they present characteristic time scales. In systems with time scaling the time taken to go from one

[12]In land locomotion, the interaction with the surrounding fluid medium (air) is neglected. That is not the case in aquatic locomotion.

configuration to another following a given path is not restricted except for the effort required to apply the forces. In systems with characteristic time scales the time taken and the path are coupled, allowing many interesting phenomena (see Chapter 2).

Scaling in kinematic chains

Here, we give a summary of the results presented in (Hollerbach and Flash, 1982). We show how torques applied to the a kinematic chain are scaled when a given trajectory is executed at a different time scale, i.e. when the same motion of the arm is done faster or slower. The motion of a kinematic chain (with frictionless joints) is described by the equations

$$\begin{aligned} M(\boldsymbol{q})\ddot{\boldsymbol{q}} + C(\boldsymbol{q},\dot{\boldsymbol{q}})\dot{\boldsymbol{q}} + N(\boldsymbol{q}) &= \boldsymbol{u}(t) \\ \boldsymbol{q}(t)\Big|_{t=0} = \boldsymbol{q}_0\ , \quad \dot{\boldsymbol{q}}(t)\Big|_{t=0} &= \dot{\boldsymbol{q}}_0 \end{aligned} \tag{1.4.16}$$

where $\boldsymbol{q} \in \mathbb{R}^{d\times 1}$ being d the dimension of the space of generalized coordinates (the total phase space has dimension $2d$). $M(\boldsymbol{q})$ is the mass matrix, which is positive definite, $C(\boldsymbol{q},\dot{\boldsymbol{q}})$ is the Coriolis matrix and $N(\boldsymbol{q})$ are the actions of potential fields. Since we work in the horizontal plane, we remove the action of gravity and we will consider kinematic chains without compliant elements, hence $N(\boldsymbol{q}) \equiv 0$. Finally, $\boldsymbol{u}(t)$ is the sum of all external torques acting on the chain.

Take a path in the postural space of the chain $\boldsymbol{q}(t)$ and the same path executed at a different time scale $\boldsymbol{q}^*(t) = \boldsymbol{q}(rt)$, where $r > 0$ is the scale. When $r > 1$ the original trajectory is executed faster and in the case $r < 1$ it is slowed down. The scaled velocities are $\dot{\boldsymbol{q}}^*(t) = r\dot{\boldsymbol{q}}(rt)$ and the accelerations $\ddot{\boldsymbol{q}}^*(t) = r^2\ddot{\boldsymbol{q}}(rt)$. Replacing these equalities in (1.4.16) and in (1.4.14) we obtain,

$$\begin{aligned} M(\boldsymbol{q})r^2\ddot{\boldsymbol{q}} + C(\boldsymbol{q}, r\dot{\boldsymbol{q}})r\dot{\boldsymbol{q}} =& r^2\left[M(\boldsymbol{q})\ddot{\boldsymbol{q}} + C(\boldsymbol{q},\dot{\boldsymbol{q}})\dot{\boldsymbol{q}}\right] = \\ &= r^2\boldsymbol{u}(rt) = \boldsymbol{u}^*(t) \end{aligned} \tag{1.4.17}$$

which shows that the torques needed to move the chain at a different time scale are scaled with the square of that scaling.

In our presentation we are going to study the system when $\boldsymbol{u}(t) \equiv 0$, then the time scale of a trajectory is defined by the initial conditions. As can be seen in (1.4.16), an initial condition is composed of an initial posture $\boldsymbol{q}_0$ and initial velocity vector $\dot{\boldsymbol{q}}_0$. Assuming that we are given a chain at an arbitrary initial posture with zero velocity, *how can we set non-zero velocities without changing the posture?* Physically this can not be done, since changing the velocity implies a change of the kinetic energy of the system, and therefore we need to do work on the system which implies a certain displacement. However, we can think that the work can be done so fast (very high power) such that the observed motion is negligible. This situation can be modeled mathematically using the Dirac delta function $\delta(t)$ (also known as the impulse function). We write

$$\begin{aligned} M(\boldsymbol{q})\ddot{\boldsymbol{q}} + C(\boldsymbol{q},\dot{\boldsymbol{q}})\dot{\boldsymbol{q}} &= \boldsymbol{p}_0\delta(t) \\ \boldsymbol{q}(t)\Big|_{t=0} = \boldsymbol{q}_0\ , \quad \dot{\boldsymbol{q}}(t)\Big|_{t<0} &= 0, \end{aligned} \tag{1.4.18}$$

by choosing the appropriate $\boldsymbol{p}_0$ (see next section), this is equivalent to

$$\begin{aligned} M(\boldsymbol{q})\ddot{\boldsymbol{q}} + C(\boldsymbol{q},\dot{\boldsymbol{q}})\dot{\boldsymbol{q}} &= 0 \\ \boldsymbol{q}(t)\Big|_{t=0} = \boldsymbol{q}_0\ , \quad \dot{\boldsymbol{q}}(t)\Big|_{t=0} &= \dot{\boldsymbol{q}}_0, \end{aligned} \tag{1.4.19}$$

Using the result of (1.4.17) in equation (1.4.18) we observe that to follow the same trajectory in a different time scale r, we must scale the amplitude of the delta function. Combining that with the scaling properties of the delta function we obtain (see eq. (1.4.26)),

$$\dot{\boldsymbol{q}}^*(t)\Big|_{t=0} = \dot{\boldsymbol{q}}_0^* = r\dot{\boldsymbol{q}}_0, \tag{1.4.20}$$

then, to follow the same postural path at a different time scale, we need to scale the initial velocity linearly with the time scale. Equivalently, two initial velocities that differ only on their norm (provided none is zero), will produce exactly the same path in the postural space, but they will be toured in different times. This gives a layered structure to the phase space.

*** Calculation of the amplitude of the Dirac delta**

The value of $\boldsymbol{p}_0$ in equation (1.4.18) is obtained in the following way. Solve (1.4.18) for $\ddot{\boldsymbol{q}}$ and integrate in a small interval around $t = 0$,

$$\begin{aligned}\dot{\boldsymbol{q}}(\tau) - \dot{\boldsymbol{q}}(-\tau) &= \int_{-\tau}^{\tau} \ddot{\boldsymbol{q}}(t)\mathrm{d}t = \\ &= \int_{-\tau}^{\tau} M^{-1}(\boldsymbol{q})\boldsymbol{p}_0\delta(t)\mathrm{d}t - \int_{-\tau}^{\tau} M^{-1}(\boldsymbol{q})C(\boldsymbol{q},\dot{\boldsymbol{q}})\dot{\boldsymbol{q}}\mathrm{d}t \qquad (1.4.21)\\ \dot{\boldsymbol{q}}(\tau) &= M^{-1}(\boldsymbol{q}_0)\boldsymbol{p}_0 - \int_{-\tau}^{\tau} M^{-1}(\boldsymbol{q})C(\boldsymbol{q},\dot{\boldsymbol{q}})\dot{\boldsymbol{q}}\mathrm{d}t \qquad (1.4.22)\end{aligned}$$

where we used the initial conditions in (1.4.18), the fact that the mass matrix is invertible (is a positive definite matrix) and the integration property of the delta. If we take the limit when τ goes to zero, i.e. we look at the speed a infinitesimal instant after $t = 0$, we get

$$\dot{\boldsymbol{q}}(0) = M^{-1}(\boldsymbol{q}_0)\boldsymbol{p}_0. \tag{1.4.23}$$

The integral term in the right hand side of Eq. (1.4.22) goes to zero under the assumption that the integrand is a bounded vector-valued function (integrable). This can be shown as follows

$$\begin{gathered}M^{-1}(\boldsymbol{q})C(\boldsymbol{q},\dot{\boldsymbol{q}})\dot{\boldsymbol{q}} = \boldsymbol{f}(\boldsymbol{q},\dot{\boldsymbol{q}})\\ 0 \le \|\boldsymbol{f}(\boldsymbol{q}(t),\dot{\boldsymbol{q}}(t))\| \le K \quad t \in (-\tau,\tau)\\ 0 \le \left\|\int_{-\tau}^{\tau} \boldsymbol{f}(\boldsymbol{q},\dot{\boldsymbol{q}})\mathrm{d}t\right\| \le \int_{-\tau}^{\tau} \|\boldsymbol{f}(\boldsymbol{q},\dot{\boldsymbol{q}})\|\mathrm{d}t \le K2\tau.\end{gathered} \tag{1.4.24}$$

Taking the limit

$$\begin{gathered}0 \le \lim_{\tau\to 0}\left\|\int_{-\tau}^{\tau} \boldsymbol{f}(\boldsymbol{q},\dot{\boldsymbol{q}})\mathrm{d}t\right\| \le \lim_{\tau\to 0}\int_{-\tau}^{\tau} \|\boldsymbol{f}(\boldsymbol{q},\dot{\boldsymbol{q}})\|\mathrm{d}t \le 0\\ \therefore \lim_{\tau\to 0}\left\|\int_{-\tau}^{\tau} \boldsymbol{f}(\boldsymbol{q},\dot{\boldsymbol{q}})\mathrm{d}t\right\| = 0\end{gathered} \tag{1.4.25}$$

Additionally, if we change the time scale, i.e. we change $\delta(t) \to \delta(rt)$, equation (1.4.23) is modified to

$$\dot{\boldsymbol{q}}^*(0) = \frac{1}{r}M^{-1}(\boldsymbol{q}_0)\boldsymbol{p}_0, \tag{1.4.26}$$

which was used to obtain relation (1.4.20).

1.4.6 Approximate solutions of differential equations

A class of methods to solve differential equations consist in proposing a parametrized solution that transforms the equations into a problem that can be solved more easily. Typically, it is assumed that the solution belongs to a certain functional space and it can be written as a combination of a basis of that space (see Funaro, 1992, for a complete overview of polynomial approximations of differential equations). A very well known method from this class is the power series method, in which solutions are decomposed into the basis of monomials $\{1, x, x^2, x^3, \ldots\}$. Similarly, spectral methods (Canuto et al., 2006) consist of proposing a solution decomposed in a generalized Fourier series. Another related family of methods is that of the Galerkin methods. In this case, the problem is transformed to its weak formulation and then the solution is projected over a known basis of the given functional space. These gave birth to the renown finite element method (Johnson, 2009). A review of most of the numerical methods used for numerically solving differential equations can be found in (Press, 2007).

Independently of the flavor of the method used, the solution is finally represented as a linear combination of certain basis functions. The parameters that generate different solutions are the coefficients of that combination. Hence, we state that the trajectory $\boldsymbol{q}(t)$ in (1.4.7) can be written as a combination of a set of functions $\boldsymbol{\theta}_i \in \boldsymbol{\Theta}$, and thus we can generate an approximation $\boldsymbol{q}(t) \simeq \tilde{\boldsymbol{q}}(t) = \sum_{i=1}^{N_\theta} a_i \boldsymbol{\theta}_i(t)$. Applying the differential operator $\mathcal{D}$ to this approximation we obtain,

$$\begin{aligned} \mathcal{D}(\tilde{\boldsymbol{q}}(t)) = \sum_{i=1}^{N_\theta} a_i L(\boldsymbol{\theta}_i(t)) + f\left(\sum_{i=1}^{N_\theta} a_i \boldsymbol{\theta}_i(t)\right) = \tilde{\boldsymbol{u}}(t), \\ g_k(\sum_{i=1}^{N_\theta} a_i \boldsymbol{\theta}_i(t), \sum_{i=1}^{N_\theta} a_i \dot{\boldsymbol{\theta}}_i(t), \ldots, t_k) = 0. \end{aligned} \tag{1.4.27}$$

Without more details about the operator $\mathcal{D}$ and the functions g_k, little else can be said. Nevertheless, it should be observed that if the inputs are given, the problem reduces to finding the parameters a_i that will make all the equalities true. Obviously, this is not always possible and in general we will obtain only approximated solutions. On the other hand, if the inputs are not given, but the task is specified by the functions g_k, the coefficients will be completely determined from the solution of the task and is equivalent to solving an interpolation problem. Mathematically, any basis $\boldsymbol{\Theta}$ of the corresponding functional space would be suitable to generate solutions. However, we are concerned not only with the mathematical problem but also with its application to robotics. If problem (1.4.27) has to be solved numerically by a machine, we would like to endow it with a generative rule for the set $\boldsymbol{\Theta}$, rather that with a priori definitions. That is, we desire that our machine is able to build the set $\boldsymbol{\Theta}$ from its experience.

Part I

Locomotion

Chapter 2

The role of *resonance*

> It seems that perfection is only attained not when there is nothing left to add, but when there is nothing left to take away.
>
> Antoine de Saint-Exupéry

Can we exploit the properties of a physical system to produce the desired behavior? Though the word "exploit" has an intelligible connotation, the details of its concrete meaning make a world of difference. The problem of concretizing this question is harder than what one may think at first glance, and there have been several attempts in the field of embodied artificial intelligence; none conclusive or complete enough to satisfy our demands for quantification. Most of the time, the interpretation of "exploiting the system's properties" is aligned with the notion of *cheap design*, characterized in Pfeifer and Scheier (1999).

One of the most appealing interpretations of this phrase, is the one that states that the properties are exploited when the observed natural behavior of a system and the desired behavior are very similar. That is, the desired behavior of the system is obtained almost directly from its construction, without requiring much external intervention. Recalling the discussion in section 1.1, a behavior is a set of measurable output signals. Hence, the dissimilarity between two behaviors can be evaluated in terms of signal measures, i.e. scalar values that quatify how different the two signals are. For example, for scalar signals we could subtract them and evaluate the integral of the square of the result.

The natural behavior of a system is the one observed when the inputs are all zero or can be neglected (we will come back to this in section 4.1). Moreover, if the desired behavior is obtained without applying inputs, we say that our agent is exploiting its physical properties, as was hinted at in the previous paragraph. Although in real agents it will rarely be possible to achieve the desired behavior in a completely effortless manner it is important to assess that, in the absence of inputs, we can produce a behavior *resembling* the desired one. In this way, we believe that the amount of energy and computation required for the control of our robots can be reduced, or that it can be rerouted to solve more complicated tasks and not just fundamental ones, as for example, basic locomotion. This is condensed in the (controversial) phrase "outsourcing parts of the computation to the physical body"(see Hauser et al., 2012, for an attempt of formalization)[1]. The cost of this reduction is ported to the design of the machine, with the hope that it will pay off during its lifetime.

The idea of including the desired behavior in the design of a machine emerged naturally

[1] However, this very interesting article lacks connections to the Church-Turing-Deutsch principle and other recent works in the field of computation, e.g. Siegelmann and Fishman (1998); Buescu et al. (2011)

in science and engineering. The iconic examples are centrifugal governors (patented around 1788) that were used to regulate the flow of a fluid in a tube. These very specialized devices, control the speed of the flow to a set-point value defined by their mechanical parameters. To vary the set-point, we must change parameters like lengths, masses, reductions of gear boxes or compliance of elastics; not very different from tuning a piano. Other examples from engineering are *autobalancing* tools built to passively minimize the oscillations of unbalanced rotating devices. Autobalancing machines appeared in the 18th century, but their effective use had to wait for better assembling technology (Adolfsson, 1997, and references therein).

During the 1990s similar devices stepped into robotics marching along with the passive dynamic walkers (McGeer, 1990). Influential work on stable running machines with simple controllers was already present at the time (Raibert et al., 1983; Thompson and Raibert, 1989). However, McGeer identified the existence of stable walking without active control, he writes (my italics):

> "There exists a class of two-legged machines for which walking is a *natural dynamic mode*"(McGeer, 1990).

Since then, the idea of building robots that *encoded* the desired locomotion patterns in their dynamics and their interaction with the environment (their ecological niche), rooted in the field of robotics and artificial intelligence.

By that time, the study of biological agents had already revealed the important role of mechanical properties in the behavior of animals. Tendons and muscles play the role of springs that can be used to orchestrate the exchange of kinetic and potential energy (in biology, however, it is difficult to separate active from passive elements). In this regard, *resonance* plays a central role in locomotion as a mechanism to use energy efficiently (Alexander, 1990; Dickinson et al., 2000; Ahlborn and Blake, 2002; Biewener and Daley, 2007; Cavagna and Legramandi, 2009; Kokshenev, 2010; Roberts and Azizi, 2011). The existence of a characteristic time scale, the *resonant frequency*, is again related to the idea that the motion itself is encoded in the morphology of the individual and its interactions. The phenomenon extends to other behaviors related to locomotion, such as breathing and thermal control. There is evidence that resonance-like phenomena are present in the control of airflow in humans, guinea pigs, panting in dogs (Mead, 1960; Crawford, 1962) and in pigeons (as cited in Vogel, 2009). Breathing at the *resonant frequency* of the respiratory system would accomplish the dual aim of maximizing flow and minimizing the work required from the respiratory muscles. However it is still under study whether this actually improves either locomotor or respiratory performance (Nassar et al., 2001, and references therein).

Due to similarities between running and swimming (Bejan and Marden, 2006; Kokshenev, 2010), it is not surprising (but not less exciting) that efficient locomotion in fluids was reported to rely on the dynamics of the body of the animal. Living trouts have been observed to exploit the energy in the flow they inhabit to reduce their swimming efforts (see Liao, 2007, for a review). Later, euthanized trouts performed natural self-propulsion when placed in the von Kármán vortex street shed by an obstacle in a flow. Therefore, it is believed that a flexible body offers the possibility of extracting energy from the environment, as shown in the technological study presented in (Allen and Smits, 2001) as well as in experiments performed on artificial platforms and with animals (Ahlborn et al., 1997; Deng and Avadhanula, 2005; Lauder et al., 2007; Epps et al., 2009). The experimental results are accompanied with mathematical models, analytical and numerical. Theoretical studies such as Cheng et al. (1998) and McMillen and Holmes (2006) focus on viscoelastic models of the body, while Eldredge (2009); Kanso (2009) and Kanso and Newton (2009) deal with the body-fluid interaction and the emergence of locomotion. In Shukla and Eldredge (2007); Eldredge and Pisani (2008)

and Alben (2009) the main interest is to understand how passive thrust is generated in vortex wakes, a question that remains open. These models do not fully agree with each other, however this is expected due to the mathematical complexity of the interaction between structures and fluids, of which the unforced case is the worst scenario: un-prescribed motion[2] of the interface boundary. This alone represents an open challenge for the mathematical modeling community. Lest the challenge remains unsolved for too long, robotic researchers design their machines with less fluid-dynamic rigor, pursuing the first *passive dynamic swimmer*. The final objective is to build a swimming machine that can perform at least as well as fish, and at comparable power ratings (Harper et al., 1997; Lauder et al., 2007). In this regard, fins as a tool for locomotion offer several appealing properties compared to propellers. From an environmental point of view, fins reduce sound pollution characteristic of propellers (Richardson et al., 1995). These aspects are of primary relevance in situations where low environmental impact and mimicry are important, as in pipes maintenance routine, or for underwater life observation. Moreover, in environments where moving parts may be clogged up due to fouling, rotatory propellers may be unfeasible for locomotion.

Readers conversant with the modeling of biological agents may have noticed that most of the systems mentioned in the previous paragraphs are nonlinear. Additionally, the words resonance, resonant frequency and natural mode were printed in italics. There is an important reason for this: we do not enjoy definitions of resonance, resonant frequency or natural mode (normal mode) for nonlinear systems. Citing Jürgen Appell et al. (2004),

> ... one could be somewhat pessimistic by stating that we do not yet have a reasonable definition of the terms "spectrum" and "eigenvalue" for nonlinear operators. All we can do ... is to choose carefully a spectrum which has at least some of the needed features.

Nevertheless, applications force us to deal with nonlinear phenomena and some useful methodologies have been developed. Among the simplest ones is the linearity plot analysis. This methodology is based on the idea that under periodic forcing, a system will behave periodically with the same frequency of the forcing (i.e. harmonic balance method). Resonance frequencies are then associated with maxima of the amplitude of the response, which is just a working definition (and probably misleading), since these so called nonlinear resonant frequencies share few or none of the algebraic properties of resonant frequencies of linear systems. In general terms, these nonlinear frequencies depend not only on the amplitude of the response (or amplitude of the forcing) but also in the particular waveform of the forcing function, i.e. its frequency spectrum. That is, the values of resonant frequencies, and how many are there, depend on the way we force the system (see Goge et al., 2005, for detailed discussions).

In this chapter we focus on understanding the behavior of our devices as functions of their physical parameters. The methodologies presented here are by no means complete but they aim to introduce a more quantitative flavor to the analysis and design of robots that are expected to "exploit" the physical properties of their bodies in their behavior.

2.1 Adapting parameters

A *parameter* is a magnitude (representing a physical property of our system or not) that is usually considered constant during the execution of a behavior. In contrast, *variables* do change during the behavior. Indeed, it is the structure of these changes what defines the behavior.

[2] Where the subsequent state of motion is determined based on the state at the current time.

We tend to consider certain magnitudes as constants due to how we build machines, e.g. the elasticity of a spring, the mass of a link, the capacitance of a capacitor or the length of a string. The more our building technology develops (new materials and building methods), the more magnitudes that can be controlled actively. The way we build is far from similar to the way natural agents are assembled. Nature's factories can assemble materials on the molecular scale and parts are rarely isolated. Nevertheless there are general principles of construction that we can learn from observation and then reproduce them in our devices (Vogel, 2003).

From a pure modeling perspective, parameters and variables are quite related. We could call parameter to any variable that changes slowly enough (relative to the system under study, as was remarked in Section 1.1) and that can be regarded as constant during the time interval of interest, e.g. we care very little about the change of length of our arms while we play tennis. Similarly, we could construct a parameter from the average of a fluctuating variable, taking into account the amplitude as well as the frequency content of the fluctuations, e.g. natural fluctuations of the concentration of oxygen in air are not relevant while we go jogging. As soon as these changes match any characteristic of our system, be it in amplitude or time scale, the magnitudes affected may not be considered parameters anymore and the description of their changes has to be included in our model, i.e. they become variables in a new model. Yet another possibility is that a magnitude remains constant for a very long time (i.e. we would call it parameter), but it suddenly suffers a considerable change. We model the damage of a machine in this way, e.g. a burned resistor or a fractured elastic element. In control and robotics, the design for coping with sudden changes in parameters has some history (Åström and Wittenmark, 1994; Sastry and Bodson, 1994), recently it can also be found in the work of Bongard (2011), focused mainly on heuristics methods.

When we build, we typically set the value of parameters based on static considerations (as stress or durability) or by the "5 oscillating digits" criterion, i.e. intuition based on experience. This selection also depends on the technology available and the knowledge we have about the consequence of variations of those magnitudes. In whatever way they are selected, they are defined at construction time and the controllers for the machine are later optimized based on them. That is, the platform is assumed to be given, and the controller is adapted to optimize behavior. Here a perspective swap is proposed: the controller is given and the only option to optimize behavior is the adaptation of parameters, i.e. the modification of the plant. Without a too much effort, we can imagine the following design cycle:

1. Initial values for parameters based on technology, knowledge and resources.
2. Construction of the device.
3. Optimization of controller based on behavior performance.
4. Optimization of parameters based on behavior performance.
5. Go back to 2 until requirements are fulfilled.

which is just another variation of many standard design cycles. For examples, see the first chapter of Ljung (1999) or related design cycles from the multidisciplinary area of Industrial design (Roozenburg and Eekels, 1995).

In biological agents, adaptation of the body parameters (or morphology) happens, at least, at two different time scales: during the lifetime of the individual through development and interactions with the environment[3], and in an evolutionary time scale due to mutation

[3]The changes of parameters due to damage of the individual are included in this time scale.

and selection. Adaptation of the controller, so to say, is readily visible in the learning of new skills or in coping with unexpected situations. Hence, we could think that nature runs the cycle just described in parallel and ad infinitum (though step 5 is controversial, since nature may not have requirements to fulfill as was mentioned at the beginning of section 1).

We could think that the design cycle is just adding the system's properties to the optimization of the controller. Synthetic approaches of this kind have been attempted in the past (popularized in Sims, 1994a,b, and continued until now). However, in most of these cases the physical reality of the models is not considered (simulation with low order integrators, unrealistic force generation, etc.) and validation is omitted. Moreover optimization is done blindly, using genetic algorithms and other heuristic methods which may be suitable to develop an application, but hardly acceptable for basic research searching for understanding underlying simplification principles, i.e. depending on the goals of the research activity. The comprehension of results, the explanation of the relations between the found parameters and the behavior, is left unfinished and represents an extremely hard reverse engineering task (Hauert et al., 2009, presents related work in evolved controllers only), and may not be the best strategy for such an objective. We could use this approach in simple situations where reverse engineering is feasible, or we could design experiments with increasing complexity to understand the role of the parameters. The former approach requires simple models that capture the essence of the observed behavior and the latter, experimental platforms whose parameters can be tuned systematically[4].

The following sections contain three case studies, two of them with experimental counterparts. In the Zürihopper example (section 2.4.1) we will show the effects on behavior due to the change of the pressure inside a pneumatic spring and its potential advantages for hopping. The results give the basis for the design of an actuator (pump and valve) to change pressure dynamically during hopping. There is evidence that humans and other animals have similar mechanisms to adapt to surfaces with changing mechanical properties (Farley et al., 1993; Farley, 1996; Ferris and Farley, 1997; Farley et al., 1998; Ferris et al., 1998; Moritz and Farley, 2003), although cockroaches apparently use another strategy (Spence et al., 2010). We encounter a similar situation in the WandaX case study (section 2.4.2) where we try to establish a link between the stiffness of the joints of an artificial fish and the observations of swimming trouts harvesting environmental energy (Liao et al., 2003; Beal et al., 2006).

As discussed in section 1.4, one of the most striking behaviors that is directly related to the physical properties of a device is the existence of resonances. This topic will be central in the forthcoming presentation, therefore a short recapitulation of the concepts is provided for the non-physicists. The specialist can read through these sections rapidly.

2.2 *Linear resonances and normal modes

One possible motivation for the calculation of normal modes is depicted in Figure 2.1. The question is as follows: Is it possible to transform a system of coupled linear systems into an equivalent set of uncoupled linear systems?
Another possible motivation is to ask whether we can understand the motion of complex systems nearby an equilibrium point. If the dynamics of the system are smooth enough, we can linearize the system at the equilibrium point. In this way, we obtain a set of coupled linear equations describing the motion on the coordinates we used to describe the dynamics. Therefore, we come back to our first question: can we decouple these equations?

[4] I call these experimental platforms *parametric robots*, and the methodology does not differ to much from the practice of experimental disciplines, e.g physics and chemistry.

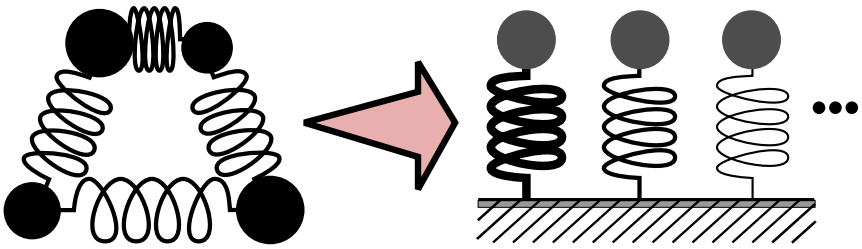

Figure 2.1: Decoupling systems of linear equations. Can the mesh of masses and springs be written as separated independent mass-spring systems?

In oder to present a succinct description of the procedure we start with a system that has already been linearized around the equilibrium position and we discuss the decoupling procedure. The whole methodology is extensively treated in most (if not all) books on mechanical engineering and classical mechanics (in physics, the historical name for the method is "small oscillations"), the classical source being the book of Goldstein et al. (2002); mathematically oriented readers may prefer Arnold (1989) where the topic is treated with rigor. Conceptual approaches can be found in the electronic book "Classical Mechanics" by Joel Shapiro or in many of the tutorials that are available on the Internet.

To start, note that the dynamics of each oscillator (the j-th) shown in the right panel of Fig. 2.1 is written

$$\ddot{n}_j + \lambda_j n_j = 0. \tag{2.2.1}$$

Where the deformation of each oscillator is denoted with n_j and the stiffness of the corresponding spring with λ_j. The dynamics of the system in the left panel are of the form

$$M\ddot{\boldsymbol{x}} + K\boldsymbol{x} = 0, \tag{2.2.2}$$

where M is a diagonal matrix with positive elements (the mass matrix, representing the mass of each oscillator in the left panel of the Fig. 2.1) and the vector $\boldsymbol{x}$ describes the displacement of each mass. By comparing the previous two dynamical systems, we see that the transformation from $\boldsymbol{x}$ to $\boldsymbol{n}$, must diagonalize K and turn M into the identity. This problem is know as simultaneous diagonalization or generalized eigenvalue problem, since we must solve $K\boldsymbol{v}_j = \omega_j^2 M\boldsymbol{v}_j$. The linearly independent vectors $\boldsymbol{v}$ are called eigenvectors of K relative to M. Details about this problem will be omitted since they are presented in all the mentioned books, and standard freely accessible numerical routines can be used to solve it[5].

Once the eigenvectors are found, general solutions of (2.2.2) can be written as linear combination of these vectors modulated with a phase evolution of frequency ω_j. That is,

$$\boldsymbol{x}(t) = V\left(C \circ e^{-i\boldsymbol{w}t}\right)V^T \tag{2.2.3}$$

where $C \in \mathbb{R}^{n\times 1}$ is a column vector of weights, $e^{-i\boldsymbol{\omega}t} = \left[e^{-i\omega_1 t}, e^{-i\omega_2 t}, \dots e^{-i\omega_n t}\right]^T$ contains the temporal evolution ($\circ$ stands for element-wise multiplication or Hadamard product) and V has each $\boldsymbol{v}_j$ as columns. In other words, for each time step the general solution is a linear mixture of the eigenvectors of K relative to M, also known as *normal modes*. Therefore, any arbitrary initial condition of the system can be represented with a unique vector of weights C, since V and $\boldsymbol{w}$ are defined by the matrices of the system. In other words, the morphology of the system, the masses represented by M and the springs mesh represented by K define the normal modes; the observed behavior is just a mixture of these. In linear systems the

[5]For example the function `eig` in GNU Octave 3.4.3 or later

normal modes are intrisinic natural motions that are usueful to explain any other observed behavior.

The main message of the previous paragraph is that once we know the normal modes of a system, any behavior can be encoded with the adequate mixture. Single modes are exited when the initial condition makes zero all but one of the coefficients in C. As can be seen from the mixture (2.2.3), if only one mode was used, time evolution will not distribute energy to other modes and they will remain inactive. The decomposition is even valid in the presence of an external stimuli and normal modes are a fundamental tool to understand the response of the system (this type of analysis is usually called "modal analysis").

Related to normal modes is the idea of resonance of a linear system. The frequency at which the amplitude of the oscillations of a system reaches a maximum is called a resonance frequency. For linear systems, resonances occur close to the frequencies of the normal modes. Additionally, a linear system can be recovered if we have full knowledge of its resonance frequencies, and estimation is possible if only a subset is known, i.e. a linear system is defined by its resonant frequencies. The concept of resonance is usually generalized to the case when an observable (e.g. the amplitude of oscillations, concentration of the product of a chemical reaction, detection level of defects in a production process, etc.) reaches a maximum when measured as a function of a property of input signals, e.g. their spectrum frequency. However in some of those cases, the so called resonances may not have the algebraic properties of resonance frequencies as described before, the name being just a metaphor. For example, "stochastic resonance" when restricted to certain systems can be considered a proper resonance even without defining an equivalent notion for the normal modes, but if we generalize it its formal meaning is lost (Douglass et al., 1993; Gammaitoni et al., 1995; Moss, 2004; McDonnell et al., 2009).

The response of a linear system as a function of the frequency content of the input can be calculated using the Fourier transform directly on the equations defining the dynamics of the system. The result is termed "Frequency Response Function" (FRF) and describes the frequency content of the output of the system for the given input. The FRF of a linear system does not depend on the intensity of the input and if the system is time invariant it does not change over time. Additionally, since the response of linear systems will have the same frequencies as the input, the FRF does not depend on the particular shape of the spectrum of the input signal[6]. Concluding, the FRF is a characteristic of a linear system, not of the particular input used to obtain it. Linear systems can be directly described by their response function (as is common in the fields of control and signal analysis).

Normal modes and frequency response functions, are tightly related in the case of linear systems and they are alternative representations of the system itself. However, because nonlinear systems can exhibit extremely complex behaviors which linear systems cannot, these representations are not generally available. Nonlinear phenomena include jumps, bifurcations, saturation, hysteresis, subharmonics, supraharmonics, internal resonances, resonance captures, limit cycles and chaos. In the next section we discuss the case of nonlinear systems, where most of the useful features of normal models and response functions are generally lost.

2.3 Nonlinear resonances and normal modes

As anticipated, the concept of normal modes and frequency response functions (FRF) are not so easy to define for nonlinear systems as it is for linear ones. In the current dark forest of nonlinear systems, we see flashes of light coming from theoretical developments aiming to

[6] In the experimental case, if there is a frequency (or frequency interval) that is not present in the input it will not be present in the output and the FRF of the system at this frequency(interval) can not be calculated.

extend these notions. However, as far as we know, there is no concept or tool that gathers all the properties of the linear case. Herein two approaches are briefly described, the first focuses on a description for nonlinear systems that can be used in a way similar to the FRF of linear systems. The second method is an attempt to extend the concept of normal modes to nonlinear systems. The descriptions are given as a review of potentially useful methodologies for researchers in the fields of embodied artificial intelligence and bioinspired robotics, where nonlinearities in the body are exploited to generate purposeful behavior.

2.3.1 Nonlinear Output Frequency Response Functions

As we discussed in the preceding section, at resonance, the frequency of an exciting force matches the natural frequency of the system causing the amplitude of vibration to become significant. Although resonance of linear systems is well understood and that resonance-like phenomena have been observed in nonlinear systems, there are no equivalent concepts of resonances and resonance frequencies for nonlinear systems. The most striking property of nonlinear system is that the frequency spectrum of the input is distributed in the spectrum of the output, therefore, even at steady state, the outputs are often richer in frequency content. Typical phenomena is the generation of supraharmonics (frequencies in the output higher then in the input), intermodulations (frequencies between the ones in the input) and the spreading of narrow band inputs. With the aim of filling the gap, nonlinear output frequency response functions (NOFRF) are defined. NOFRFs are one-dimensional functions of frequency, which allow the analysis of nonlinear systems similarly to the analysis of linear systems, however the calculations are considerably more involved and are based on the Volterra series expansion of a nonlinear dynamical system (Lang and Billings, 2005; Peng et al., 2007). The method has successfully been used to understand some characteristics of nonlinear systems, specially for polynomial nonlinearities, establishing analytical relationships between the observed outputs and the parameters of the system (Lang et al., 2007).

The idea of the method is to represent the frequency response as a linear composition of the contributions of the responses of nonlinearities of increasing degree. As can be anticipated this is perfectly suitable for polynomial nonlinearities and the general case is treated in terms of the approximation of the original system by its Volterra series. Hence, the method is applicable only to systems that accept such series (Schetzen, 1980). Currently, the method is defined for systems that under no forcing relax to an equilibrium point, however it is possible to extend it to systems that relax to a limit cycle. The output of the method are a set of one-dimensional plots, each one for each degree of nonlinearity[7] that can be interpreted similarly to frequency response functions of linear systems.

Of particular interest for robotics and locomotion is to understand how a source, generating energy in a particular range of the frequency spectrum, can be used to excite oscillations with radically different frequencies. In other words, it is ultimately useful to assess to what extent morphology can help to extract energy to be used in a purposeful manner, i.e. the body as a transducer: taking energy in one region of the spectrum and making it available at another. Understanding how to tune or entrain nonlinear systems to un-prescribed energy sources may be the key to achieving efficient locomotion in general environments. It must be noted that this is a particular instance of nonlinear energy harvesting (Cottone et al., 2009, 2011).

[7] GNU Octave code to apply the method to measured or simulated signals has been released by the author of this thesis under GPLv3 license and can be found at http://ailab.ifi.uzh.ch/images/stories/people/carbajal/NonLinearFrequencyResponse_1010.zip

2.3.2 Nonlinear Normal Modes

To extend the idea of normal modes to nonlinear systems the original Nonlinear Normal Modes method (NNMs) (Rosenberg, 1966) was revised by Vakakis et al. and Kerschen et al.. The method recovers behaviors of the system where all degrees of freedom evolve in time with the same temporal modulation; a property of linear normal modes as seen in equation (2.2.3). Though repetitively used in structural analysis, NNMs have two important limitations compared to their linear counterparts (Kerschen et al., 2009):

1. Invariance is lost: In the linear case, if motion is initiated on one specific mode, the remaining modes remain inactive for all times. In the nonlinear case this is not generally true, however, a circumvention of this drawback can be found in Pescheck (2002).

2. Can not be superimposed: in the linear case free and forced oscillations can conveniently be expressed as linear combinations of the motion of individual modes. Though the behavior of the nonlinear normal modes can be interpreted in a physical sense (source of the usefulness of the method), the motion of the system is not a linear superposition of these modes.

After these observations, the name of the methodology seems inapposite, and probably "nonlinear synchronous oscillations" would be more suitable. Nevertheless, these particular behaviors of a nonlinear system are useful to understand some basic properties of its dynamics. In particular, they are useful to design energy exchangers for mechanical systems with applications to vibration mitigation or excitation(Vakakis et al., 2009). It is this last point that may be of interest for robotics, since if a locomotion mode is characterized by a frequency of oscillation of the degrees of freedom of the robot, maximizing the energy transfered to that mode would optimize locomotion.

With all this information in mind, it is a good idea to review the systems described in the introduction in relation to the statements about resonances. It is also a good opportunity to pause a moment to consider the quote from McGeer. Hopefully the reader will realize that, in the context of nonlinear systems, statements of this kind should be considered purely colloquial and speculative, nonetheless motivating.

2.4 Case studies

In the following sections, results obtained with three parametric robotic platforms are presented. Some of these results have been published (Benker, 2009; Carbajal and Kuppuswamy, 2010; Ziegler et al., 2011), others still await the grace of the reviewers (Carbajal et al., 2011). These robots were built to test if adaptation of physical parameters could be effectively used in robots to improve their performance in hopping and energy efficient swimming.

The following list summarizes the results:

- **Zürihopper**: The relation between pressure on a pneumatic piston and hopping behavior is quantified experimentally. A leg stiffness adaptation strategy is proposed. A mathematical model of the system is provided and validated against the behavior of the robot without actuation.

- **WandaX**: A mathematical model of the joints of the parametric robotic fish is given and validated against force measurements. The model is used to approximate the dynamics of the joint with the Düffing oscillator. Results from the harmonic balance method are used to define a strategy to adapt the stiffness of the joint to cope with changes in the frequencies of an external forcing.

- **MagE**: A model for the magnetic fish is provided and its behavior analyzed. The tight relation between magnetic and mechanical properties allows us to control the frequency contents of the response of the tail. Discussions about its use for the simplification of control are provided.

All mathematical models presented in the subsequent sections were developed specifically for study of the corresponding parametric robot.

2.4.1 The Zürihopper

Zürihopper (Benker, 2009) is a 1D hopping robot, it was built to study how to tune leg stiffness to compensate for changes in the supporting surface, very much aligned with the work of Ferris and Farley (1997), where it was observed that humans compensate changes of surface elasticity by tuning the effective compliance of their legs. The robot uses the impulse generated by an oscillating mass to jump vertically. The stiffness of the ground that supports the robot can be set to a wide range of values. By changing the elasticity of the ground and sweeping the frequency of the oscillations of the mass we can detect maxima of the jump height. By repeating this procedure for different leg stiffnesses we arrive at a plausible strategy to adapt the body parameter in order to keep the jumping height around a maximum value when the ground stiffness changes. That is, we keep the overall behavior performance by adapting morphological properties of the leg of the hopper.

Platform description

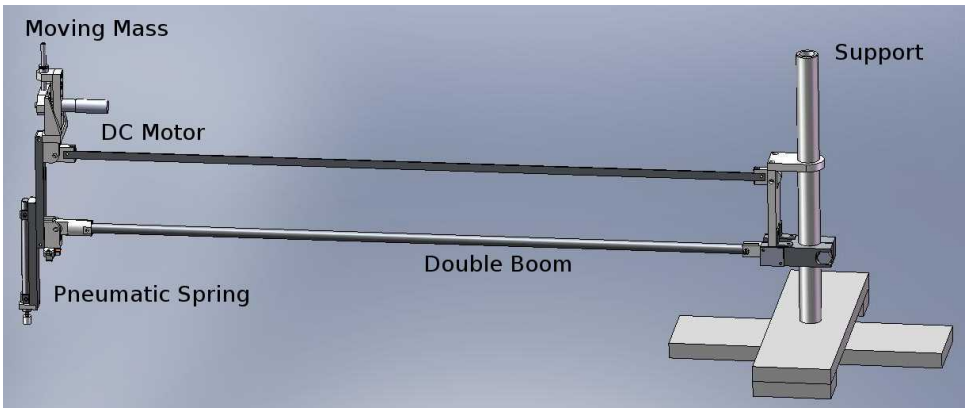

Figure 2.2: CAD of the Zürihopper. The double boom constrains the motion to the vertical direction. The pneumatic spring acting as the leg, is actuated via a moving mass connected to a DC motor.

Figure 2.2 shows a CAD file of the platform. On the left, at the end of the double boom, a pneumatic spring is connected. On top of the pneumatic spring there is a mass connected to a DC motor. The rotatory motion of the motor is converted to linear motion using a Scotch yoke[8]. The motor moves the mass up and down, and provides the energy to the hopper. The double boom guarantees that the motion of the hopper is almost vertical, the longer the boom the more vertical the motion. We used a 1 m boom , which allows a

[8] A rotating part, connected to the shaft of the motor, slides within a slot that is rigidly connected to a piston, i.e. the mass. The shape of the motion of the piston is a pure sine wave over time given a constant rotational speed. See Fig.2.3 C).

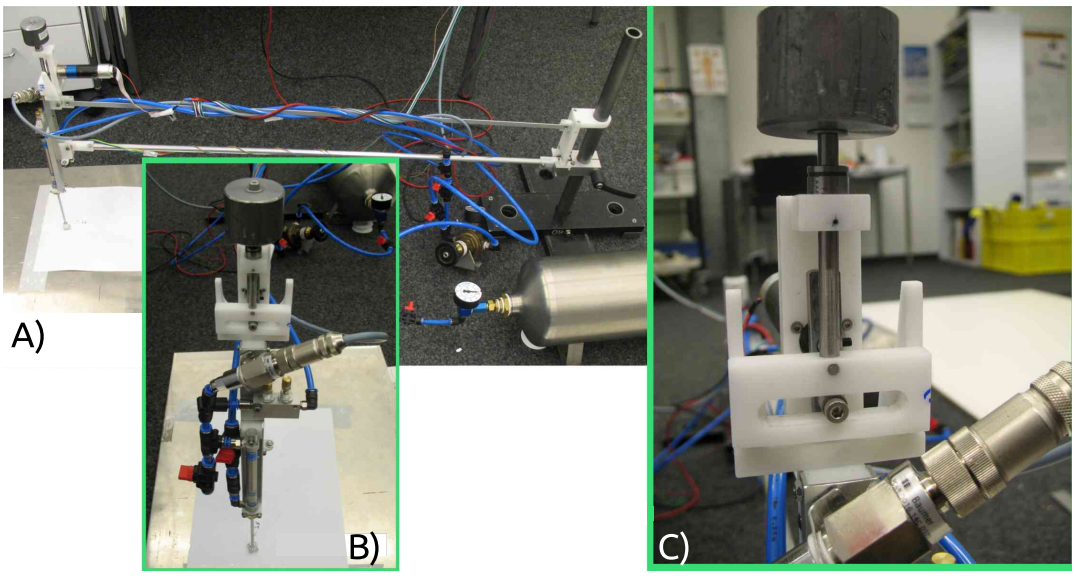

Figure 2.3: Three views of the Zürihopper. **A)** Side view: the complete set up. Boom and motor are visible. **B)** Front view: the pneumatic circuit. **C)** Detailed view: Scotch yoke. The metal pin slides sideways in horizontal slot while it follows a circular trajectory parallel to the plane of the picture.

maximal horizontal displacement of 1.3 mm. In Figure 2.3 three views of the real platform are shown. The platform has two sensors, a pressure sensor inside the pneumatic spring and a distance sensor (measuring the deformation of the leg) pointing downwards, towards the foot, as shown in diagram in Figure 2.4. The pressure on the spring, which is related to the stiffness of the leg, was not dynamically controlled but set to a given value at the beginning of each experiment. The angular velocity of the motor was set using a National Instrument DAQCard-6036E. The measurements from the pressure and the distance sensors were acquired with the same card.

To control the stiffness of the ground where the hopper bounced we used a double supported thin metallic beam. The beam has one extreme fixed and a sliding condition on the other. The longer the distance between the two supports the lower the stiffness of the ground were the Zürihopper lands. The effective elastic constant of the ground at the middle point (where the robot bounced) is proportional to the inverse cube of the distance between the supports, i.e. $K_g \propto L^{-3}$ derived from the simply supported beam with load at midspan (equation 1.42 of Kelly, 2000). Next, we present the mathematical model used to understand some of the behavior described in section 2.4.1. These details are not necessary to understand the results conceptually and the non-technical reader is free to skip forward.

*Mathematical model

There are two main aspects to model, the net force acting on the piston and the mechanics of the motion of the different parts of the hopper. The system is hybrid since there are two types of collisions to consider: foot-ground and piston-cylinder. Looking at the diagram in Fig. 2.4 we see that we have two masses (piston plus foot and cylindrical housing) coupled by the gas in the chambers. Taking z (height of piston) and d (height of cylinder base) as

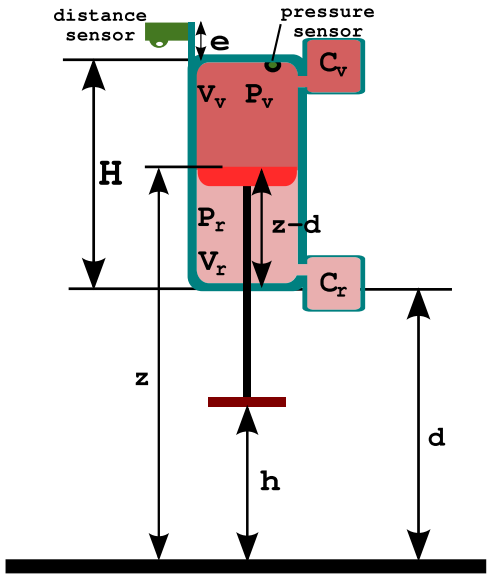

Figure 2.4: Diagram of the setup. Two chambers are separated by a piston. Each chamber is connected to an additional chamber that does not changes volume during the motion. The position of the sensors are also shown in the diagram.

our generalized coordinates, the equations of motion are,

$$\ddot{z} = \frac{F(z-d) + F_v(\dot{z} - \dot{d})}{m} - g, \tag{2.4.1}$$

$$\ddot{d} = \frac{F_v(\dot{d} - \dot{z}) - F(z-d)}{M} - g. \tag{2.4.2}$$

Where $F(x)$ is the net force acting on the piston and $F_v(\dot{x}) = k\dot{x}$ is a dissipative force modeling energy losses, g is the acceleration due to gravity. The mass of the cylinder (and the moving mass) is M and the mass of the foot and piston is denoted with m. The net force on the piston is generated by the compression of the air inside the cylinder. We assume that the hopping process does not change the temperature of the gas and that the flow is much faster than the motion of the piston, the net force can thus be estimated using the ideal gas law,

$$PV = \text{constant}. \tag{2.4.3}$$

Where P is the pressure of the chamber and V its volume at the beginning of the motion. Using the notation of Figure 2.4 we calculate the force acting on the piston in terms of all the parameters and as a function of the piston displacement $x = z - d$,

$$F(x) = \frac{A_v P_{v0}(A_r x_0 + C_r)}{A_r(A_r x + C_r)} - \frac{P_{v0}(A_v(H - x_0) + C_v)}{A_v(H - x) + C_v}. \tag{2.4.4}$$

Where A_i indicates the area of the piston facing the respective chamber. P_{v0} is the initial value of pressure, set when the system is at the rest position x_0. The constants C_i are volumes of the chambers connected to the cylinder and do not change during the motion. We have used the fact that at equilibrium $A_r P_r = A_v P_v$. The selection of signs is such that, when the force is positive the piston is pushed up and pressed down when it is negative. Equation

(2.4.4) shows that the force is proportional to the initial pressure P_{v0}. Later, we will study how changes of this parameter alter the behavior of the hopper, and how it can be exploited. Notice that other physical parameters of the Zürihopper could be used to adapt the force response of its leg (spring curve). The volumes C_v and C_r produce interesting modifications of the spring curve (Benker, 2009). These parameters could be modified utilizing an actuated piston inside the respective chamber. The piston displacement x is limited to the range $x \in (0, H)$. For the simulations, these limits where implemented as elastic collisions between the piston and the cylinder. Additionally, while the foot is in contact with the ground, it is fixed, i.e. equation 2.4.2 is zero. The condition for takeoff is $F = 0$ and $\dot{F} > 0$.

Towards the validation of the model, simulations were compared with experimental data coming from three independent drop tests, i.e. we lifted the Zürihopper 10 cm from the ground and let it fall. Table 2.1 summarizes the values of the parameters. The results of the comparison are shown in Figure 2.5. The initial pressure parameter was adjusted[9] to improve the predictive quality of the model. Additionally, the damping parameter k was not measured directly and its value is known in the simulated case only, i.e. we obtain an estimated value by fitting the simulations. However we cannot make a strict correspondence with a property of the physical device, since the physical damping might not be linear in the velocity as we are assuming here.

Table 2.1: Parameters for the drop tests. The first column corresponds to measured values of the experimental platform. The second one shows parameters values used in the simulation.

Symbol	Zürihopper	Model
P_{v0}	0.20 ± 0.04 MPa	0.205 MPa
k	??	6Ns/m
M	0.950 ± 0.001 kg	
m	10 ± 1 g	
A_r	66.00 ± 0.04 mm^2	
A_v	78.50 ± 0.04 mm^2	
C_r	188.40 ± 0.06 mm^3	
C_v	1067.60 ± 0.06 mm^3	
H	90.00 ± 0.02 mm	
e	32.00 ± 0.02 mm	
x_0	1.00 ± 0.02 mm	

Despite the strong simplifications made to arrive at equation (2.4.4), the matching between the simulated drop test and the measured one is remarkable. Increasing the mass of the cylinder improves the fitting, however we had no reasons to believe that our mass measurements were biased, therefore we show the results using the measured value given in the table. Simplified models of this kind can accelerate the design process or the search for interesting behaviors in a complex robot. In chapter 3 a similar model is used to adjust the spring curve to maximize jumping height of a nonlinear monoped under periodic forcing.

Experimental Results

We started collecting data with a setup with constant ground stiffness. We measured the amplitude of the changes in the distance and the pressure sensor for different values of frequency and pressure P_{v0}. A typical result is shown in Figure 2.6 ($P_{v0} = 2.58$ bar), the

[9] By minimizing the square error of the prediction

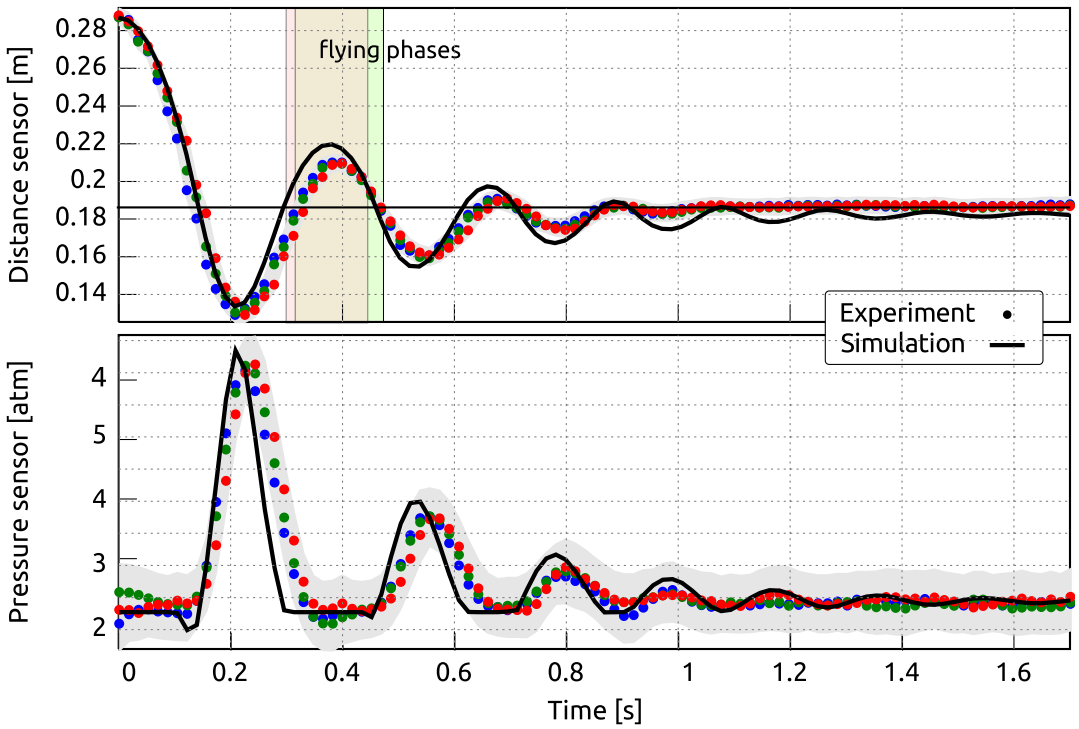

Figure 2.5: Validation of the model in drop tests. Experimental and simulated data are shown. Dots represent experimental data for several tests, solid line corresponds to the results of the simulation. Shaded areas represent uncertainty in the measurement of the experimental values due to sensor fluctuations.

signals from both sensors are normalized to highlight their similarities and the maximum values are given in the legend box. The reader should keep in mind that the values in the plot represent amplitudes of oscillations, averaged over many jumps of the Zürihopper. When the pressure P_{v0} is increased (i.e. stiffening the leg) the peaks move to higher frequencies. The nonlinear nature of the setup is made evident by a particular characteristic visible in the plot: a hysteresis-like phenomena, i.e. the frequency at which the Zürihopper starts jumping depends on the direction of change of the frequency. In Fig. 2.6 we indicated the direction of change of the frequency with black arrows.

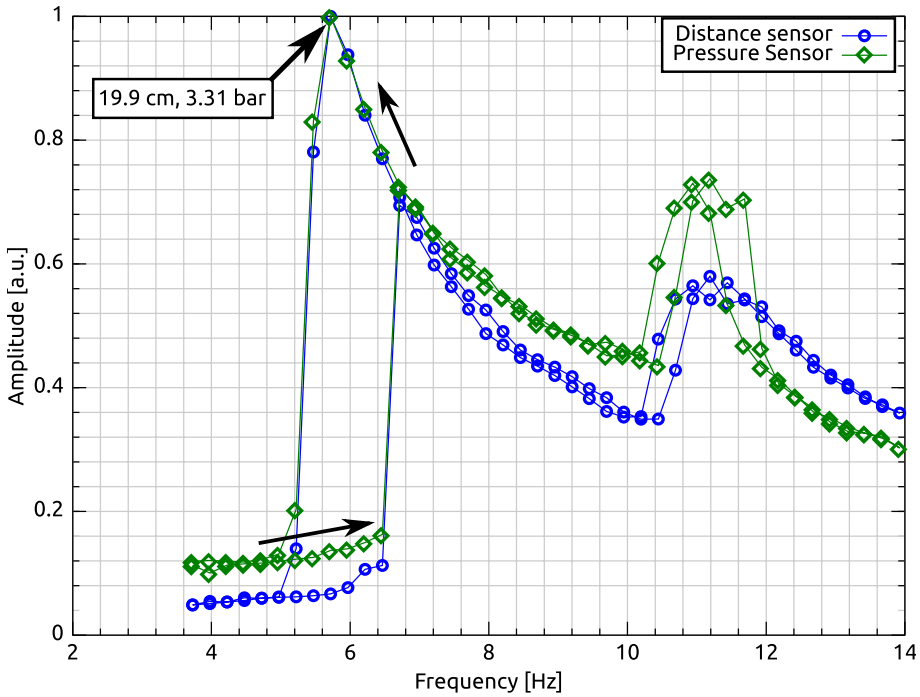

Figure 2.6: Sensor amplitude as a function of frequency. The amplitude of the pressure and distance sensor are shown as a function of the frequency of the oscillating mass. The nonlinear nature of the Zürihopper is reflected in the observed hysteresis-like phenomenon and the presence of peaks at different frequencies. The arrows indicate the direction of change of the frequency.

Figure 2.7 shows the relation between the frequency of the first maximum and the pressure P_{v0}. The dots correspond to the values obtained from measurements and the solid line is a lmse fit of a quadratic polynomial of pressure as a function of frequency (resembling the mechanical relation $f \propto \sqrt{K}$). This allows us to establish a conceptual link between the pressure P_{v0} and the frequency at which the hopper jumps, or loosely speaking, the resonance frequency of the Zürihopper.

In the second phase of the experiment, the previous measurement process (i.e. peaks in amplitude of oscillations versus P_{v0}) was repeated for three values of ground stiffness, or equivalently, three values of separation L between the supports of the metal beam used as ground. The shorter L the stiffer the ground. The results are shown in Figure 2.8. The plot shows the line of maxima of the jumping amplitude in the (f, P_{v0}) plane, each line corresponding to a different ground.

Collecting all the information provided by the experiments, allows us to devise an adaptation strategy for the leg stiffness K_L (or pressure P_{v0}) that compensates for changes in the

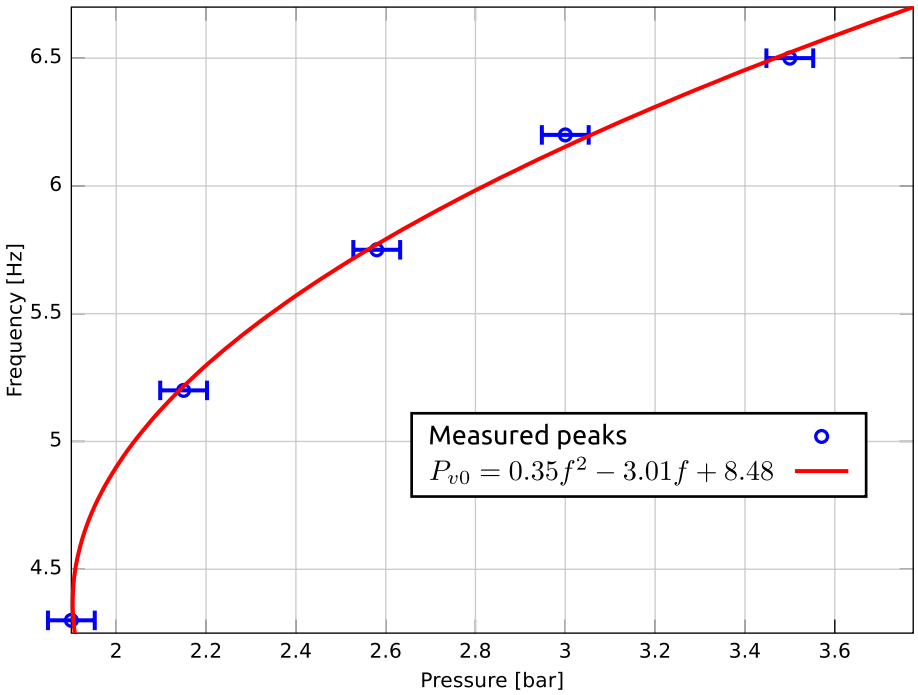

Figure 2.7: Leg stiffening. The frequency at which the jumps achieve a maximum amplitude increases with increasing pressure P_{v0}. The dots corresponds to data obtained from plots similar to 2.6 for different values of pressure. The solid line corresponds to a fitting polynomial of second degree.

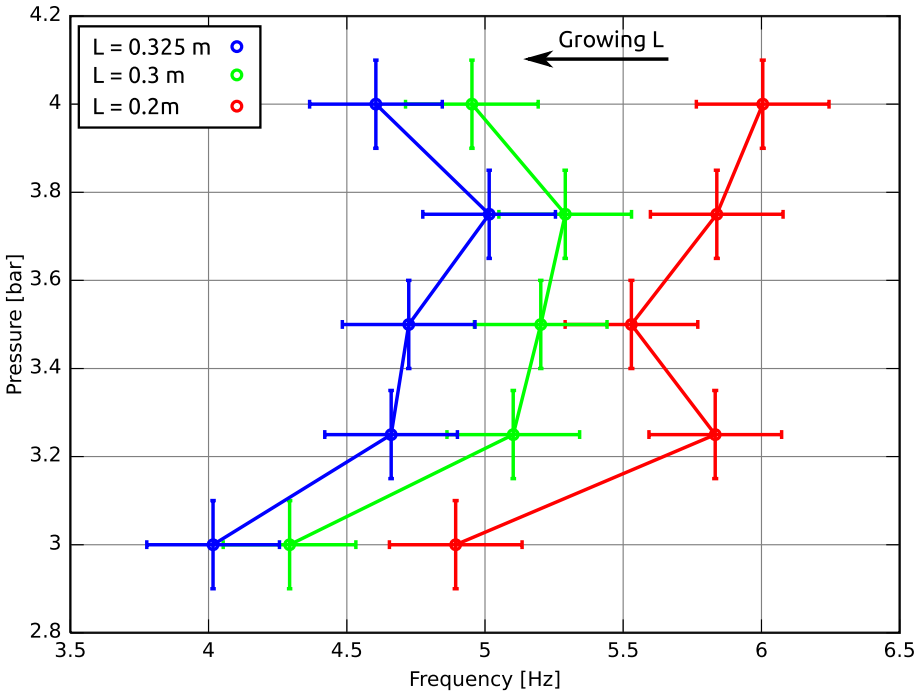

Figure 2.8: Lines of maximum amplitude. The lines of maximum jumping amplitude for different ground stiffnesses are shown in the (f, P_{v0}) plane.

ground stiffness without modifying the frequency of the forcing provided by the moving mass. This strategy is depicted in Figure 2.9. There we show the lines of maxima of the jumping height in the (f, K_L) plane, for three different ground stiffnesses K_g. While the Zürihopper is jumping using a frequency f_R, the ground stiffness is increased. Reduction of the leg stiffness is required to put the system back again in a line of maxima without changing the frequency.

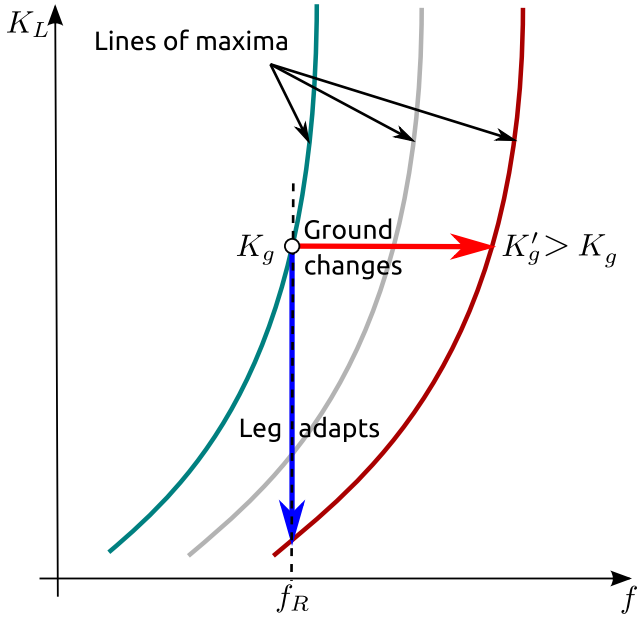

Figure 2.9: Leg stiffness (K_L) adaptation strategy. Under changes in the ground stiffness the leg properties must be adapted if the frequency of oscillation is to remain constant.

2.4.2 WandaX

The robot WandaX was built to study the role of tail fin and body stiffness in swimmers. The usual approach to this kind of studies consist in building a flexible body made of some rubbery material. One problem with such approaches is that for each test a new robot must be built, rendering the systematic study of the elastic properties extremely costly (in time, human resources and money) and error prone. Modularity can speed up this process, but it does not alleviate the difficulty to set, with controlled uncertainty, the nonlinear properties of rubbery materials. With these drawbacks in mind, WandaX was designed in a modular way, a chain of rigid segments connected between each other by means of a precisely tunable elastic revolute joint. The elastic joints are made with linear springs and to tune them, the tension (that can be measured accurately) of the spring is varied. The same chain structure was used in Ziegler et al. (2011) with the aim of learning control strategies that maximized thrust. Nevertheless, in that study we did not report the natural behavior of each segment and its response to periodic forcing (generated by fluid-structure interactions). This is the scope of the current section.

In Figure 2.10a we see the details of the joints. Each joint behaves as a rotational spring. The restoring torque is generated when the relative angle between the two connected bodies is not zero. The force producing the torque is given by the extension of a linear spring fixed to the first body. The spring is connected via an inelastic thread to an appendage of the

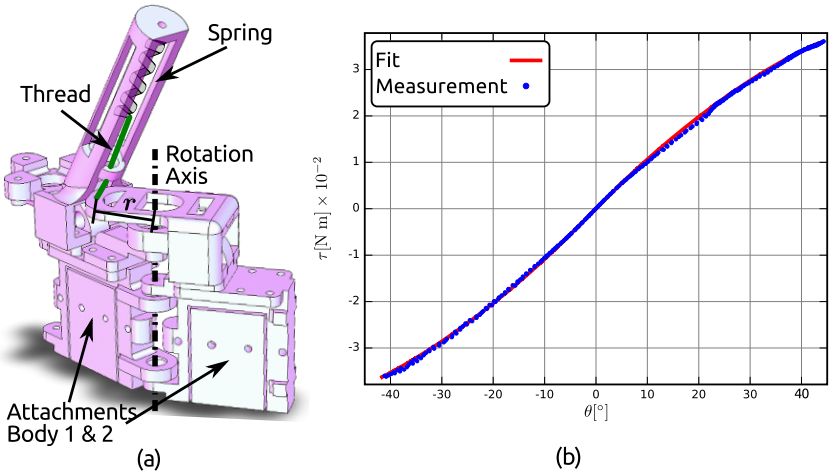

Figure 2.10: Description of the joints in WandaX. **a)** Details of the joints used in (Ziegler et al., 2011), note the axis of rotation and the appendage. **b)** Measured torques applied to the joint under controlled deflection. Replacing the parameters given in Table 2.2 into Eq. (2.4.5) the fit provides $F = 0.73 \pm 0.05$ N.

second body. When the deflection angle is zero, the extension of the spring is minimum as well as the force it exerts. We call this minimum force value *tension* and it is referred to with the letter F. Measurements of the torque for $F = 0.73$ N, are given in Figure 2.10b. The values of the parameters used throughout this section are given in Table 2.2. The two parameters r, d are distances that can be seen in the figures (r is the lever of the spring force aplpied to the rotating segment). The elastic constant of the linear spring is K and I denotes the moment of inertia of the joint around the axis of rotation. The linear specific damping coefficient of the joint is denoted with ζ. The parameters $\mathcal{Q}_0$ and Ω correspond to the amplitude and frequency of the external forcing, respectively.

Table 2.2: Value of the parameters used here and in the model studied in (Ziegler et al., 2011) .

Name	Value
r	20.24 ± 0.02 mm
d	27.68 ± 0.02 mm
K	81 ± 1 N/m
I	$(3.1 \pm 0.1) \times 10^{-5}$ kg $\cdot$ m^2
$\zeta \cdot I$	$(2.2 \pm 0.1) \times 10^{-4}$ N $\cdot$ m $\cdot$ s
$\mathcal{Q}_0 \cdot I$	1×10^{-4} N $\cdot$ m
$\Omega/2\pi$	$(0, 3]$ Hz

*Mathematical model

A geometrical representation of the joint is given in Figure 2.11. The parameters r,d and K are fixed at construction time and always $d > r$ (Table 2.2). The tension in the spring at its shortest length (F), is the controlled parameter and a servomotor can change it dynamically.

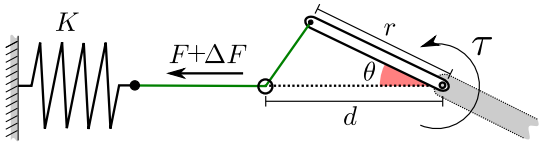

Figure 2.11: Schematic of the rotational spring used to derive Eq. (2.4.5).

The torque applied to the bodies connected to the joint is thus,

$$\tau = \frac{K\left(\sqrt{\epsilon^2 + 4S\sin^2\frac{\theta}{2}} - \epsilon\right) + F}{\sqrt{\epsilon^2 + 4S\sin^2\frac{\theta}{2}}} S\sin\theta. \tag{2.4.5}$$

Where we have defined the parameters $\epsilon = d - r$ and $S = rd$. The formula is obtained by calculating the deformation of the spring as a function of the deflection angle of the appendage (θ). The deformation is inside the parenthesis in the numerator of equation (2.4.5) and when multiplied by the stiffness K, it gives the force due to the deformation of the linear spring. The outer factors come from the product of the force and the moment arm. Note that the torque τ is linear in the controlled input F.

For $\theta \ll 1$ the third order Taylor expansion gives

$$\tau(\theta, F) = \kappa(F)\theta + \alpha(F)\theta^3 + \mathcal{O}(\theta^5). \tag{2.4.6}$$

Where

$$\kappa(F) = \frac{SF}{\epsilon}, \tag{2.4.7}$$

$$\alpha(F) = \frac{SF}{\epsilon}\left[\frac{S}{2\epsilon^2}\left(\frac{\epsilon K}{F} - 1\right) - \frac{1}{6}\right]. \tag{2.4.8}$$

And the equation of motion of the deflection angle is

$$\begin{aligned} \ddot{\theta} + \zeta\dot{\theta} + \frac{\tau(\theta, F)}{I} &\approx \\ \ddot{\theta} + \zeta\dot{\theta} + k(F)\theta + a(F)\theta^3 &= \Gamma. \end{aligned} \tag{2.4.9}$$

Where I denotes the moment of inertia around the axis of rotation. The specific damping is given by ζ, and we have defined $k = \kappa/I$, $a = \alpha/I$. Γ is the specific net effect of all other external torques acting on the joint. The approximating equation of motion is the well studied Düffing's equation.

To quantify the error introduced by the approximation, we calculated the angle at which the difference between the torque produced by equation (2.4.5) and equation (2.4.6) is equal to a reference error given by $\Delta\tau = r\Delta F$, where $\Delta F = 0.05$ N is a reasonable resolution for a force sensor working in a 10 N range. These angles are plotted in Figure 2.12 for different values of the tension.

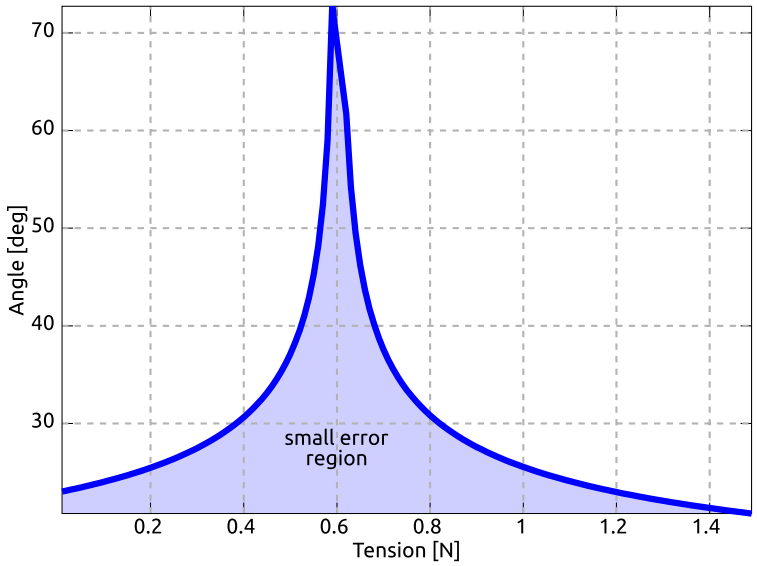

Figure 2.12: Approximation error. Values of the deflection of the joint for which the error reaches the reference value given in the text. The maximum deflection has a peak close to $F_3 = (5.90 \pm 0.01) \times 10^{-1}$ N meaning that terms of degree > 3 almost cancel each other.

Hardening, linear and softening spring

As can be seen from equation (2.4.6), $\alpha(F)$ modulates the intensity of the cubic nonlinear term. This term vanishes when the tension in the spring is

$$F = F_* = \frac{\epsilon K}{\frac{\epsilon^2}{3S} + 1}. \tag{2.4.10}$$

rendering a linear spring for the angles where the third order approximation is valid. Using the values in table 2.2 we obtain $F_* = (5.83 \pm 0.07) \times 10^{-1}$ N. For bigger values of F the spring will be softening ($\alpha < 0$) and for smaller values it will be a hardening spring ($\alpha > 0$) (Fig. 2.13). However, the full expression of the torque (Eq. (2.4.5)) contains higher order terms. Hence, the linear behavior will be even more evident if terms of higher degree cancel each other (as was for F_3 in Fig. 2.12). In Figure 2.13 curves of torque versus angle for several values of F are shown. In particular we show the curve for which up to seventh order nonlinearities give a minimum contribution ($F_0 = (5.30 \pm 0.07) \times 10^{-1}$ N)[10] together with the curve at $F = F_*$. This illustrates the power of the actuation chosen, since we can control the dynamical properties of a virtual rotational spring in the joint (more details in Ziegler et al. (2011)).

Forcing model

As explained before, the external torques acting on the joint are due to fluid-structure interaction. This kind of interaction still poses a great challenge for the mathematical modeling community. In the search for simplified models of the forces generated in the interaction

[10]This value was obtained by minimizing the sum of the squared terms of degree 3, 5 and 7 of a seventh order Taylor expansion of (2.4.5)

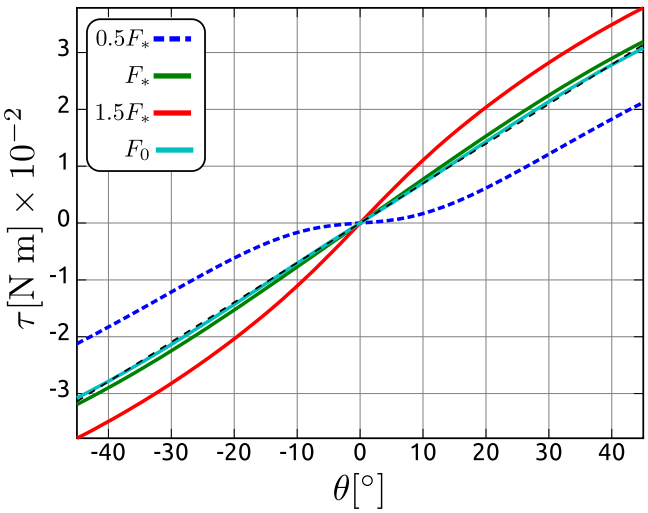

Figure 2.13: Plots of the torque function for values of tension $F = [0.5,\ 1,\ 0.9,\ 1.5] \cdot F_*$. Note the hardening behavior for small tension and softening behavior for higher tension. Almost linear curves are found for $F = F_*$ and $F = F_0$, as a reference the linear curve is shown.

between flexible bodies and turbulent flows, we found the work of (Kanso and Newton, 2009) and (Alben, 2009) instructive. Using equation (3.8) given by Alben, we can calculate the pressure difference on the boundary of a slender body in a vortex street. If the width of the body is bigger than the separation among vortices and it is placed in the middle of the vortex street, the forces on the body can be approximated by a sine function $f(t) = f_0 \sin(\Omega t + \phi)$, where t is time and ϕ is an initial offset that sets the balance between the sine and cosine behavior of the forcing. The frequency Ω is proportional to the speed of the flow plus the vorticity of the vortices (assumed to be equal for each vortex) scaled by a factor that depends on the geometrical properties of the wake. The amplitude f_0 is proportional to the density of the fluid and the square of the vorticity of each vortex. With a few additional assumptions, the torque acting on the joint can be made proportional to this force. Here we adopt this over-simplified forcing model to avoid diverting the attention of the reader from the core ideas of our work. In this manner we postpone a detailed study with a more elaborated forcing model.

Harmonic solutions of Düffing's equation

Under periodic forcing $\Gamma = \mathcal{Q}_0 \sin(\Omega t)$, equation (2.4.9) has been extensively studied (see Holmes and Rand, 1976; Luo, 1997, and references therein). Following these analyses, we show here how to maximize the amplitude of the periodic response of the joint by tuning the tension parameter.

The key point of the analysis in Luo (1997) (based in the Harmonic Balance Method, HBM), is that we search for the amplitude of solutions of (2.4.9) that are periodic (this rules out sub-harmonics, supra-harmonics and chaotic motion), $\theta(t) = A \sin(\Omega t + \psi)$. Under this assumption it can be shown that the amplitude A of such solutions is given by the roots of

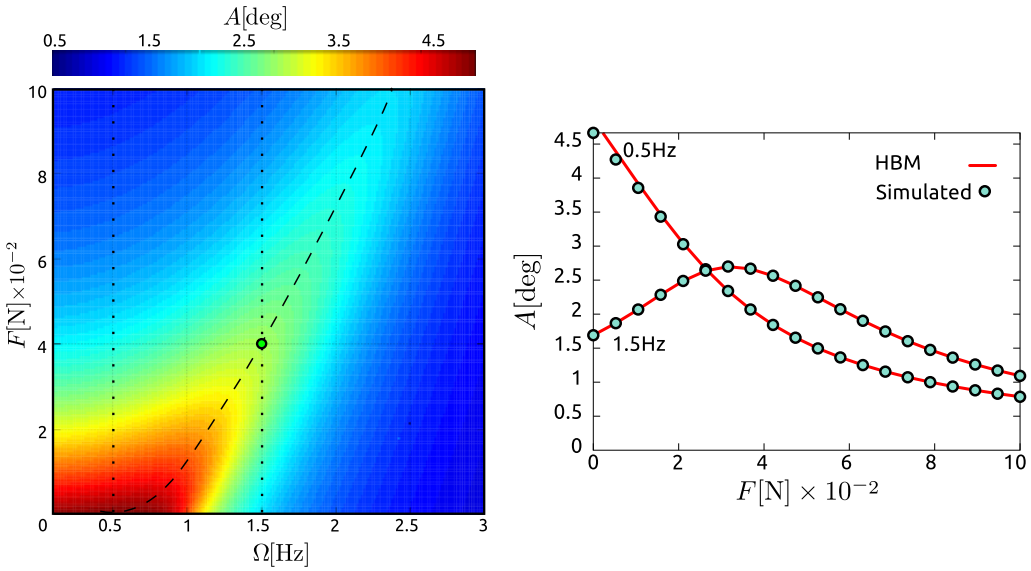

(a) (b)

Figure 2.14: Amplitude of periodic response in the plane (F, Ω). (a) shows the amplitude of the oscillations according to Eq. (2.4.11). The line of maxima is marked with dashes. The vertical dotted lines indicate a potential working configuration. (b) shows in solid lines the amplitude along the two dotted vertical lines in fig. (a). The circles represent the amplitude obtanied from simulations without any approximation, i.e. using eq. (2.4.5) directly.

the polynomial,

$$A^3 \frac{9a^2}{16} + A^2 \frac{3\left(k - \Omega^2\right) a}{2} + A\left[\left(\Omega^2 + \zeta^2 - 2k\right)\Omega^2 + k^2\right] - \mathcal{Q}_0^2 = 0. \tag{2.4.11}$$

The roots of this polynomial can be obtained analytically using a computer algebra system like Maxima and they establish the relation between the amplitude of the oscillations and the parameters of the equation, $A\left(k, a, \Omega, \mathcal{Q}_0\right)$. In the case at hand, we have $k(F)$ and $a(F)$, therefore $A\left(F, \Omega, \mathcal{Q}_0\right)$. For a given value of the parameters, only one root corresponds to the observed amplitude (there are unstable amplitudes). This implies, that is not enough to look at the roots, but we must also check their stability. This adds complexity to the evaluation of the results in addition to the limitation to pure harmonic inputs.

Figure 2.14a shows the amplitude of periodic oscillations in the (F, Ω) plane, according to Eq. (2.4.11). The line of maxima is shown with dashes. This line describes the value of the tension that produces maximum amplitude for a given forcing frequency, and is conceptually linked to the results showed in Fig. 2.7 for the Zürihopper. To compare with the observed amplitude (obtained by simulating and oscillator without any approximation), we extracted the curves of amplitude against tension for $\Omega/2\pi = 0.5, 1.5$ Hz (vertical dotted lines in Fig. 2.14a). These curves at 1.5 Hz frequency are shown in Figure 2.14b, the model predicts the simulated amplitude accurately. At 0.5 Hz, the amplitude predicted by Eq. (2.4.11) drifts away from the simulated value for lower tensions. In Carbajal et al. (2011) we compared this classical method with a more general methodology based on the Volterra series expansion, revealing a trade-off between flexibility and accuracy of the calculation.

Altogether, we have described another concrete example where the parameters of a device could be adapted to achieve the desired behavior. Once again, we remark the shift in perspective that this implies, i.e. instead of controlling the forcing of the system (which in this example it is just impossible) we look to adapt what clasically is considered a parameter of the device. In the case where the forcing can be controlled, our approach can be used to complement the optimization of the controller. The WandaX model is linear with respect to the controlled value F, hence there is little complication if it is slowly changed. However in the general case, rapidly varying values could produce complicated dynamic responses. If the elasticity of the joints is arbitrarily changed (as in the motorized version of WandaX) rather than parameters, they become inputs in a new model.

2.4.3 MagE

MagE models a swimming robot composed of a hull and a fin attached to it. We worked on the design of this robot (Carbajal and Kuppuswamy, 2010) with the aim of increasing the efficiency of swimming by means of exploiting magneto-mechanical resonances. The technology required to build a prototype turned to be too expensive for our budget, therefore we studied only simplified mathematical models. The general idea explored in this case is the variation of the interaction between magnets (by means of coils, or a battery of magnets) to produce stable and unstable oscillations in the fin of the robot.

The fin of MagE was modeled as an elastic beam (see Cheng et al., 1998; McMillen and Holmes, 2006, for detailed models), which is set into oscillatory motion. In the setup shown in Fig. 2.15, we chose to support the beam at two points. The first support is at one edge of the beam and stands for the hull of the robot. The second support is placed at some intermediate point of the beam. The section of the beam beyond this second support is meant to generate swimming thrust by interacting with the surrounding fluid. The actuation is applied in the section of the beam between the two supports using a combination of permanent magnets (one of them attached to the beam) and solenoids. In the configuration chosen, the permanent magnets serve to increase the compliance of the magnet-beam system and to reduce the force that needs to be actively applied by the solenoid. The distance between the supports defines the rigidity of the actuated section and could be tuned for optimal energy transfer. Similar working principles are described in patents of electric razors, and of active dampers of oscillations for digital cameras lenses (in these contexts the actuator is often called *motor* or *electromagnetic spring*). Similarly, the control of the resonant modes of a structure is a commonplace problem in structural dynamics Vakakis et al. (2009). Noting, however, that all those techniques exploit or require knowledge of the resonant modes of the system under study, a daunting task in a nonlinear scenario.

*Mathematical Model

The displacement of the magnet in the fin (we will refer to this point as the *fin magnet*), can be modeled by a spring-mass system under the effect of an external force field. Considering only one dimensional motion, the system is written as,

$$\begin{aligned} \dot{x} &= v \\ \dot{v} &= \frac{F_2(x) + F_1(x) + F_{s1}(x) + F_{s2}(x)}{m} - \frac{\mathcal{K}}{m}x - \frac{\Gamma}{m}v, \end{aligned} \tag{2.4.12}$$

where x is the displacement of the fin magnet, m is an effective moving mass, $\mathcal{K}$ represents an effective elastic constant of the fin setup and Γ is used to include dissipation. The F_i

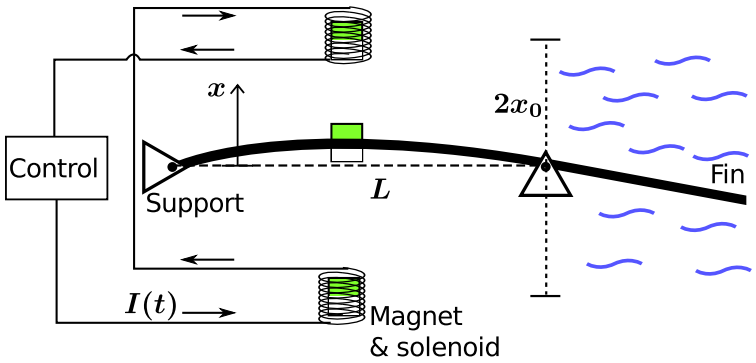

Figure 2.15: Schematic of the system described by equations (2.4.12). A beam is used to model the fin and it is simply supported at two points. The actuation is done by means of a combination of permanent magnets and solenoids. The distance between the supports defines the rigidity of the actuated section.

and F_{si} terms are forces acting on the fin due to the external magnets and the solenoids, respectively.

Magnetic forces can be highly complex; to keep our model as simple as possible we approximate each magnet as a point magnetic dipole, which is a good approximation when the distances are significantly bigger than the size of the magnet in the direction of the magnetization (Vokoun et al., 2009). In this situation the force can be expressed as follows,

$$F_i(x) = -\frac{\mathcal{C}_i}{(x - x_i)^\alpha}\,\mathrm{sign}(x - x_i), \tag{2.4.13}$$

where $\mathcal{C}_i$ is a constant that depends on the magnetic moments of the magnets and their geometry, positive values represent attractive forces and negative values repulsive forces. When solenoids are present, this constant depends also on the current, i.e. $\mathcal{C}_{si}(I) = C_{si}I(t)$ (the subindex s refers to solenoid). The position of the external magnet (or solenoid) measured from the rest position of the fin magnet is x_i. Henceforth we define $k = {}^{\mathcal{K}}/_{m}$, $\gamma = {}^{\Gamma}/_{m}$, $c_i = {}^{\mathcal{C}_i}/_{m}$ and $c_{si} = {}^{C_{si}}/_{m}$. Additionally, we assume that the deflected fin does not reach the external magnets, in mathematical terms this is expressed as $x \in (x_1, x_2)$.

Next we study the dynamics of the system without actuation, $I(t) \equiv 0$. The expression for the fixed points x^* is obtained by equating system (2.4.12) to zero. The second equation yields

$$c_2\,(x^* - x_1)^\alpha - c_1\,(x^* - x_2)^\alpha - kx^*\,[(x^* - x_1)\,(x^* - x_2)]^\alpha = 0, \tag{2.4.14}$$

where the assumption $x \in (x_1, x_2)$ was used to determine the signs.

***Linear Stability Analysis.** To classify the fixed points, we calculate the trace and determinant of the 2×2 Jacobian matrix J of (2.4.12). These are given by

$$\mathrm{Tr}(J) = -\gamma \tag{2.4.15}$$

$$\mathrm{Det}(J) = k + \alpha\left[\frac{c_2}{(x - x_2)^{\alpha+1}} - \frac{c_1}{(x - x_1)^{\alpha+1}}\right]. \tag{2.4.16}$$

In general the fixed points of the system will be saddle-nodes, centers or spirals, depending on the value of the parameters γ, k, c_i and x_i. However, the position of the fixed points (i.e. the solutions of (2.4.14)) is independent of γ.

To proceed with the analysis we introduce further assumptions. The exponent α depends on the arrangement of magnets (Vokoun et al., 2009). Here we will consider identical cylindrical magnets placed symmetrically with respect to the rest position of the fin magnet and with dipoles parallel to it (attracting); hence $\alpha = 4$, $c_1 = c_2 = c > 0$ and $x_2 = -x_1 = x_0 > 0$. By neglecting dissipation, i.e. $\gamma = 0$, we set the trace of the Jacobian to zero. Consequently, the fixed points are either saddle-nodes or centers, depending on the sign of (2.4.16). Using these assumptions to simplify the equality (2.4.14) we obtain,

$$x^* \left[8cx_0 \left(x^{*2} + x_0^2 \right) - k \left(x^{*2} - x_0^2 \right)^4 \right] = 0, \tag{2.4.17}$$

rendering evident that $x^* = 0$ is one of the fixed points, in agreement with the symmetry of the problem. The determinant (2.4.16) at this point is,

$$\mathrm{Det}(J)|_{x^*=0} = k - 8\frac{c}{x_0^5}, \tag{2.4.18}$$

which is positive for $c/k < x_0^5/8$, and the origin is a center. Although any real system will not show centers without actuation (due to dissipation) their position will match the pole of the spirals observed.

It can be shown that the nonzero solutions of (2.4.17) are saddle-nodes. Displacements beyond the saddle-nodes will bring the fin magnet into a region where the attraction is stronger than the elastic restitution, causing the fin to stick to the closest magnet. The saddles establish a natural limit for the maximal amplitude of the orbits of the system. To illustrate these ideas, we show in Fig. 2.16 three plots of the polynomial defined by (2.4.17) for different values of the ratio c/k, together with phase portraits of the system. The figure depicts the trade-off between the rigidity of the fin and the interaction of the fin magnet and the permanent magnets. Keeping x_0 fixed, the stronger the magnets (or the more compliant the fin), the smaller the region where the system can present stable orbits. At the critical ratio $c/k = x_0^5/8$, the saddle-nodes collide at the origin and the center is transformed into a saddle-node.

Phase space and time series.

Numerical results for the undamped system are presented in Fig. 2.17. We take three initial conditions on the region of the phase space to study. All the initial conditions start with zero velocity, i.e. they lie on the horizontal axis. It is important to note that the time series of the fin displacement clearly show different frequencies. This is due to the attraction of the magnets, the higher the initial displacement the lower the frequency of the orbit. These results are shown in detail in Fig. 2.18. For each initial condition we plot the power spectrum of the signal and it is visible how the main component decreases at higher amplitudes.

The offset of the oscillations corresponds to the position of the center. By breaking the symmetry of the system, either by setting $c_1 \neq c_2$ or by feeding constant current to the solenoids, we can move the center off the origin. This could be required for turning maneuvers or useful for initiating oscillations. In Fig. 2.19 we show how the center and the saddles move for different values of c_1 and c_2 (or increasing current).

2.5 Chapter summary

In this chapter we have toured around the idea of tuning the parameters of a model to adapt its behavior to our needs. The parameters in a model are many times, but not necessarily,

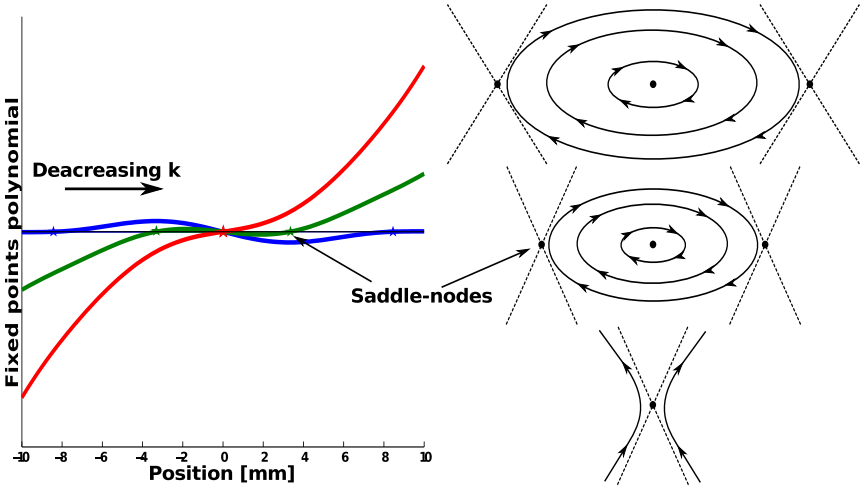

Figure 2.16: Plot of the polynomial defined in (2.4.17) for different values of c/k. The star symbols mark the position of the fixed points. The phase portraits to the right show that the saddle-nodes define a limit for the amplitude of the orbits. The figure illustrates the trade-off between the rigidity of the fin and the intensity of the magnetic interaction.

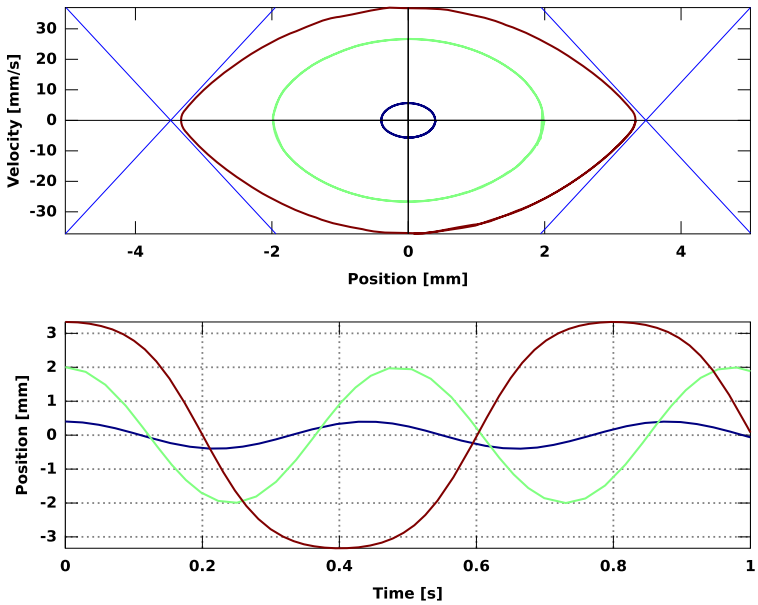

Figure 2.17: Trajectories in phase space and time series for the undamped system starting from three different initial condition. The frequency of the signal decreases with the amplitude due to the interaction of the magnets.

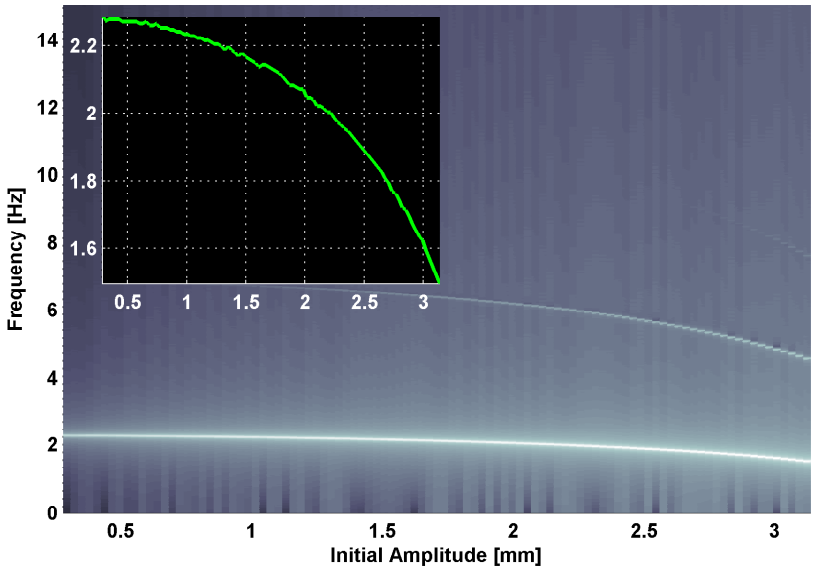

Figure 2.18: Variation of the natural frequency with the amplitude of the oscillations. The power spectrum of the orbits is plotted, brighter color implies higher energy at that frequency. Two characteristic frequencies are observed, note that the relation between them changes with the inital amplitude. The behavior of the main component is shown in detail in the inset.

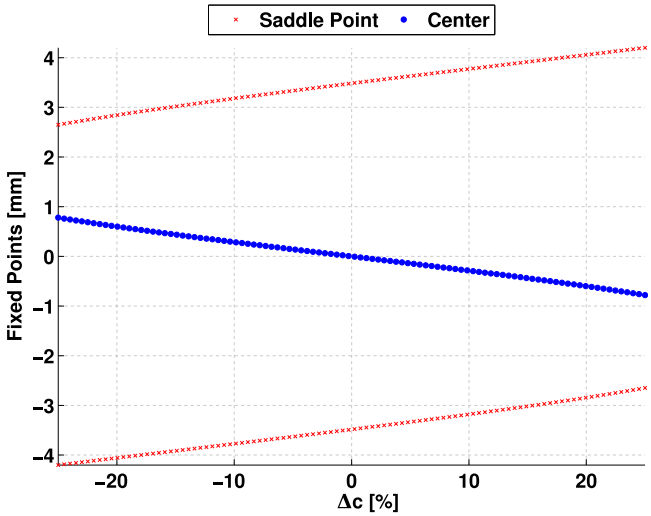

Figure 2.19: Control of the position of the center and saddles. The center moves symmetrically around the origin for differences Δc between the magnetic constants. The maximum amplitude is also compromised, because the saddle on the side of the stronger magnet come closer to the center.

related to the morphology of the system the model represents. Hence, any profit we can get from this adaptation is due to a clever use of the morphology of our device and we can concretely talk about *outsourcing* part of the control task to the body of the robot. Similar

developments have been published, specialy focused on the active control of geometrical parameters to optimize behavior (Potkonjak, 1999; Potkonjak and Vukobratovic, 2000). A quantitative comparision between active and passive adaptation, specially in terms of energy consumption, should be the aim of future research. In the next chapter we present an example in which the passive adaptation of leg parameters considerably increases the efficient utilization of an external energy source.

Though in this chapter we have used rough models, the advantages they provide to understand the role of the parameters is clear.

In the case of **MagE**, the results show that the magneto-mechanical properties of the device could be exploited to generate behavior. Though its design is not necessarily the best to reduce the actuation needed, it presents several options. For example, that the instability of the center can be used to initiate motion by forcing the system through its bifurcation. This could be achieved by on-line modification of the distance between the supports or by bringing the permanent magnets in the hull closer to the tail. Additionally, placing a permanent magnet perpendicular to the plane at the origin could be used to further reduce the frequency of the orbits or to control the offset in a more sensitive way than the one shown here. Furthermore, we saw that if MagE is too flexible, it does not possess orbits without a controller, since the center becomes a saddle point. Such a controller requires very strong actuators to produce oscillations, since it is *forcing* the system to behave unnaturally. Therefore the existence of orbits reduce the effort to produce oscillatory motion. Finally, the model presented here includes only linear dissipation proportional to the velocity and therefore the role of dissipation is marginal. Better models of the fluid dynamics and the bending of the fin will surely bring dissipation into a more primary role in the behavior of the system. In addition, thrust, heat dissipation and energy consumption could be estimated in such multi-physics models.

Zürihopper provided us with empirical results that support the idea of keeping a desired level of performance by adapting body parameters. A model of its dynamics was presented and validated against free fall data and represents a valuable tool to test controllers and parameter changes. The NOFRF method cannot be directly applied in a hybrid dynamical system as the one modeling the Zürihopper, nevertheless, as presented in the next chapter, this model can be approximated by a continuous one. Whether NOFRF will provide a tool for the design of the machine is an open research thread.

The case of **WandaX** represents an ideal opportunity to apply state-of-the-art analysis methodologies for nonlinear systems. Though conceptually related with Zürihopper, the fluid environment of WandaX provides a continuous model for the interaction allowing us to use well developed methodologies for the analysis. Notwithstanding, the mathematical problem is far from simple. Herein we presented the use of the harmonic balance method to develop a strategy that will keep oscillations of the joint to its best under periodic forcing of varying frequency. The natural next step is to analyze a chain composed of several of these joints. NNMs can be a valuable tool for the analysis and design of such systems.

These results represent a shallow scratch in the surface of an iceberg. However, concrete paths were introduced, leading to the quantification of radical and inspiring (though not suffiently precise) ideas currently advocated in the field of embodied intelligence. The methodologies presented are far from complete and many challenges remain open, waiting for the work of motivated researchers. The idea of a robot as an environmental energy harvester requires further development of the NOFRFs to be realized and promises a real enhancement in the autonomy of our robotic devices. McGeer's dream of embedding the desired behaviors in some characteristic modes of motion of the robot remains oniric for the time being. NNMs may represent the only tool we have nowadays to realize the dream, though synchronous oscillations may not be the best suited properties to describe the patterns of motion of loco-

moting devices. To be able to combine synchronous motions into a general motion, we need to find modes that obey some generalized notion of nonlinear superposition.

Nonlinear systems are generally more complicated to understand than linear ones. However the complexity is accompanied by flexibility to accommodate a vast gamma of behaviors and a nontrivial dependence on the parameters that can be exploited. Under this light we should doubt that nature, in its blind non-convergent optimization process, resorts to linearization to tackle difficulties in the control of biological agents. This is highlighted in Chapter 4 where the nonlinearity of a model will be indispensable to solve control problems.

Chapter 3

Tuning a simple hopper

> Harpists spend 90% of their time tuning their harps and 10% playing out of tune.
>
> Igor Fyodorovitch Stravinsky

In this chapter we merge the ideas discussed so far to explore the possibility of tuning a mechanical systems to use available sources of energy to generate behavior. To ease the presentation we take a very simple model, a nonlinear spring-mass system bouncing on a very stiff ground (a 1D hopper). The sources of energy for jumping are the gravitational field and the reaction force acting on the mass of the hopper due to ground contact, as shown in Figure 3.1. In general, the latter force is a reaction to changes in the internal structure of the hopper. In contrast with the model of the Zürihopper, in which the internals were described in some detail (see section 2.4.1), here we will not model the genesis of the reaction force. Due to this simplification, the ultimate source of external actions is the ground and without it (e.g. during flight phase) there is no other external force acting on the mass of the hopper apart from gravity. Consequently, during the flight phase the hopper behaves as a point mass and it cannot affect its own motion, i.e. it is in free fall. This model can be seen as an utterly simplified Zürihopper, a useful model to understand bouncing of the Puppy robot (Buchli et al., 2006) or a toy model of stotting animals. We chose to consider simplified models because the inclusion of additional degrees of freedom makes the phase portrait multi-dimensional and encumbers the presentation. Moreover, the complexity of the model would increase with the inclusion of more degrees of freedom without any further conceptual gain. However, we are aware that (as was the industrial mathematician Thornton Carl Fry, at Bell Telephone Laboratories in 1941) .

> The mathematician also tends to idealize any situation with which he is confronted. His gases are "ideal", his conductors "perfect", his surfaces "smooth". He calls this "getting down to the essentials." The engineer is likely to dub it "ignoring the facts."

Clearly we have to live with these confronted approaches to research. In my view, embodied intelligence has seen many developments of an engineering flavor, focused on "making things work" sometimes overriding nuisances (for the engineering) that may enclose fundamental understanding of the underlying mechanism. The approach taken here is maybe more aligned with that of the mathematician. The attempt is to present the simplest model that captures the phenomenon under study, adding more details would just add more phenomena out of

the scope of the initial question. Reaching this critical point in the complexity of a model is, in my view, the goal of fundamental research; that point in which removing any detail erases the phenomenon. The epigraph by Antoine de Saint-Exupéry at the beginning of chapter 2 is emblematic in this regard.

3.1 Hopper model and approximation

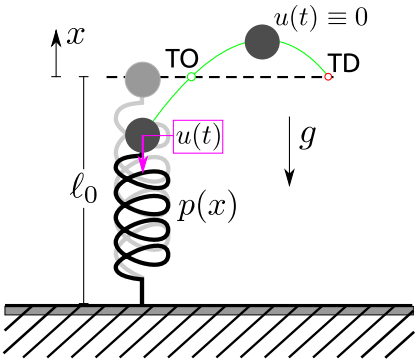

Figure 3.1: Nonlinear hopper. A simple hopper modeled with a nonlinear spring and a point mass. The natural length of the spring (root of the polynomial $p(x)$) defines the event function to switch to free fall. During flight, the hopper cannot exert net forces on its center of mass. When it is in contact with the ground there can be a nonzero external net force $u(t)$.

First, lets define the model concretely, we do this following Figure 3.1. When the hopper is in contact with the ground it obeys the following equations of motion,

$$\begin{aligned} \ddot{x} &= -g + p(x) + u(t) - 2w_0\xi\dot{x}, \\ p(x) &= a_k x^k + \cdots + a_2 x^2 - w_0^2 x. \end{aligned} \tag{3.1.1}$$

Where g is the absolute value of the acceleration due to gravity. The deformation of the spring is x and when $x = 0$ the length of the spring is equal to its natural leg length ℓ_0. When $x < 0$ the spring is compressed. The polynomial $p(x)$ models the force due to the deformation of a nonlinear spring and is always zero when $x = 0$[1]. Furthermore, in the interval $x \in [-\ell_0, 0]$ the polynomial $p(x)$ should be equal to zero only once (i.e. at $x = 0$). Additionally, since the spring can only push the ground, $p(x)$ should be positive in the interval of deformation. Note that all these conditions do not insure that $x = 0$ is the only equilibrium point since the polynomial $p(x) - g$ could have multiple roots. The hopper loses energy proportional to the velocity of the spring deformation, i.e. linear damping with ratio ξ. The reaction due to internal reconfiguration is given by $u(t)$, and to avoid abusing our simplification, it should be kept small with respect to the spring force.

The takeoff and touchdown events are given by $x = 0$, when $x > 0$ the hopper is free falling. In this phase the equation of motion is simply

$$\ddot{x} = -g, \tag{3.1.2}$$

[1]Henceforth we will talk about forces and accelerations indistinctly, either by assuming unit mass or a proper normalization.

it should be clear that we are describing a hybrid dynamical system with a switching function equal to the identity (see section 1.4.4). The system consist of two charts: spring-mass (Eq. (3.1.1)) and free fall (Eq. (3.1.2)).

Some readers may ask why a nonlinear spring is used in the model. It is the case that, in the natural world, nonlinear legs and joints are the rule rather than the exception. Additionally, the usual models of limbs of biological agents consist of rigid segments connected with revolute joints and some elastic elements (i.e. kinematic chains with elastics). Even if the elastics are linear, the geometry of the configuration of the chain of links introduces nonlinearities, frequently in the form of trigonometric functions (e.g. eq. (2.4.5) of WandaX joint torque). Therefore, the system as a whole has algebraic nonlinearities due to the geometry of the model. It may be that some models can be linearized through a change of variables, but in general the nonlinearities are "essential" and therefore we have to deal with nonlinear models. Yet, there is another important source of nonlinearity and it comes from the discrete nature of the events. This statement will be justified intuitively and an example will be given where, despite of the use of a linear leg, nonlinear behavior is observed.

To understand the nonlinearities introduced by the touchdown and takeoff events, it is important to note that the hybrid dynamical system can be made continuous (i.e. it can be made non-hybrid). When the system switches from one chart to the other, the state is conserved and the two charts can be formally unified using the Heaviside step function $\mathcal{H}(x)$,

$$\ddot{x} = -g + \mathcal{H}(-x)\left(p(x) + u(t) - 2w_0\xi\dot{x}\right). \tag{3.1.3}$$

The Heaviside step function is zero when its argument is negative, i.e. $x > 0$ and it is one otherwise. At the point of discontinuity its value is generally defined to be $\mathcal{H}(0) = 1/2$. The Heaviside function can be represented as the limit of a sigmoid curve (point-wise smooth approximation),

$$\mathcal{H}(-x) = \lim_{\beta\to\infty} \frac{1}{1+e^{\beta x}}, \tag{3.1.4}$$

and we can consider our dynamical system to be the limiting case as well. As a consequence, the discontinuity (introduced by the takeoff and touchdown events) conserves the nonlinear nature of the sigmoid function, even when $p(x)$ is linear. Figure 3.2 shows a trajectory in the phase space of a continuous system with a linear leg for increasing values of β, superimposed with a trajectory of the corresponding hybrid system. As can be seen, when β is large enough, all the properties of the hybrid system (i.e. touchdown event (TD), takeoff event (TO) and equilibrium point (EQ)) are well approximated by the continuous one. In other words, though both charts are linear, the hybrid system is approximated by a highly nonlinear system.

3.2 The nonlinear nature of a linear leg hopper

The case of a hopper with a linear leg corresponds to the polynomial $p(x)$ with $a_k = 0\ \forall k > 1$ and $w_0 \neq 0$. For this polynomial the damping ratio ξ describes the way the hopper settles down to rest. In particular if $\xi = 1$ the hopper is critically damped and will reach rest exponentially, without oscillations. For values $\xi < 1$, the lower ξ is, the longer the oscillations observed. Figure 3.3 shows the behavior of the center of mass (CoM) of the hopper for three initial conditions using $\xi = 0.3$. We mark two important values of the CoM height: the event condition $h_{CoM}(t) = \ell_0$ (horizontal red line) and the equilibrium position (thin black horizontal line), in this case unique since the equation $a_1 x - g = 0$ has one root. The trajectories observed are qualitatively similar to the oscillations of a linear spring, and exactly coincide with those in the cases where there is no takeoff event.

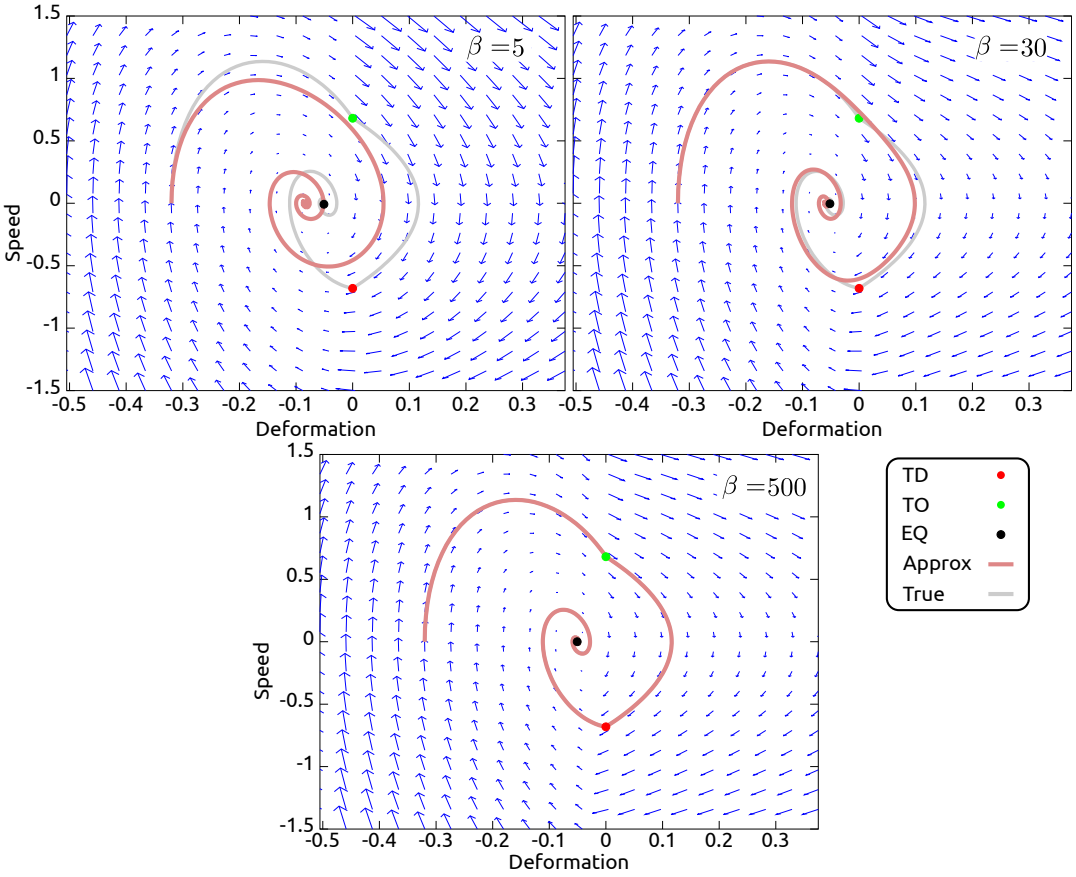

Figure 3.2: Phase space of the approximation of the hybrid system. The trajectory of the continuous system, deformation (x) versus speed ($\dot{x}$), approaches the one of the hybrid one when β (eq. (3.1.4)) increases. The panels of the figure show values of $\beta = \{5, 30, 500\}$. The touchdown (TD) and takeoff (TO) events are also approximated by the continuous system, as well as the equilibrium point (EQ). Though the chart (3.1.1) defined in $-\ell_0 \leq x \leq 0$ and (3.1.2) defined in $x > 0$ are both linear, the hybrid system is approximated by a highly nonlinear system.

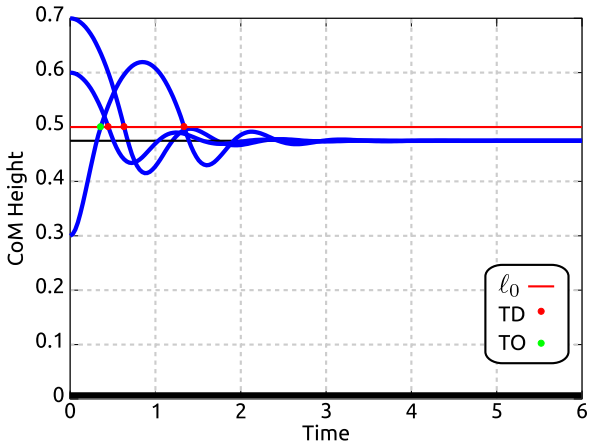

Figure 3.3: Unforced hopping. Time series of the CoM height for different initial conditions without actuation, i.e. $u(t) \equiv 0$. The horizontal lines represent the natural length of the leg ℓ_0 (red) and the equilibrium deformation (thin black). Touchdown (TD) and takeoff (TO) events are indicated with dots. Ground is depicted with a think black line.

To evince the nonlinear behavior, we set the actuation to a sine function given by $u(t) = u_0 \sin(wt + \phi)$, where u_0 is the amplitude of the forcing and ϕ its initial phase. The frequency of the actuation is set to $w = w_0\sqrt{1-2\xi^2}$, i.e. the resonant frequency of the linear system without takeoff. Figure 3.4 shows the behavior for three different amplitudes with the hopper starting from rest at the equilibrium point. The figure shows a clear dependence of the hopping behavior (i.e. the height of the jumps) on the amplitude of the forcing. This dependency is characteristic of nonlinear systems: the spectrum of the response depends on the amplitude of the input. To make the nonlinear dependence on the amplitude more clear, Figure 3.5 shows the steady state apex[2] of the flight phase (normalized with respect to the leg length) in a range of forcing amplitudes. The insets in the figure show the steady state trajectory of the hopper in the phase space. Bifurcations are clearly observed as well as regions of quasi-periodic behavior, which are impossible in a linear system.

The behavior variety observed in the figure comes from an interplay between the time of flight and the amount of energy that the actuation manage to add to, or remove from, the hopper while it is in contact with the ground. This observation lead us to think that the phase of the forcing also plays an important role. Indeed, as shown in Figure 3.6 we observe varied transient responses for a forcing with fixed amplitude but with different phases (the values were chosen to clearly show the differences). Figure 3.7 presents the same bifurcation diagram showed before, but generated with a forcing with initial phase of $\phi = \pi/4$. The qualitative behavior of the steady state apex is clearly different to the one shown in Fig. 3.5. This is evidence of the strong relation between the duration of flight, the amplitude of the forcing and its phase; introduced by the nonlinearity of the model.

3.3 Legs for optimal hopping

How can we maximize the jumping height of the hopper described by the previous model? If the objective is to maximize the height of jump in the long term we should proceed to

[2]Parameters $w_0 = 2\pi$, $g = 2$, $\xi = 0.3$, $\phi = 0$, $\ell_0 = 0.5$, the system was integrated until $t = 60$ and then data acquired for another interval of $t = 30$.

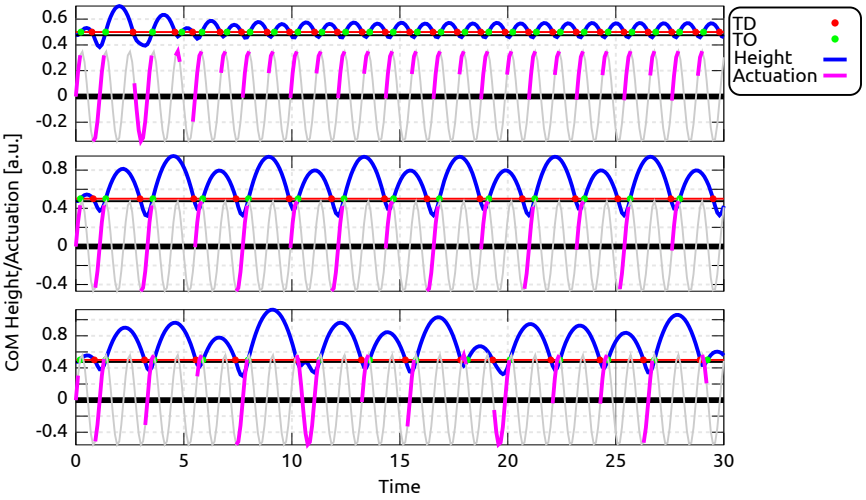

Figure 3.4: Nonlinear hopping with sinusoidal actuation with several amplitudes. Time series of the height of the center of mass of the hopper starting at rest form the equilibrium position, actuated with sinusoidal forces $u(t) = u_0 \sin(wt)$, with amplitudes $u_0 = \{3, 4, 5\}$ (from top to bottom). The actuation is normalized to fit in the same axis and is provided just as a visual reference. The center of mass of the hopper is actuated only when it is in contact with the ground (magenta thick lines). The hopping behavior shows a dependency on the amplitude of the forcing. Symbols as defined in see caption of Fig. 3.3

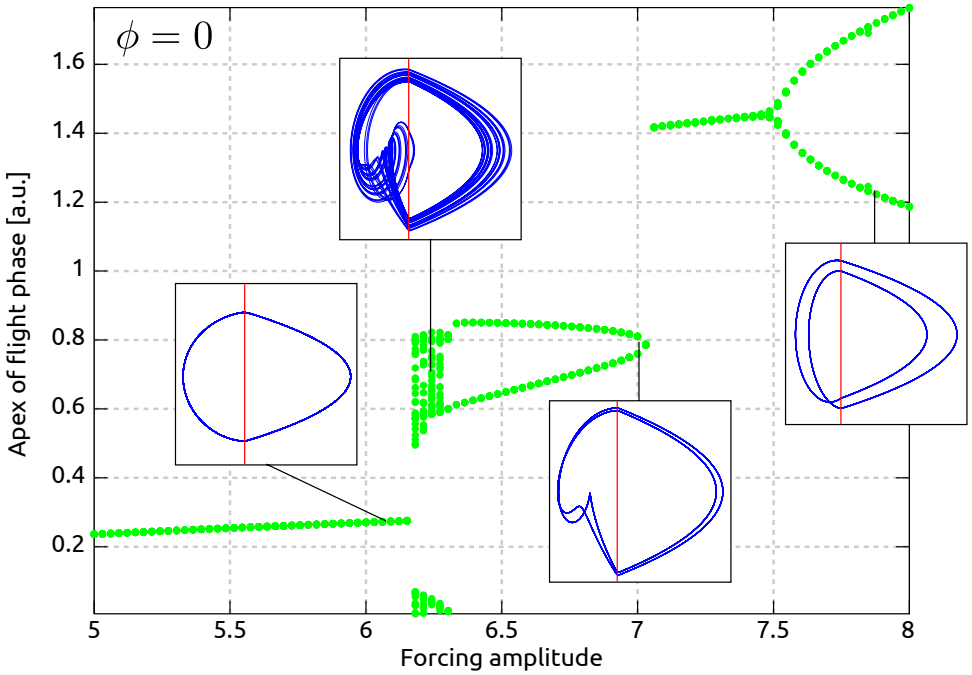

Figure 3.5: Bifurcation diagram of the apex map. The maximum hopping height is a complicated function of the forcing amplitude. The insets show the trajectory in phase space for selected values of the forcing amplitude as in Fig. 3.2. Periodic motion with the same frequency of the input can be observed as well as quasi-periodic and bistable oscillations. Though the charts composing the dynamical system are linear, the frequency spectrum of the trajectories is richer than that of the input (which contains a single frequency) due to the strong nonlinearity introduced by the takeoff and touch down events.

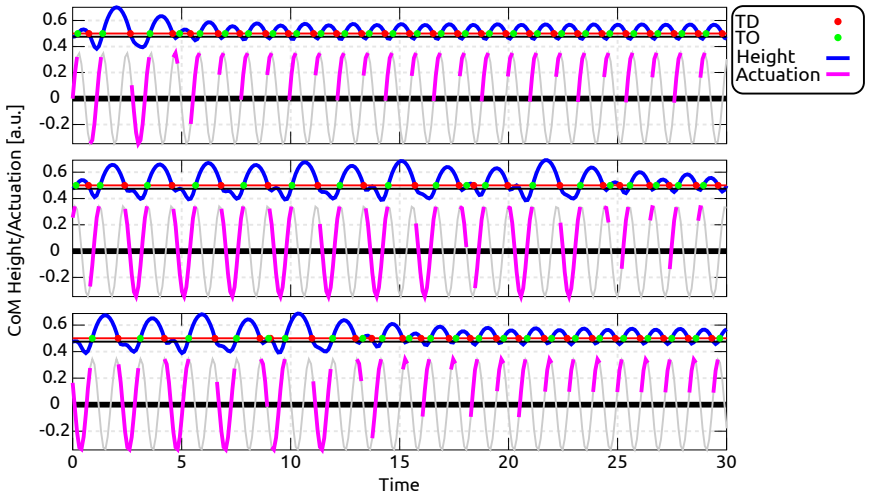

Figure 3.6: Nonlinear hopping with sinusoidal actuation with several phases. Time series of the height of the center of mass of the hopper starting at rest form the equilibrium position, actuated with sinusoidal forces $u(t) = 3\sin(wt + \phi)$, with different phases $\phi/\pi = \{0, 5/19, 16/19\}$ (from top to bottom). The actuation is normalized to fit in the same axis and is provided just as a visual reference. The center of mass of the hopper is actuated only when it is in contact with the ground (magenta thick lines). The hopping behavior shows a dependency on the phase of the forcing.

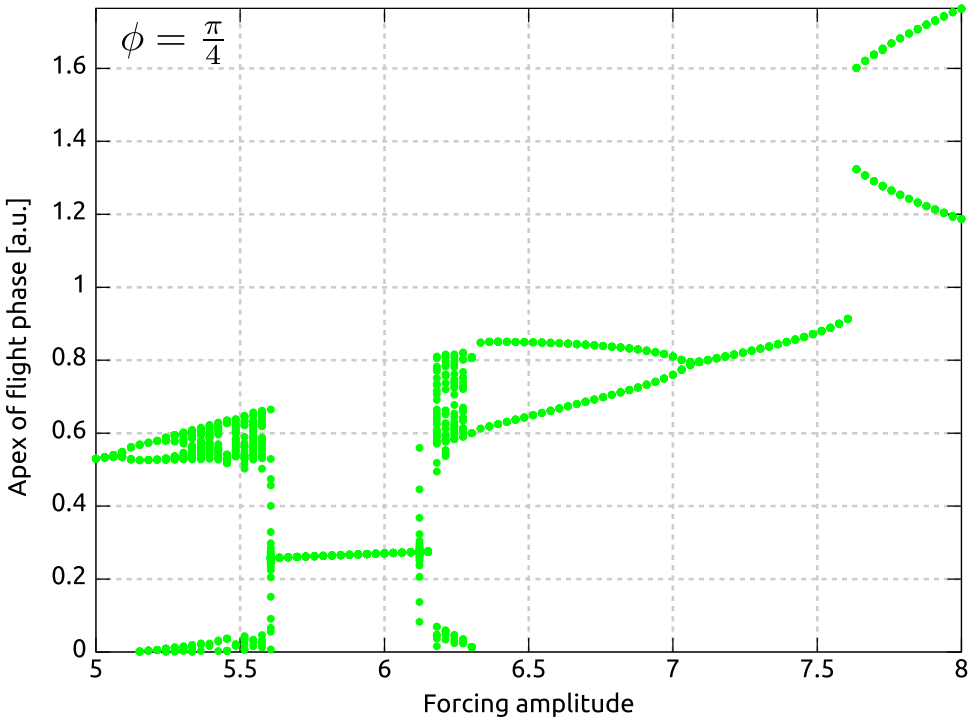

Figure 3.7: Bifurcation diagram of the apex map. The maximum height the hopper reaches while in the air is a complicated function of the forcing amplitude and initial phase $\phi = \pi/4$. The steady state behavior of the apex is sensitive to the phase of the forcing. This is evidence of the strong relation between time of flight, amplitude and initial phase of the forcing.

analyze the fixed points of the apex map (see Seyfarth et al., 2002; Geyer, 2005, for an application to running in a similar model) and establish the relation between their stability and the parameters in the model. However, we could have a more mundane objective and just desire to reach a maximum jump height in a given finite time, not caring if the system will reach this point again (as in the robot Mowgli by Niiyama et al., 2007). We will deal with the second objective, since it is suited for numerical investigation and analytical treatment is not straightforward.

In the vein of a morphological exploration, we do not adjust the forcing to achieve the objective, instead we fix the forcing and change the coefficients of the polynomial $p(x)$ in order to maximize jumping height after the first takeoff event.

For any hopper, the maximum jump height is given by the velocity at takeoff (TO). This velocity is directly related to the mechanical work done by the net force during the stance period.

$$W = K_{TO} - K_0 \tag{3.3.1}$$

Where K_0 and K_{TO} are the initial and takeoff kinetic energy, respectively. W stands for the work done by the net force. Since the hopper starts at rest we get that,

$$W = \frac{1}{2} v_{TO}^2. \tag{3.3.2}$$

This clearly shows that to maximize the velocity at takeoff, we need to maximize the work done during stance phase. The role of the leg spring becomes evident when we write W as the integral of the force along the motion path. Ignoring the work done by the damping force, since it always reduces the net work, we get:

$$W = W_u + W_p + W_g = \int_0^{t_{TO}} u(t)\dot{x}(t)\mathrm{d}t + U(x_0) + g x_0. \tag{3.3.3}$$

Here the total work is split into the contributions coming from each force: work of the actuation W_u, work of the spring force W_p and work of gravity W_g. The last two terms are calculated from the changes of the potential energies associated to the forces. $U(x_0)$ is the potential energy associated to the spring (i.e. $p(x) = -\frac{\mathrm{d}U}{\mathrm{d}x}$) and $g x_0$ the gravitational potential energy, both evaluated at the initial position[3] x_0. Hence, the only contribution subject to maximization is the integral in the first term of the right-hand side[4]. Since velocity is the time integral of Equation (3.1.1) we get,

$$\begin{aligned} &\int_0^{t_{TO}} u(t) \int_0^t \left[p(x(\tau)) - g + u(\tau)\right] \mathrm{d}\tau \mathrm{d}t = \\ &\int_0^{t_{TO}} u(t) \int_0^t p(x(\tau)) \mathrm{d}\tau \mathrm{d}t - g \int_0^{t_{TO}} u(t) t \mathrm{d}t + \int_0^{t_{TO}} u(t) \int_0^t u(\tau) \mathrm{d}\tau \mathrm{d}t. \end{aligned} \tag{3.3.4}$$

Where, t_{TO} denotes the time until takeoff. The last two terms do not depend on the leg characteristics and they can be calculated a priori if we know the actuation $u(t)$. The first term in the right hand side of (3.3.4) directly depends on the leg properties and shows that we can optimize the velocity at takeoff by modifying the function $p(x)$. Note that the upper limit t_{TO} of the integral also depends on the spring function. It is also noteworthy that the first term cannot be calculated explicitly without knowing the curve $x(t)$, i.e. the solution to the differential equation. However, this solution is explicitly accessible only in the case of

[3] x_0 is a real root of $p(x) - g$ in the interval $-\ell_0 \leq x \leq 0$

[4] Here we disregard the value of $U(x_0)$ that also depends on the spring function.

linear differential equations. Therefore, when $p(x)$ is nonlinear we cannot solve the problem analytically, nevertheless we can maximize the velocity at takeoff by performing numerical simulations.

As before, we will study actuations of the form $u(t) = A\sin(wt + \phi)$. The first case we consider here is a linear leg defined by $p(x) = -w_0^2 x$. The corresponding differential equation

$$\ddot{x} = -g - w_0^2 x + A\sin(wt + \phi), \tag{3.3.5}$$

$$x(0) = -\frac{g}{w_0^2}, \quad \dot{x}(0) = 0. \tag{3.3.6}$$

accepts solutions of the form

$$x(t) = \frac{A}{w^2 - w_0^2}\left[\frac{w}{w_0}\cos(\phi)\sin(w_0 t) + \sin(\phi)\cos(w_0 t) - \sin(wt + \phi)\right] - \frac{g}{w_0^2}. \tag{3.3.7}$$

This expression can be used to integrate (3.3.4) explicitly. However, after integration, the expression still depends on the phase of the actuation. To remove this dependency, we take the average over all possible phases to obtain a measure of the effective work. This gives,

$$\frac{1}{2\pi}\int_0^{2\pi}\int_0^T u(t)\dot{x}(t)\mathrm{d}t\mathrm{d}\phi = -\left(\frac{A}{2\omega\Omega}\right)^2\left[\omega^2\left(\cos(\Omega T) - 1\right) + \Omega^2\left(\cos(\omega T) - 1\right)\right], \tag{3.3.8}$$

where we defined $\Omega = w_0 + w$ and $\omega = w_0 - w$.

Figure 3.8 shows a color plot of Eq. (3.3.8) in the (w_0, T) plane for parameters $A = 2$, $w = 5$ and $g = 1$. For longer integration times (e.g. sustained oscillation) the high values of the integral accumulate around $w_0 = w$ as expected[5], i.e. resonance. The hopper, however, takes off before the integration can reach such favorable values. The time until takeoff for each w_0 is delimited by the minimum and maximum t_{TO} observed over all phases; these limits are shown with dashed lines. The best parameter w_0 is the one producing the highest average velocity at takeoff. Graphically stated, the optimal value of w_0 corresponds to the position of a vertical segment enclosed by the lines $\min t_{TO}$ and $\max t_{TO}$ such that it crosses the most regions with high values of the work integral. The optimization of w_0, performed on a model with damping $\xi = 0.3$, returns $w_0 = 3.94213 \pm 5{\times}10^{-4}$ corresponding to the solid line in the plot, with an average takeoff velocity of $v_{TO} = 0.392$. The optimization was carried out using the Nelder & Mead simplex algorithm[6] with regular simplex of relative size $1{\times}10^{-2}$. Parameters were initialized randomly 1000 times over the interval $w_0 \in (2, 8)$. The value function is defined as the average square velocity at takeoff over 25 values of $\phi \in (0, 2\pi)$.

We apply the same optimization procedure to a polynomial nonlinear leg given by $p(x) = \alpha x^3 + \beta x^2 + w_0^2 x$. The nonlinear parameters were initialized randomly over the ranges $\alpha \in [-600, 600]$, $\beta \in [-100, 100]$. The values obtained by the algorithm are plotted in Figure 3.9a. Note that parameters achieving the highest performance clearly show a linear trend with respect to the average velocity at takeoff. That is, the heuristic allows us to discover a relation between the parameters when they approach their optimal values. We push this

[5]Note that (3.3.8) has a singularity exactly at this value for all T, but only for longer T the singularity "spreads".

[6]Function `nmsmax` of GNU Octave.

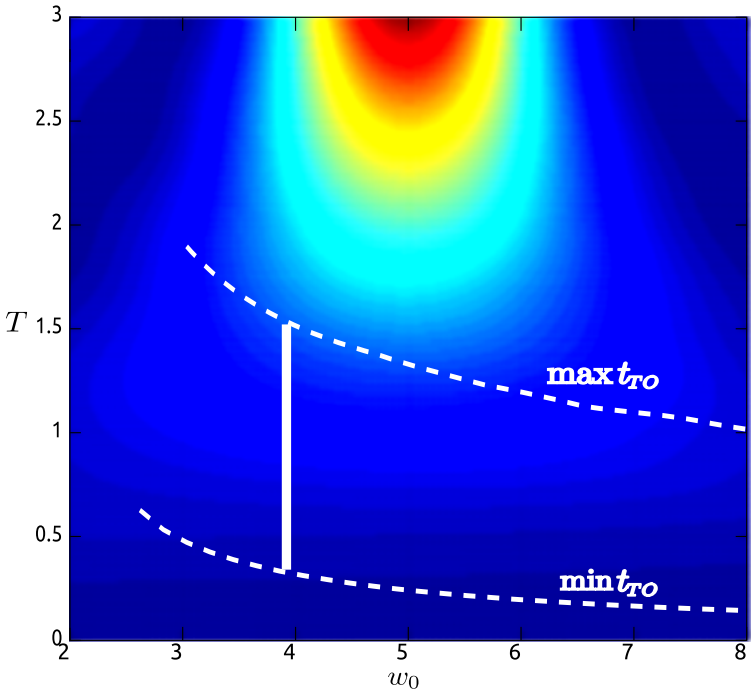

Figure 3.8: Work done by the actuation averaged over all possible phases as a function of interval of actuation (T) and actuation frequency (w_0). Color blue indicates low values and red high values, other colors are intermediate values. It can be seen that a leg in resonance with the actuation ($w_0 = 5$) becomes optimal for long periods of time. For shorter times, i.e. limited by a takeoff event, the maximum work on the first stance period is obtained with legs that have a lower resonant frequency. The result from numerical optimization is marked in the plot with a thick vertical line. See text for further explanations.

Ansatz forward and fit straight lines to the data, and use them to extrapolate leg parameters to takeoff velocities that were not found by the optimization. The results are shown in Figure 3.9b. The expected velocity is shown with solid line together with the evaluations of the value function. The extrapolation discovers a new region of optimal parameters with average takeoff velocities with a peak at $v_{TO} = 0.417$, a result about 6% better than the linear case. The corresponding parameters are $(\alpha, \beta, w_0) = (-1914.76, -424.10, 5.73)$.

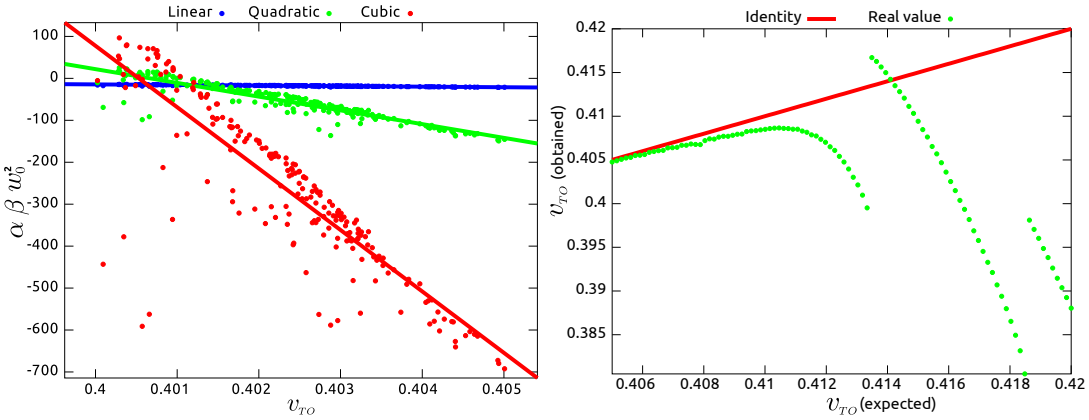

(a) Optimization results (b) Extrapolation

Figure 3.9: Optimization results. Different solutions obtained by optimization with parameters initialized randomly.(a) The optimal values of parameters (coefficients: linear (w_0^2), quadratic (β), and cubic (α)) show a linear trend with the velocity at takeoff. (b) Plot of the expected velocity following this trend versus obtained value from simulation. The extrapolation reveals a new optimal region of parameters.

The force function of the linear and nonlinear leg are compared in Figure 3.10a. The plot shows the force generated by the spring for negative values of the deformation (compression). The horizontal line marks the value of gravity; the equilibrium deformation of the leg corresponds to the intersection of that line with the leg curves. The shape of the nonlinear leg force curve accepts a straightforward interpretation above the equilibrium point: the spring tries to act as a gravity compensator.

Figure 3.10b shows $x(t)$ for different values of the phase of the actuation. Observe the variety of responses to changes of this phase. To summarize them, Figure 3.10c shows v_{TO} for both legs in a polar plot. The angle with respect to the positive x-axis corresponds to the phase of the actuation and the value of v_{TO} is represented as the radius. Compared with the nonlinear leg, the linear one achieves higher velocities for actuations with $\phi/\pi \in [1/2, 11/4]$, i.e. actuations that begin by compressing the leg. However, the nonlinear leg outperforms the linear one in the ranges $\phi/\pi \in [0, 3/4] \cup [11/4, 0)$, i.e. achieving high jumps for actuations that do not begin by compressing the leg. On average, the nonlinear leg performs better. However, there are intervals of phases for which a linear leg generates higher jumps (note the intersection in Fig. 3.10c).

Based on these results we could think that a combined leg curve, as the one shown in Fig.3.10a(dashed line) could make the best of the whole phase interval: linear when the leg is being compressed below the equilibrium point and nonlinear for smaller compressions. Such a leg curve is of much higher degree than the cubic polynomial considered here. The seventh

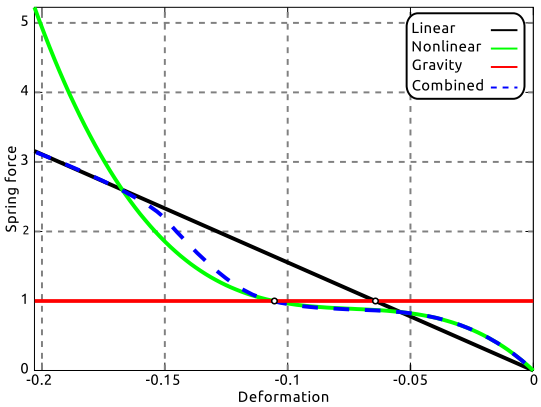

(a) Leg force curve

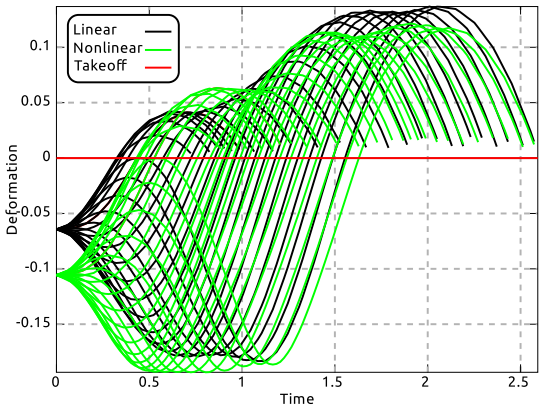

(b) Motion

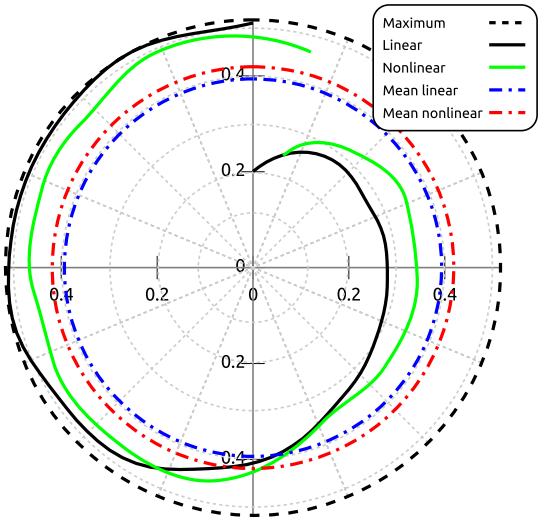

(c) v_{TO} vs. ϕ

Figure 3.10: Jumping performance. (a) Show the force generated by the linear and nonlinear legs when they are compressed. A "combined", potentially better leg is also shown. In (b) we show $x(t)$ for both legs for actuation with different phases. (c) Is a polar plot comparing v_{TO} as a function of the phase of the actuation. Note that velocity at take off is not a continuous function of the phase of the actuation.

degree polynomial

$$p(x) = -3.33\times10^7x^7 - 2.21\times10^7x^6 - 5.59\times10^6x^5 - 6.87\times10^5x^4 \\ - 4.47\times10^4x^3 - 1.70\times10^3x^2 - 47.7x, \tag{3.3.9}$$

in the interval of deformation $x \in [-0.2, 0]$ has the desired behavior. The motion corresponding to this leg is shown in Figure 3.11. The line of maxima for the linear and the cubic leg are shown for comparison, the performance of this highly nonlinear leg is outstanding for most of the actuations. The linear leg would perform better only when the phase of the actuation could be precisely controlled. Hence, achieving higher jumps requires less control in the case of a nonlinear leg.

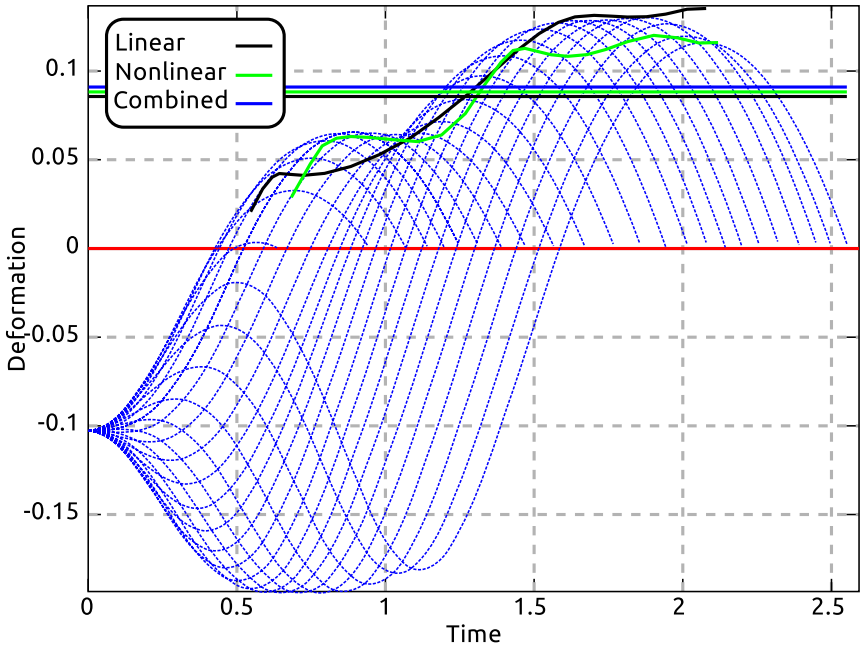

Figure 3.11: Performance of a seventh degree polynomial leg. The combined leg showed in Fig.3.10a (dashed line) outperforms, on average, both other legs, linear and cubic. Maximum hopping heights averaged over all phases are shown with horizontal solid lines.

3.4 Chapter summary

In Section 3.2, we briefly studied a hopper with a linear spring leg to show that the linearity of the charts of the hybrid system does not reduce the complexity of its behavior. A robotic quadruped jumping with its four legs in unison, as described in Buchli et al. (2006) can be qualitatively modeled in this way. Due to the observations herein, the use of a linear model to understand such a highly nonlinear system seems inapposite. Moreover, the concept of "resonant frequency" should not be summoned in this situation because, first it is not defined for nonlinear systems, and second it is misleading; since the behavior shows non-trivial dependencies on the amplitude and phase of the actuation not only on the frequency. Additionally, we showed that the behavior is strongly sensitive to variations of the characteristics of the actuation signal, thus it is not surprising that the results reported in the mentioned

publication can hardly be reproduced independently. Therefore the question of how to actuate a nonlinear leg becomes of primal importance, however our focus was on improvements due to the morphology for a given fixed actuation. Studying co-optimization of morphology and behavior for a hopping robot is not a simple task. The parameter space becomes huge and we are left with almost no tools for analysis. The emphasis should be on understanding the relation between the parameters and the fitness (see Fig. 3.9a), not only on finding an (local)optimal design.

Altogether, with a simple example, we showed that when dealing with nonlinear systems we cannot talk about resonances considering only the frequency of the input since the behavior depends (in a non-trivial way) on other properties of the input signal, e.g. amplitude and phase. Thus, resonance (if ever defined for this system) should be observed in the frequency-phase-amplitude plane. This was already highlighted in Section 2.3.1 when we discussed the effect that the input signal spectrum has on the frequency content of the output of a nonlinear system.

By studying the role of morphology in hopping, we underlined a change in perspective: optimize body, not controller. Though this approach is not completely novel, the bottom-up procedure used here provided fruitful insights, allowing the progressive design of nonlinear legs for hopping. The take-home message of this chapter is that there is little to gain by jumping[7] straight into a complicated model and be forced to base our investigations on purely heuristic approaches. Not only numerical integration becomes less accurate and expensive, but also the insights gained are diffused due to the lack of ground truths, i.e. the computational model is as complicated and puzzling as the physical device itself.

The nonlinear legs reported in this chapter have not been realized in an experimental platform. Nevertheless, we believe that robots such the Zürihopper and WandaX could be tuned to generate forces as the ones described here. The task is left for new researchers to pick it up.

Mathematical roboticist face the same problems that abound in other scientific disciplines (Holmes, 2005; Ellner and Guckenheimer, 2006), the difficulties ahead are the development of simplified models that capture the main aspects of the behaviors studied, the understanding of the role of parameters in these models, and then the reverse engineering of more complex models. Once the sensibility of the behavior with respect to several parameters is quantified using a simple model, heuristic approaches may help us discover the interaction between these parameters, paving the road for the construction and experimental validation of more complete models. An example of application of this procedure for the understanding of gait transitions in bipedal locomotion, is presented in Martinez Salazar and Carbajal (2011a), which itself is based on similar approaches lead by the Locomotion Laboratory[8].

[7] No pun intended.

[8] Locomotion Laboratory, Sports Biomechanics department, Technische Universität Darmstadt, Darmstadt, Germany.

Part II

Reaching

Chapter 4

Dynamic response decomposition method

> The limbs that function as nothing more than a pendulum, swinging freely, will follow the movement in their own fashion without anyone's aid.
>
> "Über das Marionettentheater" by Heinrich von Kleist (1810)(Translated by T. G. Neumiller)

To study the behavior of robots and to design controllers, we create models of them based on differential equations. In the introduction of this thesis, we described the types of equations that are frequently used (section 1.2). In this chapter, we present a method to solve a class of control problems stated in terms of differential equations. The method is aimed to provide the machine with the capability to solve problems using knowledge of its own dynamics and to reduce the need of *a priori* models. It is rooted in several ideas and hypotheses that orbit the fields of robotics, biomechanics, and artificial intelligence at the time of writing this document. First, it tries to deal with nonlinear systems, without resorting to linearizations. Second, it is based upon the idea that biological machines reuse their experience to generate solutions to new problems. Finally, it directly takes into account the behavior defined by the physical properties of the machine. We have already mentioned the notion of naturality before, but since its use was purely metaphorical, this chapter starts with a timely discussion on natural dynamics. The subsequent sections form the conceptual and technical background for the understanding of the proposed methodology. In Chapter 5 we present applications of the method to generalized reaching problems in nonlinear oscillators and kinematic chains.

4.1 Natural dynamics

We have already mentioned the notion of *naturality*, but it was not discussed in depth. It plays an important role in the sections that follow, therefore a digression is in order. The phrase "natural dynamics" is frequently used in the field of control and embodied artificial intelligence, but a proper definition is seldom given[1]. It refers to the behavior that physical

[1] Other common phrases are "passive dynamics" and "unforced dynamics", that are also seldom defined. The concept of "passivity" has a definition in the context of feedback control. In that field, passivity means

systems present in the absence of external actions. This is an amenable description of the idea, however it is still ambiguous. *What are external actions?*. The classification between external and internal actions depends on the physical system, i.e. the portion of the physical universe chosen for analysis (see section 1.1). Therefore, if the physical system is not explicitly stated, two observers may classify actions differently and consequently conclude differently about the naturality of the behavior of the system. Lets take a pendulum as an example: a point mass (the bead) hangs from a rigid rod of negligible mass that is connected to another body of infinite mass (the wall or ceiling) via an ideal revolute joint (it can rotate without friction). We start the system with the bead away from the rest position and let it fall under the action of its weight. Is the motion we observe natural? Many people will rush into an affirmative answer, however we will go slowly and hopefully flawlessly. First, we have to define what is internal and what is external to our system. If we take the bead and the massless rod as the system, there are two external actions: the weight of the bead and the force from the wall. Therefore, considering natural as "no external actions", the behavior of this system is not natural. We could include gravity as part of the system, by including the Earth in it, and a similar thing could be done with the force from the wall. In this extended system, the pendulum (plus all the other things) shows a natural behavior, because there is no other external influence acting on the system. We closed the system, i.e. all forces and their reactions belong to the system under study. It should be clear that this is rather a cumbersome way to go just to achieve naturality. Moreover, we will be driven to conclude that all behaviors are natural, based on the belief that the universe is a closed system. Therefore, due to the uselessness of this notion, we will drop the idea of "natural" as "no external actions" and take one that emerges from the semantic meaning given to some of the variables describing the behavior of the system.

As we mentioned in section 1.1 once a mathematical model is built, those variables that we can change arbitrarily are called inputs. Once the model, inputs and outputs are determined, our system is fully defined. We can assign the role of input to variables already existing in the model or we can include new ones (usually, inputs are additive but other type of inputs could be used). The key point here is that we are giving semantic meaning to some variables in the model. The notion of naturality emerges from this semantic meaning and we will motivate this idea with an example and finally provide a working definition of *natural dynamics*.

Remove gravity from the previous example and consider the physical system consisting of the bead alone, with no inputs. Give a push to the bead, so as to set an initial nonzero velocity; then, the external action is due to the force that the rod exerts on the bead. In this situation, the bead moves in a circle around the revolute joint. Lets compare this motion with the one of a spacecraft always accelerating towards a reference point (a beacon in the center of rotation). The comparison is pictorially presented in Figure 4.1. Which system behaves naturally? Most of us would agree that the behavior of the bead is natural while the one of the spacecraft is not. That is, we see the motion of the spacecraft as "unnatural" because of the meaning we give to the force produced by the propellers: since it can be controlled (e.g. by the pilot), this force is an input. However, its effects are physically equivalent to the force acting on the bead, which is not an input. Clearly, the notion of naturality is linked to the existence of inputs. It is the meaning of the force produced by the propellers, not its physical

that the system's energy changes only due to the work of the inputs(Desoer and Vidyasagar, 2009; Ortega et al., 1998). However, in that context energy has a physical meaning only when the product of input and output has units of power, otherwise it is just the signal theoretic measure of energy, i.e. the norm of a signal in a given normed space (usually $L^2(\mathbb{R}^n)$ or its discrete counterpart). In that context passivity is defined as a property of the system with respect to its inputs. I use the word "naturality" to avoid a confusing clash of naming conventions. Though widely used, the term "unforced" does not make any sense, and is a source of confusion and obscure sentences, e.g *the damping force acting on the unforced system.*

properties, what makes us think of one behavior as natural and the other as unnatural.

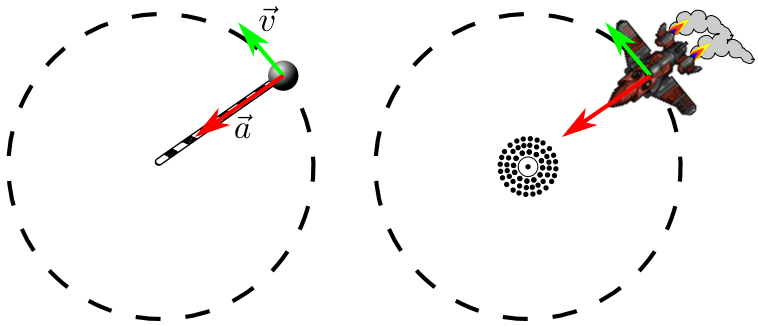

Figure 4.1: A bead with initial velocity rotating around a revolute joint due to the force transmitted by the massless rigid rod. The same motion could be obtained with a hypothetical spacecraft accelerating towards a beacon.

In what follows we study systems that are properly modeled by a differential equation (in our context second order ordinary differential equations) of the form,

$$\begin{aligned} \mathcal{D}(\boldsymbol{q};\boldsymbol{\lambda}) = L(\boldsymbol{q};\boldsymbol{\lambda}) + f(\boldsymbol{q};\boldsymbol{\lambda}) = \boldsymbol{u}(t), \\ \boldsymbol{q}(0) = \boldsymbol{q}_0, \dot{\boldsymbol{q}}(0) = \dot{\boldsymbol{q}}_0 \end{aligned} \tag{4.1.1}$$

Where $\boldsymbol{q} \in \mathbb{R}^d$ is the generalized configuration vector (loosely, what one would measure from a snapshot of the system), and $\dot{\boldsymbol{q}}$ its derivatives with respect to time. $\mathcal{D}(\ \cdot\ )$ represents a system of differential equations that we can think of as a differential operator acting on $\boldsymbol{q}$. $L(\ \cdot\ )$ is the linear part of that operator and $f(\ \cdot\ )$ is the nonlinear part. The functions of time $\boldsymbol{u}(t)$ are inputs to our system. The system is parametrized with a vector of parameters $\boldsymbol{\lambda} \in \mathbb{R}^p$ that represent physical magnitudes (lengths, masses, moments of inertia, etc...). The state vector of the system, $\boldsymbol{s}(t) = [\boldsymbol{q}(t), \dot{\boldsymbol{q}}(t)]$ is the concatenation of the configuration and velocity of the system.

Definition 1 (Natural dynamics)**.** The natural dynamics of the system defined by (4.1.1) is the set of all solutions $\boldsymbol{\Theta} = \{\boldsymbol{\theta}_i(t)\}_{i=0}^{\infty}$, when all inputs are zero, i.e. $\boldsymbol{u}(t) \equiv 0$.

We have defined natural behavior as the trajectories generated when all inputs are zero, i.e. naturality is a property of the trajectory[2]. It should be noticed, however, that to place the system at an arbitrary initial condition some nonzero inputs are required.

Another important property to notice is that if $\boldsymbol{u}(t)$ is replaced by a feedback law $\boldsymbol{u}(\boldsymbol{q}, \dot{\boldsymbol{q}})$, it ceases to be arbitrary, hence it is not an input anymore and consequently the observed trajectories under this actuation belong to the natural dynamics of a different system $D' = \mathcal{D}(\boldsymbol{q}) - \boldsymbol{u}(\boldsymbol{q}, \dot{\boldsymbol{q}})$. There may be other definitions that would fulfill the intuitive notion of naturality, the definition used here is the basis for the presented results, using an altered definition might be part of future directions of research.

If a system evolves in time under the influence of non-zero inputs, the cost of producing the inputs is a measure of naturality. This means that to effectively know how natural a behavior is, we need to describe how the inputs are generated, that is, we need to specify the *actuators* of the system. This cannot be done in a general case. The most general consideration about the nature of the actuators is that the higher the inputs generated the

[2]Readers familiar with operator theory may have noticed that the natural dynamics is nothing but the nullspace of $\mathcal{D}$.

more energy required. In this very general sense, a weighted norm of $\boldsymbol{u}$, i.e. $||\boldsymbol{u}|| = \boldsymbol{u}^T Q \boldsymbol{u}$ (where Q is a positive definite matrix), measures the naturality of a behavior. This is however, just a general statement that has to be revised when specific actuators are used.

4.1.1 *Solving reaching tasks using dynamic bases

Herein we will discuss in detail a class of boundary value problems (BVP, see 1.4): reaching tasks. A general point-to-point reaching task consists of moving from an initial state $(\boldsymbol{q}_0, \dot{\boldsymbol{q}}_0)$ to a final state $(\boldsymbol{q}_T, \dot{\boldsymbol{q}}_T)$, in a given amount of time T:

$$\begin{aligned} \boldsymbol{q}(0) &= \boldsymbol{q}_0, \quad \dot{\boldsymbol{q}}(0) = \dot{\boldsymbol{q}}_0, \\ \boldsymbol{q}(T) &= \boldsymbol{q}_T, \quad \dot{\boldsymbol{q}}(T) = \dot{\boldsymbol{q}}_T. \end{aligned} \tag{4.1.2}$$

Controlling a system to perform such tasks amounts to finding the actuation $\boldsymbol{u}(t)$ that fulfills the point constraints (4.1.2). The solving procedure consists of, first, solving the problem in kinematic space (i.e. finding the appropriate $\boldsymbol{q}(t)$), and then computing the corresponding actuations through inverse dynamics. As was discussed in Section 1.4, solving a differential equation can be posed as an algebraic problem if solutions can be decomposed into a suitable base of functions. Additionally, from the kinematic point of view, the task can be seen as an interpolation problem; i.e. $\boldsymbol{q}(t)$ is a function that interpolates the data in (4.1.2). Therefore, a set of functions is used to build the interpolant trajectory that satisfies the constraints imposed by the task

$$\boldsymbol{q}(t) = \sum_{i=1}^{N_\theta} \boldsymbol{\theta}_i(t) a_i := \boldsymbol{\Theta}(t)\boldsymbol{a}, \tag{4.1.3}$$

where the vector of combinators $\boldsymbol{a}$ is chosen such that the task is solved. $\boldsymbol{\Theta}(t)$ describes a formal matrix where each column is a different (multivariate) function, we will call this set *dynamic basis*. If we consider a time discretization, $\boldsymbol{\Theta}(t)$ becomes a $N \dim(\boldsymbol{q})$-by-N_θ matrix, where N is the number of time steps, $\dim(\boldsymbol{q})$ the dimension of the configuration space and N_θ the number of functions in the set.

Consider configurations vectors $\boldsymbol{q} \in \mathbb{R}^d$ and propose the controlled trajectory $\boldsymbol{q}_{\text{ND}}(t) = \sum_{i=0}^{N_\theta} c_i \boldsymbol{\theta}_i(t)$ that obeys the boundary conditions of (4.1.2),

$$\begin{cases} \boldsymbol{q}_{\text{ND}}(0) = \sum_{i=0}^{N_\theta} c_i \boldsymbol{\theta}_i(0) \doteq \boldsymbol{q}_0 \\ \boldsymbol{q}_{\text{ND}}(T) = \sum_{i=0}^{N_\theta} c_i \boldsymbol{\theta}_i(T) \doteq \boldsymbol{q}_T \\ \dot{\boldsymbol{q}}_{\text{ND}}(0) = \sum_{i=0}^{N_\theta} c_i \dot{\boldsymbol{\theta}}_i(0) \doteq \dot{\boldsymbol{q}}_0 \\ \dot{\boldsymbol{q}}_{\text{ND}}(T) = \sum_{i=0}^{N_\theta} c_i \dot{\boldsymbol{\theta}}_i(T) \doteq \dot{\boldsymbol{q}}_T, \end{cases} \tag{4.1.4}$$

where each $\boldsymbol{\theta}_i(t)$ is an element of the dynamic basis. Since $\boldsymbol{\theta}_i(t)$ are known beforehand, this is a system of $4d$ linear equations with N_θ unknown coefficients c_i. In general, the dynamics basis will be bigger than the dimension of the task to solve, i.e. $N_\theta \geq 4d$, rendering the

system of equations undetermined. Using matrix notation we can write,

$$P = \begin{bmatrix} \theta_{1,1}(0) & \dots & \theta_{1,N_\theta}(0) \\ \vdots & \ddots & \vdots \\ \theta_{d,1}(0) & \dots & \theta_{d,N_\theta}(0) \\ \theta_{1,1}(T) & \dots & \theta_{1,N_\theta}(T) \\ \vdots & \ddots & \vdots \\ \theta_{d,1}(T) & \dots & \theta_{d,N_\theta}(T) \\ \dot{\theta}_{1,1}(0) & \dots & \dot{\theta}_{1,N_\theta}(0) \\ \vdots & \ddots & \vdots \\ \dot{\theta}_{d,1}(0) & \dots & \dot{\theta}_{d,N_\theta}(0) \\ \dot{\theta}_{1,1}(T) & \dots & \dot{\theta}_{1,N_\theta}(T) \\ \vdots & \ddots & \vdots \\ \dot{\theta}_{d,1}(T) & \dots & \dot{\theta}_{d,N_\theta}(T) \end{bmatrix}, \; \boldsymbol{c} = \begin{bmatrix} c_1 \\ \vdots \\ c_{N_\theta} \end{bmatrix}, \; R = \begin{bmatrix} q_{c,1}(0) \\ \vdots \\ q_{c,N_\theta}(0) \\ q_{c,1}(T) \\ \vdots \\ q_{c,N_\theta}(T) \\ \dot{q}_{c,1}(0) \\ \vdots \\ \dot{q}_{c,N_\theta}(0) \\ \dot{q}_{c,1}(T) \\ \vdots \\ \dot{q}_{c,N_\theta}(T) \end{bmatrix}, \tag{4.1.5}$$

$$P\boldsymbol{c} = R. \tag{4.1.6}$$

The matrix P is sometimes referred to as the *alternat matrix*. The problem is linear and any known method can be used to solve it. In particular, we could use $\boldsymbol{c} = P^+R$ where P^+ is the Moore-Penrose pseudoinverse of matrix P, giving the minimum norm solution for the coefficients $\boldsymbol{c}$. This is equivalent to solving the boundary condition problem in the least square error sense, however, other criteria could be used (for example minimization of the L^1-norm, see Candes et al. (2006)). It is noteworthy that the condition $N_\theta > 4d$ permits us to impose additional constraints on the trajectories $\boldsymbol{q}(t)$. For example, we could ask that the acceleration at the end-points of the trajectories is also constrained as we will be do in Section 5.1 for a nonlinear spring. It should be evident that, if the system of equations is overdetermined (i.e. $N_\theta < 4d$) the solution cannot fulfill all constraints unless they are trivial. Finally, when the alternant matrix has linearly dependent columns, the vector of coefficients $\boldsymbol{c}$ is not unique. To obtain other solutions we use the formula

$$\boldsymbol{c} = P^+R + \left(I - P^+P\right)\boldsymbol{w}. \tag{4.1.7}$$

Where I is the identity matrix and $\boldsymbol{w}$ an arbitrary vector. This formula will be used in Section 5.3 to optimize reaching motions.

4.2 Natural dynamics decomposition

How can we use the natural dynamics to calculate the inputs that solve (4.1.2)? The answer is hidden in the nonlinear properties of the differential operator $\mathcal{D}$. A nonlinear operator maps a linear combination of elements of its nullspace (i.e. the natural dynamics) into a function of time. This transformed signal represents the input necessary to produce the given linear combination, and can be associated with a controller. This indicates that if we are able to solve tasks with linear combinations of the natural dynamics, we could calculate controllers based on them. To do this, we take the natural dynamics as the set of functions used to build interpolants solving the task. In other words, we consider solutions to the tasks that can be written in terms of functions $\boldsymbol{\theta}_i \in \boldsymbol{\Theta}$ that obey the relation

$$\begin{aligned} \mathcal{D}(\boldsymbol{\theta}_i) = L(\boldsymbol{\theta}_i) + f(\boldsymbol{\theta}_i) = 0, \\ \boldsymbol{\theta}_i(0) = q_i, \quad \dot{\boldsymbol{\theta}}_i(0) = \dot{q}_i. \end{aligned} \tag{4.2.1}$$

Where the initial conditions are arbitrarily chosen. Using this relation in the original problem,

$$\begin{aligned} \mathcal{D}(\boldsymbol{q}(t,\boldsymbol{s}_0)) = \sum_{i=1}^{N_\theta} a_i L(\boldsymbol{\theta}_i(t)) + f\left(\sum_{i=1}^{N_\theta} a_i \boldsymbol{\theta}_i(t)\right) = \boldsymbol{u}(t), \\ g_k(\sum_{i=1}^{N_\theta} a_i \boldsymbol{\theta}_i(t), \sum_{i=1}^{N_\theta} a_i \dot{\boldsymbol{\theta}}_i(t), \ldots, t_k) = 0. \end{aligned} \tag{4.2.2}$$

we obtain

$$f\left(\sum a_i \boldsymbol{\theta}_i\right) - \sum a_i f(\boldsymbol{\theta}_i) = \boldsymbol{u}(t), \tag{4.2.3}$$

$$g_k(\sum a_i \boldsymbol{\theta}_i(t), \sum a_i \dot{\boldsymbol{\theta}}_i(t), \ldots, t_k) = 0. \tag{4.2.4}$$

This replacement makes evident an interesting relation between the inputs and the nonlinearity of the system. Namely, the inputs are described in terms of the nonlinear operator applied to the natural dynamics. This means that the linear part of $\mathcal{D}$ plays a role in defining the natural dynamics, but not in the solution of the task at hand. Hence, if the problem can be solved with this approach, the inputs are functions generated by the natural dynamics transformed by the nonlinear part of $\mathcal{D}$. Note that if the left-hand side of (4.2.3) is zero for all times for a given vector of coefficients $\boldsymbol{a}$, it is as if the nonlinear part of the operator was behaving linearly with respect to $\boldsymbol{\Theta}$. Vectors $\boldsymbol{a}$ for which this is true, generate trajectories that belong to the natural dynamics and will be discussed in section 5.4. In particular, vectors $\boldsymbol{a}$ with only one non-zero element (i.e. $a_i = 1$ $a_k = 0\ \forall k \neq i$) do make the left-hand side of (4.2.3) zero (this renders (4.2.3) into (4.2.1)), but in general they do not fulfill the goals g_k.

When $\mathcal{D}$ is a linear operator, i.e. $f \equiv 0$, the left-hand side of (4.2.3) is always zero, since linear combinations of solutions of a linear homogeneous ODE are also solutions of the equation. This implies that for a linear system, the natural dynamics cannot be used to solve the control problem (1.4.7), except for the trivial cases when the solution itself, belongs to the natural dynamics.

Example 4 (Boundary conditions)**.** Consider the one dimensional harmonic oscillator (spring-mass system) with boundary conditions[3]

$$\mathcal{D}(x) := \ddot{x} + x = u(t) \tag{4.2.5}$$

$$x(0) = 0, \quad \dot{x}(0) = 0 \tag{4.2.6}$$

$$x(T) = 1, \quad \dot{x}(T) = 0 \tag{4.2.7}$$

The natural dynamics of the harmonic oscillator is the span of the trigonometric functions $\sin(t)$ and $\cos(t)$, therefore we assume that the solution to the given problem is $x_c(t) = A\cos(t) + B\sin(t)$. It is easy to verify that $\mathcal{D}(x_c(t)) = 0$, i.e. $x_c(t)$ belongs to the natural dynamics. Replacing x_c into the boundary condition (4.2.6) we obtain $A = B = 0$ and nothing else can be done to satisfy the conditions at T. This shows that the natural dynamics solve trivial boundary value problems, i.e. problems imposing conditions that are a consequence of the initial condition. The example also shows that a linear system cannot generate inputs from linear combinations of its natural dynamics. ◀

Consequently, since the trajectories in the natural dynamics of a linear system do not fulfill the boundary conditions of arbitrary tasks, we cannot solve them with this method. In the

[3]More details can be found in any introductory book on differential equations.

nonlinear case, a linear combination of functions is generally mapped to a non-zero function of time. If this combination is able to satisfy the boundary conditions, then we have found a solution to the problem. In essence, the method presented here relies fundamentally on a property that is characteristic of nonlinear systems: the linear superposition principle does not hold. Namely, that a linear combination of elements of the natural dynamics does not belong to the natural dynamics. Examples are provided in section 5.1.

4.3 Dynamic response decomposition

Modifying equation (4.2.1) by adding an input to the generation of the function set, we obtain the general form of the dynamic response decomposition (DRD) method. Doing this we move away from a natural dynamic decomposition to a decomposition based on the behavioral response of the system to a given set of inputs. Although this increases the complexity of the formulation, it provides an interesting and fruitful link to the synergy hypothesis, a current biomechanical explanation for the versatility of animal motor control.

Define *dynamic responses* (DR) of a set of inputs as the responses $\boldsymbol{\theta}_i(t) \in \boldsymbol{\Theta}$ of the system to each input $\boldsymbol{\phi}_i(t) \in \boldsymbol{\Phi}$ (i.e. forward dynamics):

$$\mathcal{D}(\boldsymbol{\theta}_i(t)) = \boldsymbol{\phi}_i(t) \qquad i = 1...N_\phi. \tag{4.3.1}$$

with initial conditions chosen arbitrarily.

Inspired by the hypothesis of muscle synergies (D'Avella et al., 2003), we formulate the actuation as a linear combination of predefined motor co-activation patterns:

$$\boldsymbol{u}(t) = \sum_{i=1}^{N_\phi} \boldsymbol{\phi}_i(t) b_i := \boldsymbol{\Phi}(t)\boldsymbol{b}, \tag{4.3.2}$$

where the functions $\boldsymbol{\phi}_i(t) \in \boldsymbol{\Phi}$ are called *motor synergies*. Intuitively, each motor synergy $\boldsymbol{\phi}$ represents the coordinated actuation of the degrees of fredoom of the system. For example, scratching our head requieres coordination of the joints in the shoulder, the elbow as well as the wrist (among many others!). In this case $\boldsymbol{\phi}$ is the torques to be applied to each of these joints that generate the scratching motion. If a big set of motions could be decomposed using the same basic coordinations then, the solutions of motion tasks could rendered into the simpler problem of finding the right mixture of synergies. Everytime we propose a solution of the form of (4.3.2) we are neglecting all other potential solutions that do not belong to the linar span of $\boldsymbol{\Phi}$ (all linear combinations of the synergies). Coloquially we could say that our body can do much more than what we use it for, but that does not prevet us from solving a plethora of useful tasks.

The notation $\boldsymbol{\Phi}(t)$ describes a formal matrix where each column is a different synergy. As before, if we consider a time discretization, $\boldsymbol{\Phi}(t)$ becomes a $N\dim(\boldsymbol{q})$-by-N_ϕ matrix, where N is the number of time steps, $\dim(\boldsymbol{q})$ the dimension of the configuration space and N_ϕ the number of functions in the set. Once a kinematic solution has been found (linear combination of DRs as was shown in 4.1.1), the corresponding actuation can be obtained by applying the differential operator; i.e. $\mathcal{D}(\boldsymbol{\Theta}(t)\boldsymbol{a}) = \tilde{\boldsymbol{u}}(t)$. Finally, the vector $\boldsymbol{b}$ can be computed by projecting $\tilde{\boldsymbol{u}}(t)$ onto the synergy set $\boldsymbol{\Phi}$. If $\tilde{\boldsymbol{u}}(t)$ does not belong to the linear span of $\boldsymbol{\Phi}$, the solution can only be approximated in terms of a defined norm (e.g. Euclidean):

$$\boldsymbol{b} = \arg\min_{\boldsymbol{b}} ||\tilde{\boldsymbol{u}}(t) - \boldsymbol{\Phi}(t)\boldsymbol{b}||. \tag{4.3.3}$$

When the time is discretized, all functions of time become vectors and this equation can be solved explicitly using the psuedoiverse of the matrix $\boldsymbol{\Phi}$,

$$\boldsymbol{\Phi}^{+}\tilde{\boldsymbol{u}} = \boldsymbol{\Phi}^{+}\mathcal{D}\left(\boldsymbol{\Theta}\boldsymbol{a}\right) = \boldsymbol{b}. \tag{4.3.4}$$

This equation highlights the operator $\boldsymbol{\Phi}^{+} \circ \mathcal{D} \circ \boldsymbol{\Theta}$ ($\circ$ denotes operator composition) as the mapping between the kinematic combinators $\boldsymbol{a}$ (kinematic solution) and the synergy combinators $\boldsymbol{b}$ (dynamic solution). Generically, this operator represents a nonlinear mapping $\mathcal{M} : \mathbb{R}^{N_\theta} \to \mathbb{R}^{N_\phi}$, and it will be discussed in Chapter 6. This expression also underlines the relation between the set of functions chosen to solve the problem and the system morphology (i.e. the $\mathcal{D}$ operator). In this sense, there may exist sets $\boldsymbol{\Theta}$ and $\boldsymbol{\Phi}$ that simplify the action of $\mathcal{D}$ generating a global map $\mathcal{M}$ that, for example, could behave almost linearly.

4.3.1 *Multiple initial conditions per synergy

The constitutive relation defined in Eq. (4.3.1) can be generalized to the case when more than one initial condition is used per synergy. This generalization becomes important if one considers the generation of dynamics response process as a system identification procedure (Ljung, 1999). In this case, the elements of $\boldsymbol{\Theta}$ are obtained from the elements in $\boldsymbol{\Phi}$ through the relation,

$$\mathcal{D}(\boldsymbol{\theta}_{ij}) = \boldsymbol{\phi}_j, \tag{4.3.5}$$

$$\boldsymbol{\theta}_{ij}(0) = {}_0\boldsymbol{\theta}_i \ \ldots \ \boldsymbol{\theta}_{ij}^{(n-1)}(0) = {}_0\boldsymbol{\theta}_i^{(n-1)}, \tag{4.3.6}$$

$$1 \leq j \leq N_\phi, \ i \in {}_0N(j), \ N_\theta = \sum_{j}^{N_\phi} |{}_0N(j)|.$$

Where the left-subscript 0 indicates an initial condition and the superscript between parenthesis indicates the derivatives with respect to time. Implicitly, it is assumed that $\mathcal{D}$ stands for a "smooth" system of n-th order ordinary differential equations, therefore the initial values of the first n derivatives define a unique trajectory (for a specified actuation). As a result, a unique dynamic response can be defined by the initial conditions of the system and a specified synergy. The initial conditions can be chosen arbitrarily, and are indexed by the set of integers ${}_0N(j)$ (see Fig. 4.2). The first subindex in $\boldsymbol{\theta}_{ij}(t)$, refers to the initial condition and the second subindex to the synergy of $\boldsymbol{\phi}_j(t) \in \boldsymbol{\Phi}$ used as an input to the system.

With this formulation, the problem of finding $\boldsymbol{q}(t)$ and $\boldsymbol{u}(t)$ reduces to finding the vector of combinators $\boldsymbol{a}$ and $\boldsymbol{b}$, which now can have different dimension (e.g. $\dim(b) \ll \dim(a)$).

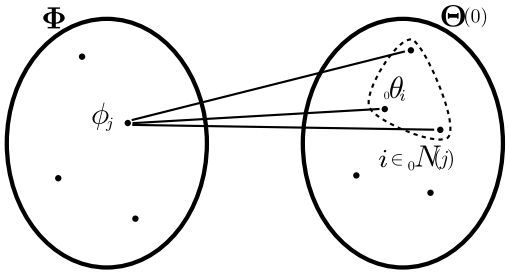

Figure 4.2: For each indexed synergy $\boldsymbol{\phi}_j$ a subset of initial conditions ${}_0\boldsymbol{\theta}_i$ is used to generate dynamic responses. The selection of initial conditions is specified by the indices $i \in {}_0N(j)$.

Chapter 5

Applications of DRD

> It is well known that a vital ingredient of success is not knowing that what you're attempting can't be done.
>
> "Equal Rites" by Terry Pratchett (1987)

Herein we present several examples where the methods described in the previous chapter are applied. Sections 5.1 and 5.2 show the use of the natural dynamics of a system to solve reaching tasks. As mentioned, this method is applicable only to nonlinear systems. Section 5.5 applies the dynamic response decomposition (DRD) method to kinematic chains and sketches a developmental framework to synthesize synergies. Altogether, we prove the feasibility of the methodology, though in some sense still rudimentary, promises interesting approaches to the control of complex nonlinear dynamical systems.

5.1 Nonlinear 1D springs

We want to solve the boundary value problem for a general nonlinear oscillator,

$$\begin{aligned} \mathcal{D}(x) &:= \ddot{x} + p(x) + g(\dot{x}) = u(t) \\ p(x) &= a_k x^k + \cdots + a_1 x^1. \\ g(\dot{x}) &= b_n \dot{x}^n + \cdots + b_1 \dot{x}^1. \\ x(0) &= 0,\ \dot{x}(0) = 0 \\ x(T) &= 1,\ \dot{x}(T) = 0. \end{aligned} \tag{5.1.1}$$

Where the parameters a_i and b_i define the physical properties of the model[1]. The boundary conditions mean that we want to bring the oscillator from its rest length with zero velocity to a state of nonzero deformation with zero velocity (i.e. a 1D reaching problem). The first step is to generate the natural dynamics of the system. Therefore we solve the initial value problem for a set of initial conditions

$$\begin{aligned} \ddot{\theta}_i + p(\theta_i) + g(\dot{\theta}_i) &= 0 \\ \theta_i(0) \doteq x_i,\ \dot{\theta}_i(0) &\doteq \dot{x}_i, \end{aligned} \tag{5.1.2}$$

[1] Strictly speaking, this model will describe an oscillator when the polynomial $p(x)$ has at least one root and this root is a stable equilibrium point. i.e $p(x_0) = 0$ and $g'(0) - 4p'(x_0) > 0$.

Where x_i and $\dot{x}_i$ are initial positions and velocities generated by

$$\begin{aligned} \boldsymbol{s}_i &= \begin{bmatrix} x_i \\ \dot{x}_i \end{bmatrix} = r\hat{e}_i,\ i = 1, \ldots, N \\ \boldsymbol{s}_i &= \begin{bmatrix} x_i \\ \dot{x}_i \end{bmatrix} = \begin{bmatrix} 1 \\ 0 \end{bmatrix} + r\hat{e}_{i-N},\ i = N+1, \ldots, 2N, \end{aligned} \tag{5.1.3}$$

where $\hat{e}_i$ are $N = 8$ (i.e. $N_\theta = 16$) preselected directions in the plane (we will use 8 directions equally distributed in the circle of radius 1) and r is a scale factor $r = 0.1$. Using the notation we defined in (1.4.7), we have the following vector constraints functions,

$$g_0(x, t_0 = 0) := \begin{bmatrix} x(0) \\ \dot{x}(0) \end{bmatrix} = \begin{bmatrix} 0 \\ 0 \end{bmatrix}, \tag{5.1.4}$$

$$g_1(x, t_1 = T) := \begin{bmatrix} x(T) - 1 \\ \dot{x}(T) \end{bmatrix} = \begin{bmatrix} 0 \\ 0 \end{bmatrix}, \tag{5.1.5}$$

using a solution of the form $x(t) = \sum c_i \theta_i(t)$ they can be written as,

$$\begin{aligned} \sum_{i=1}^{16} c_i x_i = 0, \quad \sum_{i=1}^{16} c_i \dot{x}_i = 0, \\ \sum_{i=1}^{16} c_i \theta_i(1) - 1 = 0, \quad \sum_{i=1}^{16} c_i \dot{\theta}_i(1) = 0. \end{aligned} \tag{5.1.6}$$

where we used the initial conditions of the natural dynamics explicitly.

We show solutions for the oscillators defined by the following parameters (parameters that are not specified are zero).

$$a_1 = 1, \text{ (linear oscillator without damping)} \tag{5.1.7}$$

$$a_1 = 1,\ b_1 = 0.25 \text{ (underdamped linear oscillator)} \tag{5.1.8}$$

$$a_1 = 1,\ b_1 = 4 \text{ (overdamped linear oscillator)} \tag{5.1.9}$$

$$a_1 = 1, b_2 = 0.25 \text{ (linear oscillator with quadratic damping)} \tag{5.1.10}$$

$$a_1 = 1,\ a_3 = 4,\ b_1 = 0.25 \text{ (Duffing's oscillator)} \tag{5.1.11}$$

$$\begin{aligned} a_1 = 1,\ a_2 = -2,\ a_3 = 4, \\ b_1 = 0.25 \text{ (Stiffening cubic spring with quadratic softening)} \end{aligned} \tag{5.1.12}$$

Figure 5.1 shows the resulting trajectories in phase space for all these oscillators and their inputs as function of time. Since we need to satisfy 4 boundary conditions (2 in position and 2 in velocities) with a combination of 16 coefficients (one per each solution of (5.1.2)), they are satisfied in a least square error sense (absolute error for all solvable cases is of order 10^{-16}). Observe that the linear problems (5.1.7)-(5.1.9) cannot be solved with this method and therefore the boundary conditions are not satisfied.

Since in equations (5.1.6) there are more free coefficients than boundary conditions, we can add more constraints to the system. As an example, we extend the constraints to include null acceleration at both extrema $g_0(x, 0) := [x(0), \dot{x}(0), \ddot{x}(0)] = 0$, $g_1(x, T) := [x(T) - 1, \dot{x}(T), \ddot{x}(T)] = 0$. Figure 5.2 shows the solutions under these conditions for the spring defined by (5.1.11). To ease comparison, the solution of the previous boundary value problem is shown in the same plot. As a side remark, it should be noticed that the solution with constraints on the accelerations achieves a higher maximum velocity, but the bounds of the input are lower than in the unconstrained acceleration case. Additionally, note that zero conditions on the accelerations set the final posture as an equilibrium position of the system.

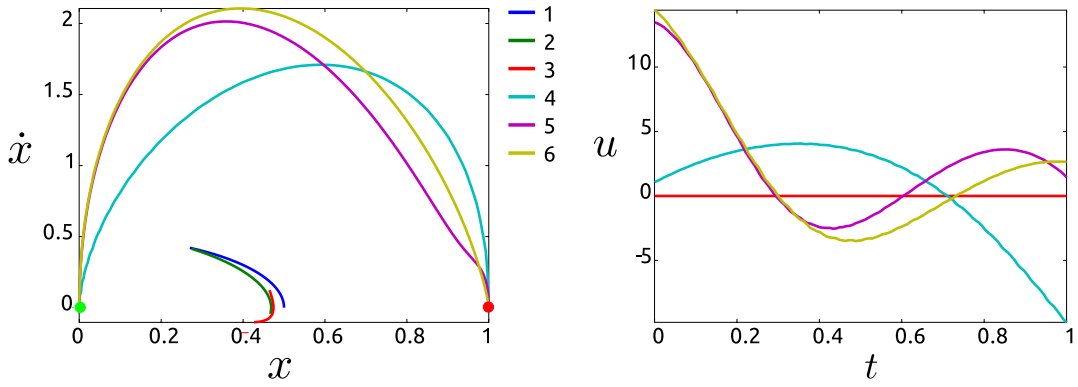

Figure 5.1: Trajectories of the oscillator in phase space and inputs as function of time for each case described in the text. Notice that with linear operators, problems (5.1.7)-(5.1.9) (1-3 in the plot) cannot be solved.

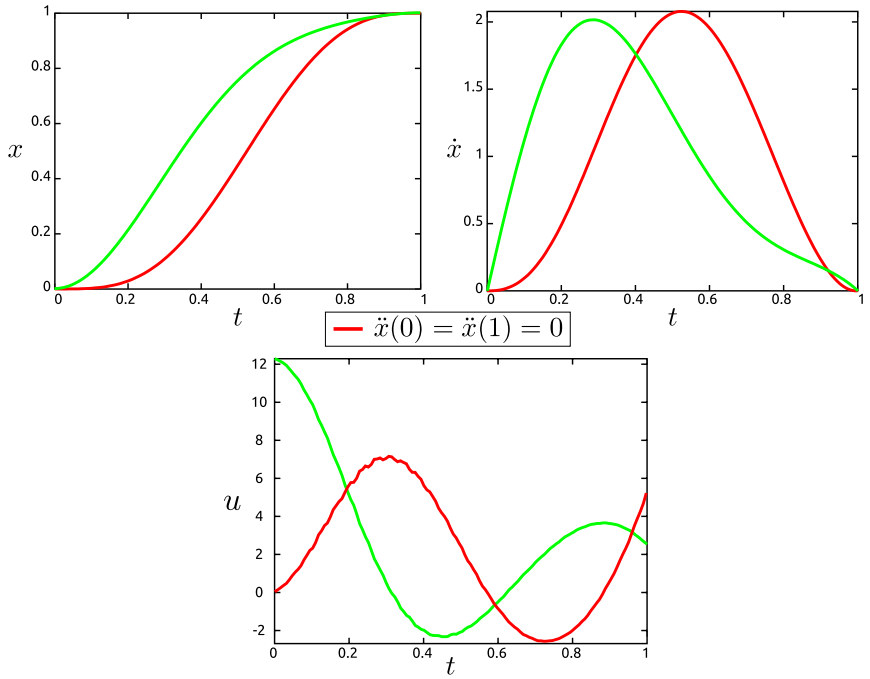

Figure 5.2: Comparison of the solutions obtained for the boundary problem defined in (5.1.1) and solutions of the same problem extended with null boundary values for the acceleration. The nonlinearity corresponds to the spring in (5.1.11).

5.1.1 Parameter dependency

We ask whether the natural dynamics of a given system is better to solve the problem than the natural dynamics of a different system. In order words we are asking whether there is an intrinsic optimal relation between the natural dynamics of the system and the solution of the given task. As can be expected we will find that the natural dynamics is by no means special to solve the problem. This can be understood by realizing that solutions of any Sturm-Lioville problem are the bases used in generalized Fourier series (e.g. trigonometric functions, Legendre polynomials, etc.), and therefore will be excellent bases to represent the trajectories $x(t)$ satisfying the point constraints in (5.1.1); nevertheless, in general, the elements of these bases are not natural dynamics of the nonlinear system.

To illustrate this, we choose $p(x)$ and $g(x)$ such that Eq. (5.1.1) becomes Duffing's equation,

$$\mathcal{D}(x, \boldsymbol{\lambda}) := \ddot{x} + w^2 x + \alpha x^3, \tag{5.1.13}$$

where $\boldsymbol{\lambda} = (w^2, \alpha)$ is the vector of parameters. In Figure 5.3 we show the natural dynamics of this system for two different parameter vectors. When the parameter α is positive, Duffing's equation represents a cubic spring that gets stiffer as it is moved off the origin. When the parameter α is negative, the spring gets softer. In this later case, it is clear that when the term $w^2 x - |\alpha| x^3 < 0$ the system is not stable anymore and trajectories will explode (for the parameters chosen this happens at $x \approx 1.1426$). When the two terms cancel each other exactly, we are in a saddle point of the dynamical system, that can be seen on the left panel of the Fig.5.3.

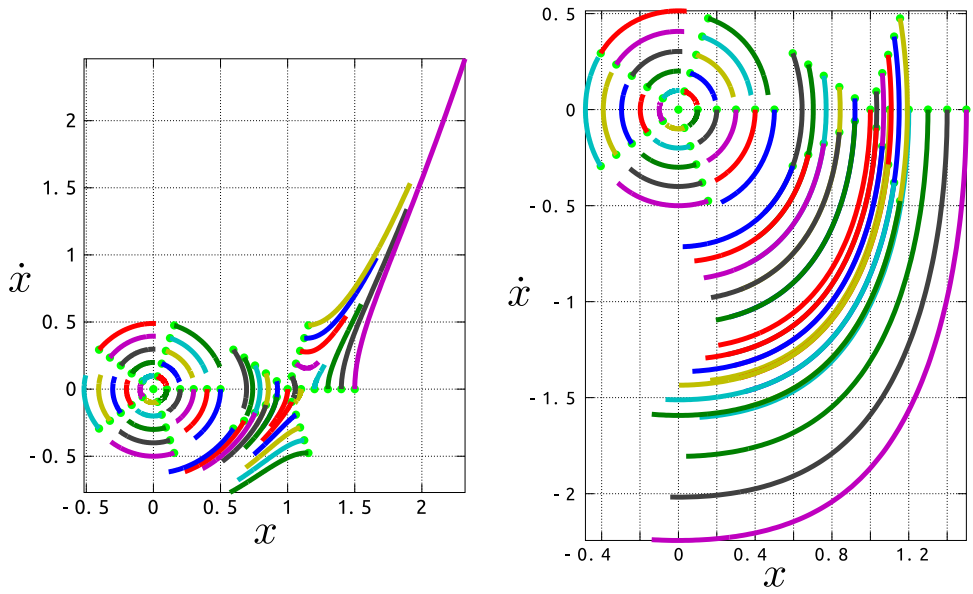

Figure 5.3: Generated orbits. Orbits of the system in (5.1.13) generated with different initial conditions and parameters $\boldsymbol{\lambda} = (1, -0.766)$ left (saddle point at $x \approx 1.1426$) and $\boldsymbol{\lambda} = (1, 1.100)$ right. The starting point of each orbit is shown with a circle.

We seek to solve the reaching task for a reference oscillator, namely $\boldsymbol{\lambda}_0 = (w^2, \alpha_0) = (1, 0.5)$. The task will be solved using the natural dynamics of other oscillators defined by $\alpha \in [-1.5, 2.5]$, including $\alpha = 0$ corresponding to the linear oscillator. First we proceed as before, we find $\theta_j(t, \boldsymbol{s}_i, \boldsymbol{\lambda}_j)$ for initial conditions around the point constraints. We repeat this

for each value of the parameter α. Secondly, we solve the reaching task for each parameter, producing a vector of coefficients $\boldsymbol{c}_j$ for the controlled trajectory $x_j = \boldsymbol{c}_j \theta_j$. Finally, we obtain and compare the inputs required to achieve these trajectories in the reference oscillator, i.e. $u_j(t) = D(x_j, \boldsymbol{\lambda}_0)$. In Figure 5.4, the trajectories $x_j(t)$ obtained by solving the problem with parameter vectors $\boldsymbol{\lambda}_j$ are shown. The trajectory obtained with the reference parameter vector $\boldsymbol{\lambda}_0$ is highlighted. The trajectory generated when the system is linear (i.e $\alpha_j = 0$) is indicated, as we know this trajectory fails to solve the boundary value problem.

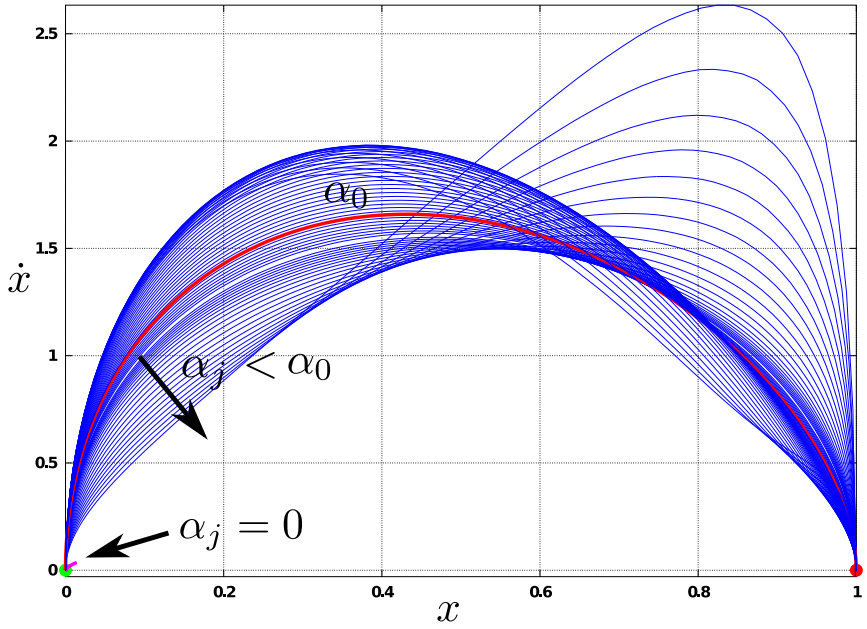

Figure 5.4: Controlled trajectories. Trajectories generated using the orbits of systems with different parameters. The trajectories obey the boundary conditions given in (5.1.1) which are shown with circles. The trajectory generated with reference parameters $\boldsymbol{\lambda}_0 = (1, 0.5)$ is highlighted. The solutions to the linear problem $\alpha_j = 0$ cannot solve the boundary value problem.

Figure 5.5 shows the L^2-norm of $u_j(t)$ as a function of the parameter α_j (solid line). The figure also shows the sum of the errors for the boundary conditions (dashed red line) and the square ℓ^2-norm of the of coefficient vector, i.e. $||\boldsymbol{c}_j|| := \sqrt{\sum_i c_{ij}^2}$ (dot-dash green line). All magnitudes are normalized to their maximum values. Observe how the norm of the coefficient vector diverge for $\alpha \to 0$, showing that the more linear the system, the harder to solve the task.

From these results we see that the natural dynamics with $\boldsymbol{\lambda} = (1, -0.5)$ generate the input $u_j(t)$ with lowest norm, and it represents the most natural solution (as understood in this thesis) to the task imposed to a system with parameters $\boldsymbol{\lambda}_0 = (1, 0.5)$. Figure 5.5 also shows that a certain degree of instability helps to reduce the norm of the inputs, but if the instability grows too large, the actuation has to work to bring the system to a rest at $x = 1$, considerably increasing the norm of the controller. Note that for this comparison we solved the problem in a LMSE sense (as was done in section 4.1.1) and no further optimization is coerced over the solution obtained. The question of which parameter set is the best to minimize $||u(t)||$ is postponed until Section 5.3.

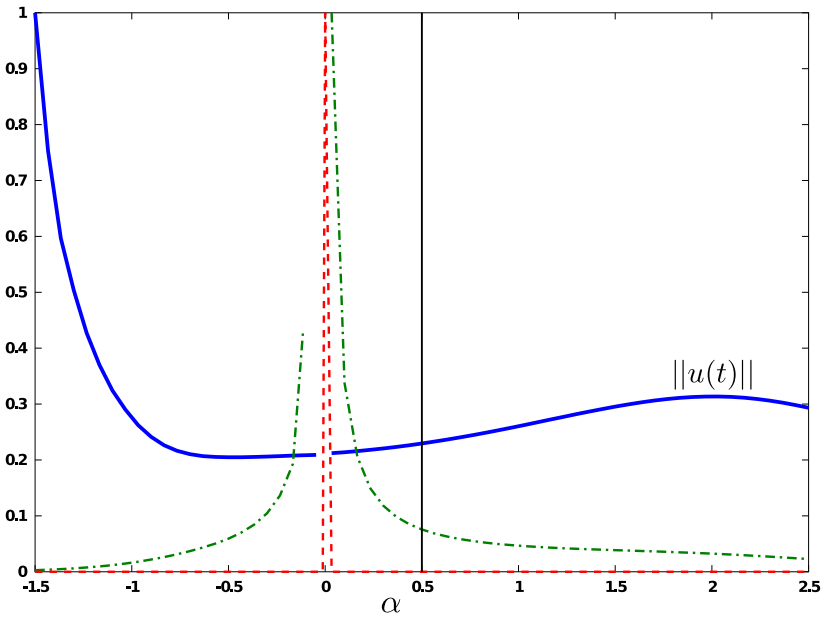

Figure 5.5: Controller norm. The L^2-norm of $u(t) = D(x_j(t))$ for different values of α_j (solid line), the sum of the errors for the boundary conditions (dashed red line), and the square ℓ^2-norm of the of weights (dot-dash green line). All magnitudes are normalized to their maximum value. The vertical black line marks the parameter value used as reference $\alpha_0 = 0.5$. The value $\alpha = 0$ corresponds to a linear problem. The divergence of the error of the solution and the coefficients norm occurs when the system is linear, showing that the metohd is only suited for nonlinear systems.

5.2 Planar arm motion

We start analyzing a 2DoF kinematic chain used to model horizontal planar reaching behavior observed in humans (see Hollerbach and Flash, 1982, for the details of the model). This model is a standard starting point for the study of reaching behaviors and it is commonly used in biomechanical studies (Muceli et al., 2010). The kinematic chain and its relation to the upper limbs is depicted in Figure 5.6.

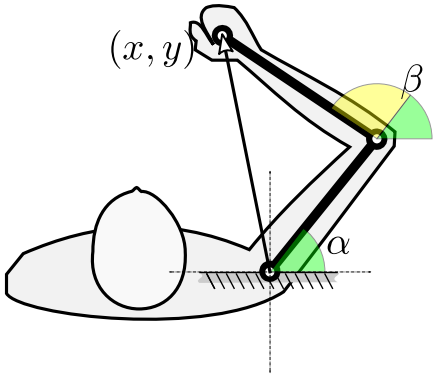

Figure 5.6: 2DoF Kinematic chain modeling the motion of a human arm in the horizontal plane. The chain is described by the angles of its joints (absolute or relative). The parameters involved are the lengths, masses and positions of the center of mass of each segment. Goals are usually described in terms of the position of the end-effector (x, y), in this case the hand.

Table 5.1: Parameter values used in the 2DoF kinematic chain. The values are derived from anthropometric scalings corresponding to a subject of height 1.80 m and weighting 80 kg(Winter, 2009).

Mass	m_1, m_2	2.18 kg, 1.75 kg
Length	l_1, l_2	0.335 m, 0.454 m
Center of mass (fraction of length)	f_1, f_2	0.59, 0.39
Joint limits (relative angles)	elbow, shoulder	$[-7°, 100°]$, $[0°, 160°]$

The chain is composed of two straight segments (arm and forearm) connected via a revolute joint with vertical axis (the elbow). One of the ends of the first segment (arm) is connected to a body of infinite mass via another revolute joint with vertical axis (the shoulder); this end of the segment is fixed respect to the laboratory's frame of reference[2]. The configuration (or posture) of the chain is described by the angle that each segment spans with respect to the abscissas (absolute joint angles). The relative elbow angle is given by the difference of the absolute angles. The shoulder and elbow joint angles are limited to the ranges $[-7°, 100°]$ and $[0°, 160°]$, respectively. The parameters used are given in Table 5.1, they where obtained using the identification methods in Winter (2009) provided by Mattia Dandola (Fundazione Santa Lucia, 2011, priv. comm.).

The goal of a reaching task is given in terms of position of the end-effector (the hand) that, for this simple case, is directly mapped one-to-one into a posture (multiple solutions are ruled out by the joint limits). We will not discuss the redundant scenario, where a single end-effector position can be achieved with multiple postures. That situation adds a layer of complexity to the formulation without adding new concepts. To deal with such a scenario,

[2]This represent a holonomic constraint that is included in the model by the use of polar coordinates.

we would obtain the representation of the task in the configuration space of the system[3], and then follow the procedure illustrated here.

We will solve the reaching of several targets distributed in a circle with center at the initial position of the hand. To apply the method described in section 4.1.1 we first need to generate the natural dynamics of the system. This set is obtained by starting the system at an initial posture with different joint angular velocities and recording the resulting trajectories. Due to the scaling property described in Sec. 1.4.5, to obtain two different trajectories in the postural space, the initial joint angular velocities vectors $\dot{\boldsymbol{q}}_0 = (\dot{\alpha}, \dot{\beta}) = \omega(\cos\theta, \sin\theta)$, must have different phases $\theta = \tan^{-1}(\dot{\beta}/\dot{\alpha})$. The modulus ω of the velocity vector only influences the time taken to go along the trajectory. The paths of the end-effector generated this way are shown in Figure 5.7.

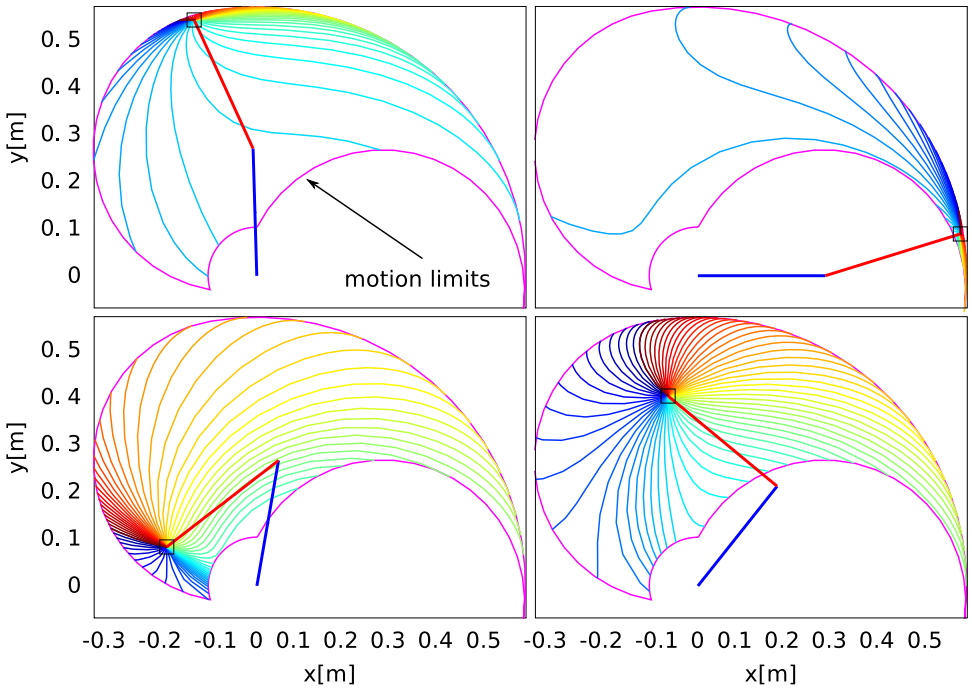

Figure 5.7: Natural dynamics of 2DoF kinematic chain. The color of the paths indicates the phase of the initial velocity vector $\dot{\boldsymbol{q}}_0$.

Once the set of natural dynamics is built, we use the pseudoinverse approach to solve the task. We use Eq. (4.1.5) with $d = 2$, since the configuration space is bidimensional. The initial and final posture should be motionless, thus we set $\dot{\boldsymbol{q}}_0 = \dot{\boldsymbol{q}}_T = 0$. Using the pseudoinverse of the alternant matrix we obtain a vector of coefficients that is used to generate the trajectory that interpolates the data. The corresponding end-effector paths are shown in Figure 5.8 together with the corresponding torques $\boldsymbol{u}(t) = \mathcal{D}(\boldsymbol{q}(t))$.

In the same plot we show the paths generated with the iterated LQG (ILQG) algorithm from (Todorov, 2005). ILQG is intended to solve general nonlinear, non-quadratic and stochastic optimization problems. For the case of a 2DoF kinematic chain we ask that the controller minimizes the square norm of the torques, the hand-target distance at the end of the trajectory, as well as the velocity of the hand at the target (see Todorov, 2005). For

[3]Such calculation can be daunting, and perhaps the redundancy could be exploited by the method presented here. We just obviate the situation in order to provide a clean and easy to grasp example of application.

several targets the difference between these paths and the ones generated with the natural dynamics is remarkably small.

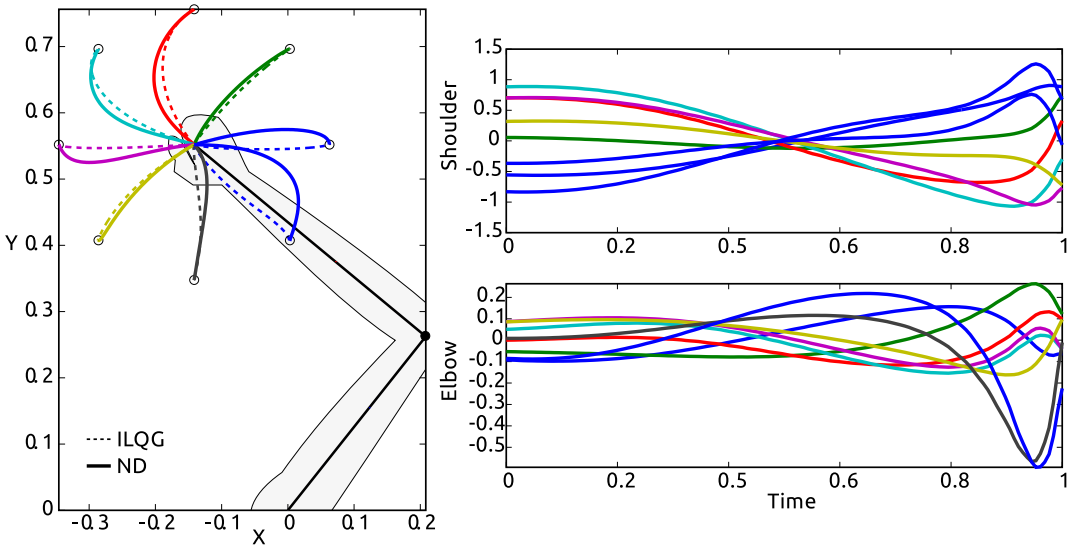

Figure 5.8: Trajectories generated by linear combinations of the natural dynamics. Target positions are depicted with hollow circles. On the left panel, the initial posture of the arm is shown in black straight lines, end-effector trajectories generated by the ILQG method are shown in dashed lines and the ones generated with the natural dynamics in solid lines (ND). On the right panel, the torques applied to the elbow and shoulder are shown as functions of time.

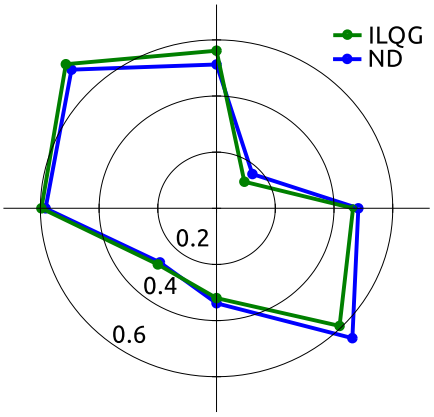

Figure 5.9: Comparison of L^2-norm of torques. For each target we show the norm of the controller generated by the ILQG method and the natural dynamics of the arm in a polar plot. The distance between the center of the plot and the data-point is the L^2-norm of the respective controller.

Figure 5.9 shows the comparison between the norms of the torques obtained with the natural dynamics and the ones obtained with the ILQG method. In the plot, the distance of each point to the origin is proportional to the L^2-norm of the torque signals. The angular position of the values in the plot coincides with the angular position of the targets in the task. Though the norm of the torque signals is comparable, we make no claim that the trajectories generated by the natural dynamics are optimal. We cannot rule out that the similarity might be due to the flatness of the cost function. However, the natural dynamics can indeed be

used to minimize the norm of the controller, this will be presented in Section 5.3, where the problem is modified to include optimality criteria in the generation of solutions.

5.3 Relation to optimal control

In Eq. (4.2.3) we found that the span of the natural dynamics (i.e. all possible linear combinations) of a nonlinear system can generate controllers that solve a given task. These controllers belong to a surface described by the span of the natural dynamics transformed by the model of the system (e.g. the body of a robot), succinctly

$$\mathcal{D}\left(\text{span}(\boldsymbol{\Theta})\right) = f\left(\boldsymbol{\Theta}\boldsymbol{a}\right) - f(\boldsymbol{\Theta})\boldsymbol{a} = \boldsymbol{u}(t). \tag{5.3.1}$$

As before, f denotes the nonlinear part of the differential operator $\mathcal{D}$ which models the agent. This relation is depicted in Figure 5.10, the span of the natural dynamics (linear combinations of its elements) are mapped into a surface that can accommodate inputs solving a given task (note that this only holds for problems with nonlinear models).

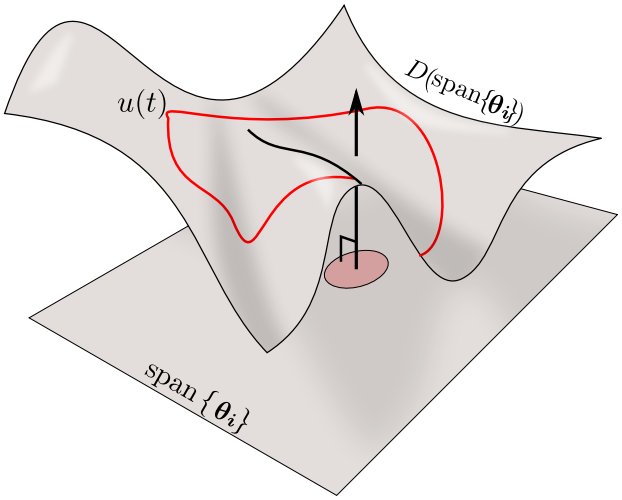

Figure 5.10: Geometric intuition for the generation of controllers using the natural dynamics. Through the action of the nonlinear differential operator $\mathcal{D}$, the trajectories generated with linear combinations of the natural dynamics are mapped to a set of functions of time used as inputs to control the system.

In this section we investigate if inputs produced in this way can fulfill optimality criteria. First, we proceed to verify that the span of natural dynamic contains optimal trajectories, i.e. we verify that optimal controllers are hosted in the transformed natural dynamics. Subsequently, we propose a simple methodology to generate optimal controllers.

5.3.1 Representing optimal trajectories

Can optimally controlled trajectories be decomposed into the natural dynamics of the system? To answer this question we project trajectories generated with optimal controllers into the natural dynamics and observe the relative error of their reconstruction, defined by

$$\text{err} = \sqrt{\frac{\int_0^T \|\boldsymbol{q}_c - \boldsymbol{q}_{\text{ND}}\|^2 \text{d}t}{\int_0^T \|\boldsymbol{q}_c\|^2 \text{d}t}}, \tag{5.3.2}$$

where $\boldsymbol{q}_c$ is the trajectory generated by an optimal controller and $\boldsymbol{q}_{\text{ND}}$ is its reconstruction using a linear combination of the natural dynamics. We study the situation for the kinematic chain described in section 5.2. Controlled trajectories reaching targets with zero velocity of the end-effector are generated using two controllers from the available scientific literature. Namely, minimum jerk control (Flash and Hogan, 1985) and iterative LQG control (Todorov, 2005).

Minimum jerk trajectories are those that minimize the norm of the jerk[4]. The jerk is defined as the rate of change of the acceleration of a parametrized curve. If $\boldsymbol{r}(t)$ denotes the vector position, the jerk is $\boldsymbol{j} = \frac{\mathrm{d}^3\boldsymbol{r}}{\mathrm{d}t^3}$. Here we use a straight minimum jerk trajectory to reach the target.

Figure 5.11 shows the errors of the reconstruction for each of the targets in Fig. 5.8. The maximum error incurred is of order 10^{-3}, meaning that in the worst case the modulus of the difference between the controlled trajectory and its reconstruction is approximately 0.1%. These results support the idea that the natural dynamics can be used to generate optimal solutions to control problems. It is noteworthy that the error we defined in (5.3.2) can be used to measure the "naturality"(in the sense used here) of a given controller. Whenever this error is not negligible, there is a component of the optimal trajectory that cannot be represented in terms of the natural dynamics, suggesting that the motion is not natural.

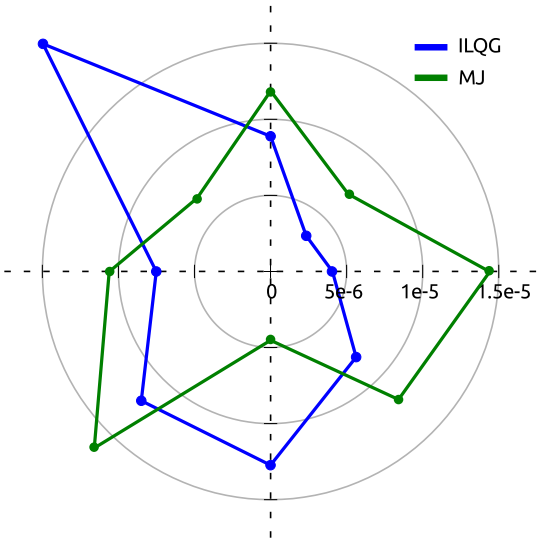

Figure 5.11: Error of the reconstructed controlled trajectories using the natural dynamics of the arm as defined in equation (5.3.2). Two controllers where used, ILQG and minimum jerk (MJ). Each point corresponds to a target in Fig 5.8.

[4]In a more recent paper, Todorov and Jordan (1998) used minimum jerk to optimize the velocity profile of a given trajectory.

5.3.2 Generating optimal inputs

The formulation of the general optimal control problem is the following: Find $\boldsymbol{u}(t)$ such that

$$\begin{gathered}\boldsymbol{u}(t) = \arg\min \int_0^T ||\boldsymbol{u}(t)||^2 \mathrm{d}t \quad \text{subject to} \\ \mathcal{D}(\boldsymbol{q}(t)) = \boldsymbol{u}(t), \\ \begin{pmatrix} \boldsymbol{q}(0) - \boldsymbol{q}_0 \\ \dot{\boldsymbol{q}}(0) - \dot{\boldsymbol{q}}_0 \end{pmatrix} = \mathbf{0} \quad \begin{pmatrix} \boldsymbol{q}(T) - \boldsymbol{q}_T \\ \dot{\boldsymbol{q}}(T) - \dot{\boldsymbol{q}}_T \end{pmatrix} = \mathbf{0}.\end{gathered} \tag{5.3.3}$$

Note that if $\boldsymbol{u}(t) \equiv 0$ the trajectory $\boldsymbol{q}(t)$ belongs to the natural dynamics of the operator. Using Eq. (5.3.1) the problem reduces to finding the vector of coefficients $\boldsymbol{a}$ such that,

$$\boldsymbol{a} = \arg\min_{\boldsymbol{a}} \int_0^T ||f\left(\boldsymbol{\Theta}(t)\boldsymbol{a}\right) - f(\boldsymbol{\Theta}(t))\boldsymbol{a}||^2 \mathrm{d}t \tag{5.3.4}$$

$$P = \begin{bmatrix} \boldsymbol{\Theta} & \dot{\boldsymbol{\Theta}} \end{bmatrix}\Big|_{0;T} \tag{5.3.5}$$

$$P\boldsymbol{a} - \begin{pmatrix} \boldsymbol{q}_0 \\ \dot{\boldsymbol{q}}_0 \\ \boldsymbol{q}_T \\ \dot{\boldsymbol{q}}_T \end{pmatrix} = \mathbf{0}. \tag{5.3.6}$$

Where P represents the alternant matrix of the natural dynamics (and its time derivatives) evaluated at $t = 0$ and $t = T$. Once the set $\boldsymbol{\Theta}$ is given, Eq. (5.3.6) can be solved using the pseudoinverse method (details were given in Section 4.1.1),

$$\boldsymbol{a} = P^+ \begin{pmatrix} \boldsymbol{q}_0 \\ \dot{\boldsymbol{q}}_0 \\ \boldsymbol{q}_T \\ \dot{\boldsymbol{q}}_T \end{pmatrix} + \left(I - P^+ P\right) \boldsymbol{w}, \tag{5.3.7}$$

and then search for the vector $\boldsymbol{w}$ that minimizes the integral in Eq. (5.3.4). The integrand can be evaluated as shown there, i.e. using only the nonlinear part of the operator, or simply as $||\mathcal{D}(\boldsymbol{\Theta}\boldsymbol{a})||^2$. The selection of the integrand depends on the computational advantage given by the evaluation of only the nonlinear part of the operator against the complete operator. The optimization procedure can alternatively be carried out using, for example, a sequential quadratic programming method[5] with Eq. (5.3.6) used as equality constraints.

Figure 5.12a shows the results of this procedure when applied to several reaching problems with zero velocities at $t = 0$ and $t = T$. The maximum error incurred in the initial and final postures is of order 10^{-6}, a highly satisfactory solution. The resulting actuations can be seen in Figure 5.12b. Note that the shoulder, as well as the elbow, have nonzero net torques at the extremes of the time interval. This means that at the beginning and at the end, the acceleration of the limbs is not zero. If the torque signals were set to zero for $t < 0 \cup t > T$, we would observe that the arm does not remain in the initial and final posture, since at those points velocity is still changing. In other words, these two postures are not equilibrium positions.

Forcing the initial and final postures to be equilibrium positions using our formulation is straight forward. We simply extend the matrix P to,

$$P = \begin{bmatrix} \boldsymbol{\Theta} & \dot{\boldsymbol{\Theta}} & \ddot{\boldsymbol{\Theta}} \end{bmatrix}\Big|_{0;T}, \tag{5.3.8}$$

[5] Function `sqp` in GNU Octave.

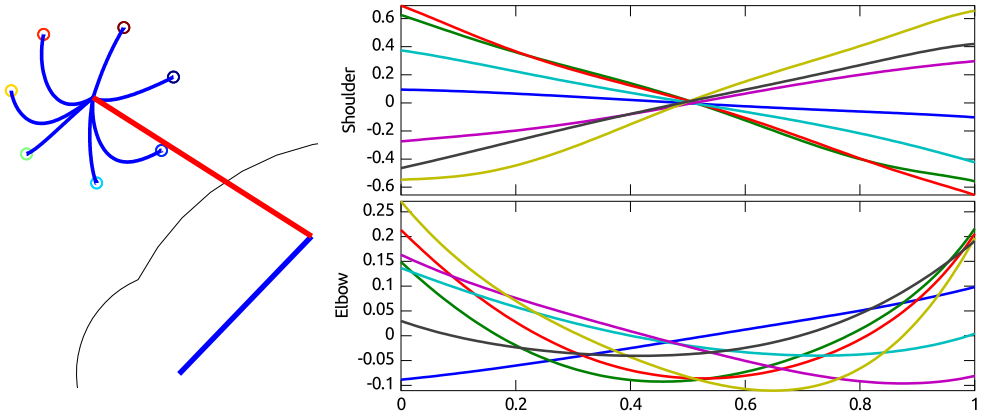

(a) End-effector trajectories (b) Torques

Figure 5.12: Optimal solutions generated by linear combinations of the natural dynamics. Target positions are depicted with hollow circles.(a) Shows the initial posture of the arm and the end-effector trajectories solving the tasks.(b) The torques applied to the elbow and shoulder are shown as functions of time.

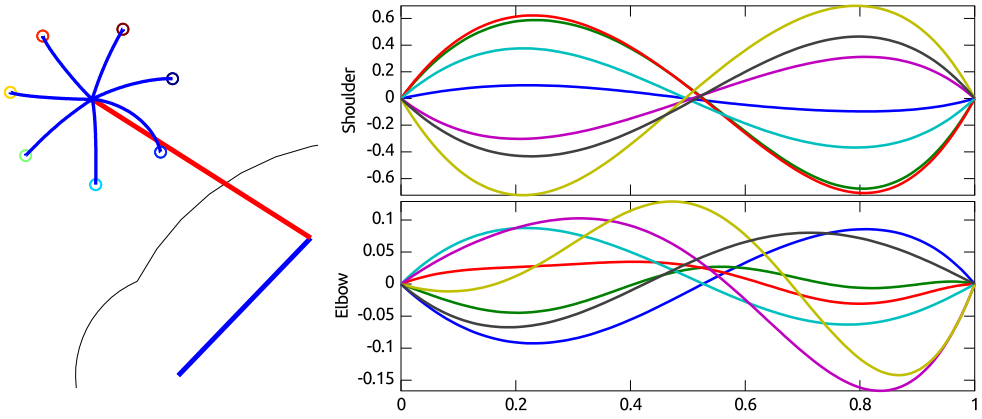

(a) End-effector trajectories (b) Torques

Figure 5.13: Optimal solutions generated by linear combinations of the natural dynamics with equilibria at end-points. Target positions are depicted with hollow circles.(a) Shows the initial posture of the arm and the end-effector trajectories solving the tasks.(b) The torques applied to the elbow and shoulder are shown as functions of time.

and solve the problem exactly as before using a data vector that includes $\ddot{\boldsymbol{q}}_0 = 0$ and $\ddot{\boldsymbol{q}}_T = 0$. The solution trajectories of the end-effector can be seen in Figure 5.13a and the corresponding torques in Figure 5.13b. The maximum error in the initial and final postures is again of order 10^{-6}. However, in this case the trajectories are closer to straight lines, i.e. the equilibria at end-points induces straighter end-effector paths.

Figure 5.14 shows a comparison of the torque activity (squared sum of the elbow and shoulder torques) in the two cases studied. Enforcing the end and initial postures as equilibrium postures, redistributes the peak activity and it can be segmented into acceleration burst (first bump) and deceleration burst (second bump).

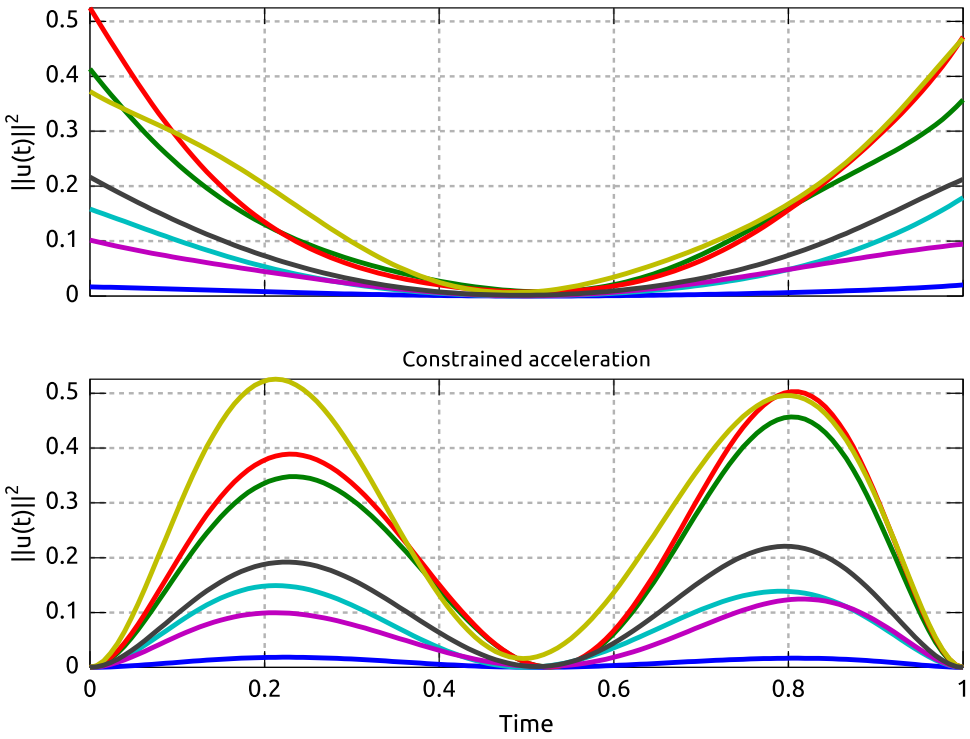

Figure 5.14: Torque activity in reaching. The modulus of the torque vector is plotted for reaching with and without acceleration constraints in the end-points. Torque activity corresponding to constrained acceleration present a bursting structure identified in biomechanical data.

The procedure presented in the previous sections relies strongly on the explicit knowledge of the operator $\mathcal{D}$. We should consider several scenarios in which the methodology takes different flavors. First, the model of the system (i.e. $\mathcal{D}$) is known and the input is given: the projection into the mapped natural dynamics can be used to measure the naturality of the controller; the method can be used as an analysis tool, as we have done in Section 5.3.1. Second, only $\mathcal{D}$ is know and we want to calculate an optimal input that solves a given task: we state an optimization problem and search for the coefficients of the linear combination of the natural dynamics that minimizes a cost function, as we did in this section. Finally, $\mathcal{D}$ is partially unknown (e.g. certain properties of the nonlinearity can be assumed) we can approximate it using an expanded set of functions (see Section 5.4). This case comes very close to system identification, and it will be discussed further in Section 5.5 in relation with the biological plausibility of the method.

5.4 *Polynomial nonlinear systems

In this section we consider the class of systems with polynomial nonlinearities. For these systems, the manifold depicted in Fig. 5.10 can be obtained explicitly. This class of system is general enough to be of practical interest; any system with smooth algebraic nonlinearities can be approximated by its polynomial expansion[6]. Additionally, we explore the possibility of using natural dynamics known a priori to generate additional natural trajectories. This last exploration can be rephrased into a mathematically provocative statement: We find solutions to a nonlinear BVP by linearly combining solutions of the nonlinear IVP problem.

Let's begin with the explixit representation of the mapped natural dynamics. We work with a system of the form,

$$\mathcal{D}(x) := L(x) + x^n = 0 \tag{5.4.1}$$

where $n > 1$ is a natural number and L is a linear differential operator (the linear part of $\mathcal{D}$). From Equation (4.2.3) and the discussion therein, the linear part of $\mathcal{D}$ can be replaced with any linear operator and the following algebraic development remains unchanged.

Lets assume that we have a set of initial conditions $X = \{x_i\}$ for which we know the set of orbits $\boldsymbol{\Theta}(T, X) = \big\{\theta_i(t) \big\backslash\, \theta_i(0) = x_i \wedge t \in [0, T]\big\}$, i.e, we know the natural dynamics of the system restricted to the set X and the time interval $[0, T]$. Now we take a linear combination of these orbits and replace it in equation (5.4.1).

$$\begin{aligned} L(x) + x^n = \boldsymbol{a}L(\boldsymbol{\Theta}) + (\boldsymbol{a}\boldsymbol{\Theta})^n = \\ = \sum_{i=1}^{N_\theta} a_i L(\theta_i) + \left(\sum_{i=1}^{N_\theta} a_i\theta_i\right)^n = \\ = \left(\sum_{i=1}^{N_\theta} a_i\theta_i\right)^n - \sum_{i=1}^{N_\theta} a_i\theta_i^n. \end{aligned} \tag{5.4.2}$$

In the last equality we used the fact that each θ_i is a solution of the homogeneous equation and got rid of the explicit linear part. We could have arrived to the same expression using directly equation (4.2.3). To expand the parenthesis we use the multinomial expansion,

$$(x_1 + \cdots + x_m)^n = \sum_{|\alpha|=n} \binom{n}{\alpha} x^\alpha. \tag{5.4.3}$$

where $\alpha = (\alpha_1, \alpha_1, \ldots, \alpha_m)$, $|\alpha| = \sum_{i=1}^m \alpha_i$ and $x^\alpha = x_1^{\alpha_1} x_2^{\alpha_2} \cdots x_m^{\alpha_m}$. The combinatorial number is defined as

$$\binom{n}{\alpha} = \frac{n!}{\alpha_1!\alpha_2! \cdots \alpha_m!}. \tag{5.4.4}$$

Using this expansion in (5.4.2) we obtain,

$$\mathcal{D}(x) = \sum_{|\alpha|=n} \binom{n}{\alpha} \boldsymbol{a}^\alpha \boldsymbol{\Theta}^\alpha - \sum_{i=1}^{N_\theta} a_i\theta_i(t)^n. \tag{5.4.5}$$

These expression can be rearranged to give

$$\mathcal{D}(x) = \sum_{|\alpha'|=n} \binom{n}{\alpha'} \boldsymbol{a}^{\alpha'} \boldsymbol{\Theta}^{\alpha'} - \sum_{i=1}^{N_\theta} \left(a_i^n - a_i\right) \theta_i(t)^n, \tag{5.4.6}$$

[6]Some nonlinear differential operators also accept approximations similar to polynomial expansions, but the procedure is mathematically involved and requires the use of notions of Fréchet and Gâteaux derivatives.

where α' are all the vectors $|\alpha| = n$ with at least two nonzero components. Equation (5.4.6) is a linear combination of $\binom{n+N_\theta-1}{n}$ functions, i.e. the set of homogeneous monomials of degree n in $\theta_i(t)$. Note that a general polynomial nonlinearity

$$f(x) = \sum_{n=2}^{K} c_n x^n, \tag{5.4.7}$$

produces linear combinations of the functions in the set

$$\boldsymbol{\Theta}^* := \bigcup_{2\leq n\leq K} \{\boldsymbol{\Theta}^\alpha,\ \forall\, \alpha \setminus |\alpha| = n\}, \tag{5.4.8}$$

i.e. all homogeneous monomials of degree $2 \leq n \leq K$. That is, smooth algebraic nonlinearities of the operator $\mathcal{D}$ could be approximated with this expanded set. Additionally, observe that the manifold depicted in Fig. 5.10 is a subset of the linear span of $\boldsymbol{\Theta}^*$. This is so, because the coefficients in Equation (5.4.6) are not completely independent from each other: they are functions of the original coefficients[7] $\boldsymbol{a}$.

5.4.1 *Generating additional natural trajectories

In Section 5.3 we minimized the norm $||\mathcal{D}(x)||^2$. When this norm is exactly zero, we have found a natural trajectory of the system. There are no such trajectories passing through arbitrary point constraints and to achieve that, we need to make sure that the norm is not zero, i.e. we need a nonzero input that forces the system through the point constraints. However, if we relax the initial point constraint (i.e we do not set its value), we can search for natural solutions that go through one arbitrary point constraint. For example, we could ask what is the natural solution of $\mathcal{D}(x) = 0$ that fulfills $x(T) = x_T$, $\dot{x}(T) = \dot{x}_T, \ldots$. In this section we will solve this problem for the system defined by the first order nonlinear differential equation

$$\mathcal{D}(x) = \dot{x} - x + 5x^3 - 4x^5. \tag{5.4.9}$$

This system has 5 fixed points, $x = \{0, \pm 0.5, \pm 1\}$, being $x = 0$ stable, $x = \pm 0.5$ unstable and $x = \pm 1$ stable again. We take 5 randomly chosen initial conditions to generate the natural dynamic set $\boldsymbol{\Theta}$. Using this set we solve the problem

$$\begin{gathered}\min_{\boldsymbol{a}} \int_0^T ||5\left[(\boldsymbol{\Theta a})^3 - \boldsymbol{\Theta}^3\boldsymbol{a}\right] - 4\left[(\boldsymbol{\Theta a})^5 - \boldsymbol{\Theta}^5\boldsymbol{a}\right]||^2 \mathrm{d}t \\ \text{such that} \quad \boldsymbol{\Theta}(T)\boldsymbol{a} = x_T.\end{gathered} \tag{5.4.10}$$

where we take 1000 values of $x_T \in [0, 1]$. The situation should be compared with the linear case, in which any linear combination of the natural dynamics is also natural. Here however, we are in the search for **some** vector $\boldsymbol{a}$ such that the linear combination is a natural solution fulfilling the given final value; in contrast to the linear case, this situation does not hold for any $\boldsymbol{a}$.

To solve the problem we apply the pseudoinverse method described in Section 4.1.1. Figure 5.15a shows the value of the integral in Eq. (5.4.10), indicating the level of non-naturality of the solution found, $x_{\text{ND}}(t) = \boldsymbol{\Theta}(t)\boldsymbol{a}$. The same figure shows the L^2-norm of difference between $x_{\text{ND}}(t)$ and the trajectory $x_r(t)$ obtained by integrating the system with

[7] The reader may find it useful to explore this using the fuction `multinom` in GNU Octave, programmed by the author of this thesis.

initial condition $\boldsymbol{\Theta}(0)\boldsymbol{a}$. This error is labeled Δx and is shown with green dashed line. Additionally, we plot the difference between the final values of these two trajectories; labeled *target error* and shown with a dashed blue line. Vertical straight lines indicate the final value of the natural dynamics used to solve the problem. The maximum non-naturality is of order 10^{-1} and is marked 3 in the figure. To give a qualitative sensation of the meaning of this non-naturality, we plot the corresponding time series in Figure 5.15b. The estimated time series is plotted using circles; $x_r(t)$ is shown with a solid red line, and thick gray lines correspond to the natural dynamics. Though the non-naturality of the solution labeled 3 is the highest, the error incurred in the time series is remarkably low.

5.5 The synergy hypothesis in biomechanics: a developmental approach

In Section 4.3 we hinted at a relation between the dynamic response decomposition (DRD) method and the synergy hypothesis in biomechanics. In this section we extend the description of this relation. The contents of this section are derived from Alessandro et al. (2012).

Humans are able to perform a wide variety of tasks with great flexibility; learning new motions is relatively easy, and adapting to new situations (e.g. change in the environment or body growth) is usually dealt with no particular effort. The strategies adopted by the central nervous system (CNS) to master the complexity of the musculoskeletal apparatus and to provide such performance are still not clear. However, it has been speculated that an underlying modular organization of the CNS may simplify the control and provide the observed adaptability. There is evidence that the muscle activity necessary to perform various tasks (e.g. running, walking, keeping balance, reaching and other combined movements) may emerge from the combination of predefined muscle patterns, the so-called *muscle synergies* (D'Avella et al., 2003). This organization seems to explain muscle activity across a wide range of combined movements (Ivanenko et al., 2005; Cappellini et al., 2006; D'Avella et al., 2006, 2008).

The scheme of muscle synergies is inherently flexible and adaptable. Different actions are encoded by specific combinations of a small number of predefined synergies; this reduces the computational effort and the time required to learn new useful behaviors. The learning scheme can be regarded as developmental since information previously acquired (i.e. synergies) can be reused to generate new behaviors(Dominici et al., 2011). Finally, improved performance can be easily achieved by introducing additional synergies. Thus, the hypothetical scheme of muscle synergies would contribute to the autonomy and the flexibility observed in biological systems, and it could inspire new methods to endow artificial agents with such desirable features. In what follows, we propose a strategy to synthesize a small set of synergies that is tailored to the task and the agent, based in the DRD method described in the preceding sections. The overall method can be interpreted in a developmental fashion; i.e. it allows the agent to autonomously synthesize and update its own synergies to increase the performance of new reaching tasks.

Other researchers in robotics and control engineering have recently proposed architectures inspired by the concept of muscle synergies. In Nori (2005) the authors derive an analytical form of a set of primitives that can drive a feedback linearized system (known analytically) to any point of its configuration space. In Alessandro and Nori (2012) the authors present a numerical method to identify synergies that optimally drive the system over a set of desired trajectories. This method does not require an analytical description of the system, and it has the advantage of assessing the quality of the synergies in task space. However, it is

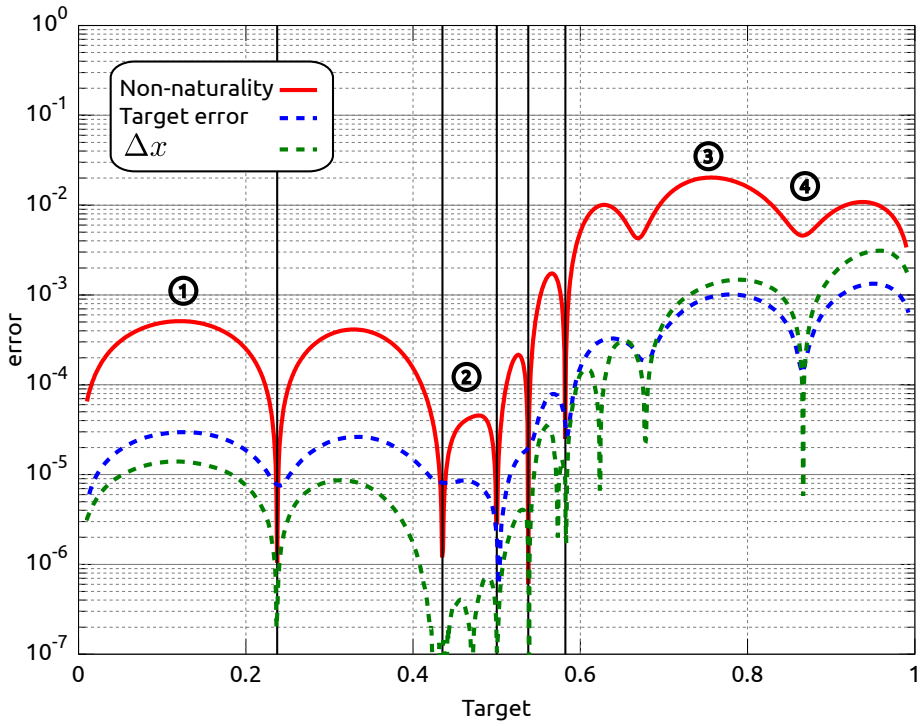

(a) Error measures

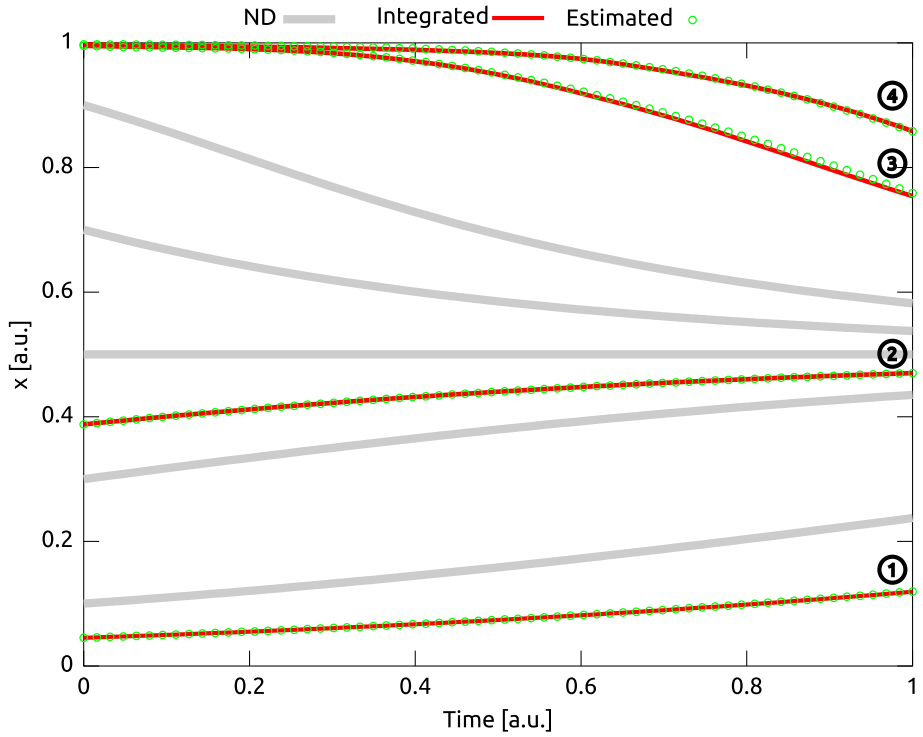

(b) Estimated time series

Figure 5.15: Generation of natural solutions.(a) Shows the non-naturality of the estimated solution in solid red line. The L^2-norm of the error of the estimated trajectory is shown with green dashed line. The error of the final value is shown with blue dashed line. Vertical straight lines indicate the final value of the natural dynamics used to solve the problem.(b) Plots several time series corresponding to the labeled regions. Solid red lines show the integrated trajectory and the estimated one is shown with circles. The natural dynamics are plotted with thick gray lines.

computationally expensive as it involves heavy optimizations. In Todorov and Ghahramani (2003) muscle synergies are identified by applying an unsupervised learning procedure to a collection of sensory-motor data obtained by actuating a robot with random signals. In Schaal et al. (2005) the architecture of the dynamic movement primitives (DMP) is proposed as a novel tool to formalize control policies in terms of predefined differential equations. Linear combinations of Gaussian functions are used as inputs to modify the attractor landscapes of these equations, and to obtain the desired control policy.

In contrast to these works, our method to synthesize synergies does not rely on feedback linearization, nor on repeated integrations of the dynamical system. The method is grounded on the input-output relation of the dynamical system, and it provides a computationally fast method to obtain the synergy combinators to solve a given task. Furthermore, our method is inherently adaptable as it allows the on-line modification of the set of synergies to accommodate to new reaching tasks.

5.5.1 Synthesis and development of synergies

The synthesis of synergies is carried on in two phases: exploration and reduction. The exploration phase consists in actuating the system with an extensive set of motor signals $\mathbf{\Phi}_0$ in order to obtain the corresponding dynamic responses (DRs, see Section 4.3) $\mathbf{\Theta}_0$. The reduction phase consists in solving a small number of point-to-point reaching tasks in kinematic space (that we call *proto-tasks*) by creating the interpolants using the elements of set $\mathbf{\Theta}_0$, as described in Section 4.1.1. These solutions are then taken as the elements of the reduced set $\mathbf{\Theta}$. Finally, the synergy set $\mathbf{\Phi}$ is computed using relation (4.3.1), i.e. inverse dynamics. As a result, there will be as many synergies as the number of proto-tasks (i.e. $N_\phi = N_\theta$). The intuition behind this reduction is that the synergies that solve the proto-tasks may capture essential features both of the task and of the dynamics of the system. Despite the non-linearities of $\mathcal{D}$, linear combination of these synergies might be useful to solve point-to-point reaching tasks that are similar (in terms of Eq. (4.1.2)) to the proto-tasks.

We need to define measures of "badness" for the different stages of the process:
Interpolation error: Measures the quality of the interpolant $\mathbf{\Theta}(t)\boldsymbol{a}$ with respect to the task. Strictly speaking, only the case of negligible errors corresponds to interpolation. A non-zero error indicates that the trajectory $\mathbf{\Theta}(t)\boldsymbol{a}$ only approximates the task

$$\underset{I}{\text{err}} = \sqrt{||\boldsymbol{q}_T - \mathbf{\Theta}(T)\boldsymbol{a}||^2 + ||\dot{\mathbf{\Theta}}(T)\boldsymbol{a}||^2}, \tag{5.5.1}$$

where $||\cdot||$ denotes the Euclidean norm, and the difference between angles are mapped to the interval $(-\pi, \pi]$.
Projection error: Measures the distance between the actuation that solves the task $\tilde{\boldsymbol{u}}(t)$, and the linear span of the synergy set $\mathbf{\Phi}$

$$\underset{P}{\text{err}} = \sqrt{\int_0^T ||\tilde{\boldsymbol{u}}(t) - \mathbf{\Phi}(t)\boldsymbol{b}||^2 \mathrm{d}t}. \tag{5.5.2}$$

Forward dynamics error: Measures the error of a trajectory $\tilde{\boldsymbol{q}}(t, \boldsymbol{\lambda})$ generated by an actuation $\mathbf{\Phi}(t)\boldsymbol{\lambda}$, in relation to the task.

$$\underset{F}{\text{err}} = \sqrt{||\tilde{\boldsymbol{q}}(T, \boldsymbol{\lambda}) - \boldsymbol{q}_T||^2 + ||\dot{\tilde{\boldsymbol{q}}}(T, \boldsymbol{\lambda}) - \dot{\boldsymbol{q}}_T||^2}. \tag{5.5.3}$$

Replacing $\tilde{\boldsymbol{q}}(t, \boldsymbol{\lambda})$, $\boldsymbol{q}_T$ and $\dot{\boldsymbol{q}}_T$ with their corresponding end-effector values provides the *forward dynamics error of the end-effector*.

The number of proto-tasks as well as their specific instances determine the quality of the synergy-based controller. To obtain good performance in a wide variety of point-to-point reaching tasks, the proto-tasks should cover relevant regions of the state space. Clearly, the higher the number of different proto-tasks, the more regions that can be reached with good performance. However, a large number of proto-tasks (and the corresponding synergies) increases the dimensionality of the controller. In order to tackle this trade-off, we propose a procedure that parsimoniously adds a new proto-task only when and where it is needed: if the performance in a new reaching task is not satisfactory, we add a new proto-task in one of the regions with highest projection error or we modify existing ones.

We apply the method just described to the simulated planar kinematic chain used in Section 5.2. In the exploration phase, we employ an extensive set of motor signals $\mathbf{\Phi}_0$ to actuate the arm model and generate the corresponding dynamic responses $\mathbf{\Theta}_0$. The panels in the first row of Fig. 5.16 show the end-effector trajectories resulting from the exploration phase. We test two different classes of motor signals: actuations that generate minimum jerk end-effector trajectories (100 signals), and low-passed uniformly random signals (90 signals). In order to evaluate the validity of the general method, we use the sets $\mathbf{\Phi}_0$ and $\mathbf{\Theta}_0$ to solve 13 different reaching tasks without performing the reduction phase. The second row of Fig. 5.16 depicts the trajectories drawn by the end-effector when the computed mixture of synergies are applied as actuations (i.e. forward dynamics of the solution). It has to be noted how the nature of the solutions (as well as that of the responses), depends on the class of actuations used. The maximum errors are reported in Table 5.2. The results are highly satisfactory for both classes of actuations, and show the validity of the method proposed. Since the reduction phase has not been performed, the dimension of the combinator vectors $\boldsymbol{a}$ and $\boldsymbol{b}$ equals the number of actuations used in the exploration.

Table 5.2: Order of the maximum errors obtained by using $\mathbf{\Phi}_0$ and $\mathbf{\Theta}_0$ (no reduction phase).

	Min. Jerk	Random
err_I	10^{-15}	10^{-15}
err_P	10^{-5}	10^{-3}
err_F	10^{-4}	10^{-3}

The objective of the reduction phase is to generate a small set of synergies and DRs that can solve desired reaching tasks effectively. This is achieved by solving a handful of proto-tasks. The number (and the instances) of these proto-tasks determines the quality of the controller. Figure 5.17 shows the projection error as a function of the number of proto-tasks. The reduction is applied to the low-passed random signal set. Initially, two targets are chosen randomly (top left panel); subsequent targets are then added on the regions characterized by higher projection error. As it can be seen, the introduction of new proto-tasks leads to better performance on wider regions of the end-effector space, and eventually the whole space can be reached with reasonable errors. In fact, the figure shows that this procedure decreases the average projection error to 10^{-3} (comparable to the performance of the whole set $\mathbf{\Phi}_0$, see Tab. 5.2) and reduces the dimension of the combinator vector to 6, a fifteen-fold reduction. This result shows that a set of "good" synergies can drastically reduce the dimensionality of the controller, while maintaining similar performance. The bottom right panel of the figure shows the forward dynamics error of the end-effector obtained with the 6 proto-tasks. Comparing this panel with the bottom left one, it can be seen that the forward dynamics error of the end-effector reproduces the distribution of the projection error, rendering the latter a good estimate for task performance.

To further demonstrate that the reduction phase we propose is not trivial, we compare

the errors resulting from the set of 6 synthesized synergies, with the errors corresponding to 100 random subsets of size 6 drawn from the set of low-passed random motor signals. Figure 5.18 shows this comparison. The task consists in reaching the 13 targets in Fig. 5.16. The boxplots correspond to the errors of the random subsets, and the filled circles to the errors of the synergies resulting from the reduction phase. Observe that, the order of the error of the reduced set is, in the worst case, equal to the error of the best random subset. However, the mean error of the reduced set is about 2 orders of magnitude lower. Therefore, the reduction by proto-tasks can produce a parsimonious set of synergies out of a extensive set of actuations. Evaluating the performance with different classes of proto-tasks (e.g. catching, hitting, via-points) is postponed to future works.

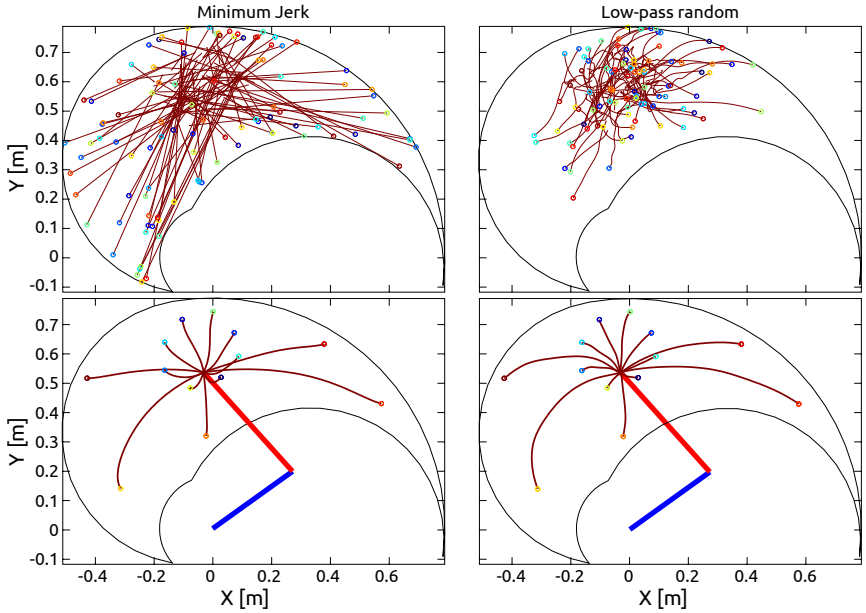

Figure 5.16: Comparison of explorations with two different classes of actuation: minimum jerk and low-passed random signal. Each panel shows the kinematic chain in it initial posture (straight segments). The limits of the end-effector are shown as the boundary in solid line.

These results justify the interpretation of the methodology as a developmental framework. Initially, the agent explores its sensory-motor system employing a variety of actuations. Later, it attempts to solve the first reaching tasks (proto-tasks), perhaps obtaining weak performance as the exploration phase may not have produced enough responses yet (see the box-plots in Fig. 5.18). If the agent finds an acceptable solution to a proto-task, it is used to generate a new synergy (populating the set $\mathbf{\Phi}$), otherwise it continues with the exploration. The failure to solve tasks of importance for its survival, could motivate the agent to include additional proto-tasks; Figure 5.17 illustrates this mechanism. As it can be seen, the development of the synergy set incrementally improves the ability of the agent to perform point-to-point reaching. Alternatively, existing proto-tasks could be modified by means of a gradient descent or other learning algorithms. In a nutshell, the methodology we propose endows the agent with the ability to autonomously generate and update a set of synergies (and dynamic responses) that solve reaching tasks effectively.

Despite the difficulty of the mathematical problem (i.e nonlinear differential operator), our method seems to generate a small set of synergies that span the space of actuations required

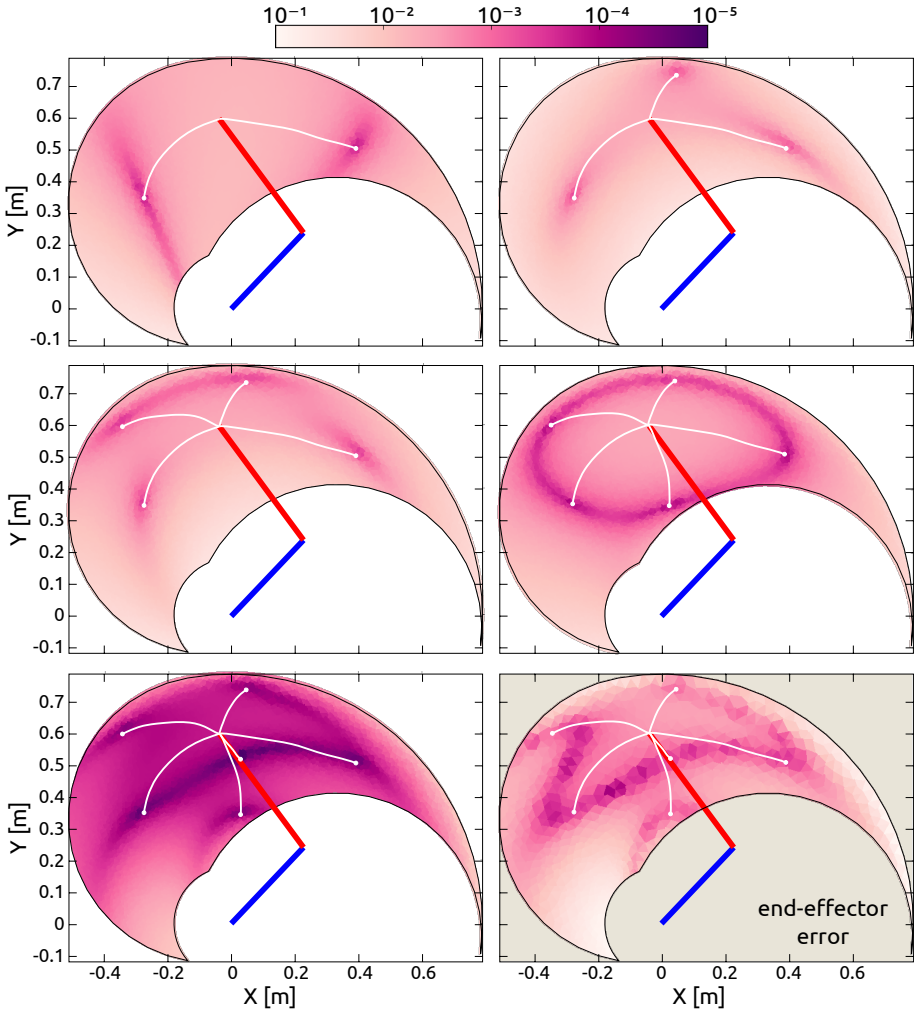

Figure 5.17: Selection of targets based on projection error. Each panel shows the kinematic chain in its initial posture (straight segments). The limits of the end-effector are the boundary of the colored regions. The color of each point indicates the projection error produced to reach a target in that position. The bottom right diagram shows the forward dynamics error of the end-effector using 6 proto-tasks (6 synergies).

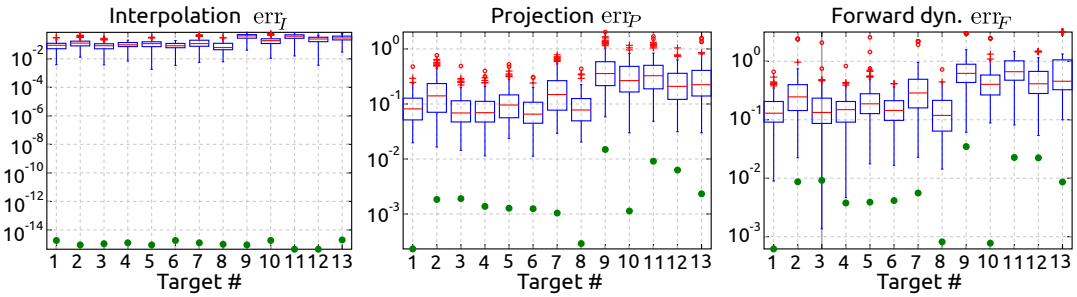

Figure 5.18: Evaluation of the reduction phase. Errors produced by subsets randomly selected from the exploration-actuations (boxplots) are compared with the errors obtained after the reduction phase (filled circles).

to solve reaching tasks. This is not a trivial result, since these synergies out-perform many other set of synergies randomly taken from the set $\mathbf{\Phi}_0$ (see Fig. 5.18). It appears as if the reduction phase builds features upon the exploration phase, that are necessary to solve new reaching tasks. To verify whether solving proto-tasks plays a fundamental role, our synergies could be compared with the principal components extracted from the exploration set.

An important aspect of our method is the relation between $\mathbf{\Theta}$ and $\mathbf{\Phi}$ (see Eq. (4.3.1)). This mapping makes explicit use of the body parameters (embedded in the differential operator $\mathcal{D}$), hence the synergies obtained can always be realized as actuations. The same cannot be said, in general, for synergies identified from numerical analyses of biomechanical data. Though some studies have verified the feasibility of extracted synergies as actuations (Neptune et al., 2009), biomechanical constraints are not explicitly included in the extraction algorithms. Additionally, Eq. (4.3.1) provides an automatic way to cope with smooth variations of the morphology of the agent. That is, both the synergies and their dynamic responses evolve together with the body. In line with Nori (2005); Alessandro and Nori (2012), these observations highlight the importance of the body in the hypothetical modularization of the CNS.

Summarizing, the current work introduces a simple framework for the generation of open loop controllers based on synergies. The framework is applied to a planar kinematic chain to solve point-to-point reaching tasks. Synergies synthesized during the reduction phase outperform hundreds of arbitrary choices of basic controllers taken from the exploration motor signals. Furthermore, our results confirm that the introduction of new synergies increases the performance of reaching tasks. Overall, this shows that our method is able to generate effective synergies, greatly reducing the dimensionality of the problem, while keeping a good performance level. Additionally, the methodology offers a developmental interpretation of the emergence of task-related synergies that could be validated experimentally.

Chapter 6

Closing remarks

> The work of the eyes is done. Go now and do the heart-work on the images imprisoned within you.
>
> "Wendung" by Rainer Maria Rilke (1914)(Translated by Stephen Mitchell)

The first part of the thesis explored the possibility of adapting parameters of robotic devices to optimize their behavior. Several robots where built to test hypothesis and results from biomechanics, thus continuing with the task of bringing together robotics and biological sciences. We demonstrated with three examples: Zürihopper, WandaX and MagE (two of them with a physical robotic counter part) how nonlinear aspects of a plant (which, as the quote from Brilliant in chapter 1 points out, are usually undesired) are accommodators for useful optimizations. Therefore, whenever a body should be suitable for morphological optimizations, it is expected and desired that it possesses nonlinear properties. With Zürihopper we described a strategy to adapt leg stiffness in order to compensate for changes in the ground compliance. Similarly, with WandaX we showed that the variable stiffness of the tail fin could be used to extract energy from external forcing due to vortices in the flow. MagE was proposed to demonstrate an alternative mechanism for underwater propulsion based on magneto-mechanical resonance. The strong nonlinear coupling between the body of MagE and the propeller can be used to encode several behaviors, e.g. turning.

We tried to emphasize (and show with results) the importance of a validated model of a parametric robot. When we are searching for the understanding of the interaction between certain aspects of a complicated robot (a flexible humanoid, for example) for which a model might be impossible to produce and validate, the construction of a simplified version of it comes handy. This simplified version should allows us to perform systematic studies of the effect of changes in body properties on the behavior observed. This parametric robot (WandaX, Zürihopper, etc.) can be modeled and should be validated. With these tools at hand the quantification and formal understanding of the phenomenon investigated, though still hard, is possible. Indeed, a careful review of a linear leg hopper showed that this simple model already presents a zoo of complex behaviors that has to be considered in order to properly understand the concept of "Walking and Running at resonance".

The methodology advocated here is (by no means) considered better than the exciting engineering approach which hurls us directly into complex machines, almost extracted from science fiction. On the contrary, it is presented as a complementary approach to those endeavors. The role of a scientist is not only to impress with new technological devices,

but also to provide understanding of the underlying principles of nature and to unify (when possible) the different explanations already provided to the observed phenomena. Quoting Richard P. Feynman

> Nature uses only the longest threads to weave her patterns, so that each small piece of her fabric reveals the organization of the entire tapestry.

In the chapters of the second part of the thesis, we showed that a nonlinear system can be used as a generator of solutions for generalized reaching problems. In the context of this thesis, the system is a model of the body of an agent, artificial or natural. We defined *natural dynamics* based on current interpretations of this notion in the fields of embodied artificial intelligence, robotics and biomechanics; and arrived at a formal definition that is closely related to the *evolution function* of a homogeneous dynamical system. Indeed, as was used here, it is the projection of the evolution function into the configuration space of the dynamical system. The formalization allowed us to developed a simple methodology, relying on pseudoinverses, to solve generalized reaching tasks: interpolation problems, that require the matching of an unknown function both in desired value, and the desired value of its time derivatives. An important property of the methodology described is that it only works when the plant is nonlinear, i.e. a nonlinear plant is controllable with a extremely simple method. This makes a nonlinear plant preferable to a linear one, whenever there is the option. It also illustrate the fact that, since most biological systems are nonlinear, linear methodologies need not be pervasive in nature as it is often suggested.

This natural dynamics interpolation machinery was applied in several scenarios, demonstrating its feasibility. Once the task is solved in configuration space, the corresponding actuation is computed using the explicit model of the agent (i.e. the differential operator $\mathcal{D}$). In fact, the natural dynamic approach for the solution of problems strongly depends on this knowledge and does not provide tools to circumvent this issue. As a consequence, to apply this method we require a process of system identification. The identification of the model could be done prior to the application of the method, or it could run in parallel with the attempts to solve tasks. Such a combination of techniques is worth exploring and may constitute a fruitful direction for future researchers.

Taking natural dynamics out of the focus of the approach, we proposed an extension of the methodology to include predefined actuations: the Dynamic Response Decomposition (DRD) method. This method includes the natural dynamic approach as a particular case, and it also offers a link to the widely accepted *synergy* hypothesis for biological motor control. The DRD method could represent the first predictive model based on such hypothesis.

The method proceeds as in the natural dynamics case, but the obtained actuations are projected into a set of preexisting synergies. It might appear that there is no particular advantage in this projection. However, as in the case of natural dynamics, if the differential operator is unknown, an identification procedure is required. The advantage of the projection is that it offers a direct mapping between two finite low-dimensional vector spaces (instead of a differential relation), and the estimation of this map may turn to be easier than estimating the differential operator $\mathcal{D}$. Furthermore, we believe that the explicit use of $\mathcal{D}$ may harm the biological plausibility of our method. In order to estimate the map $\mathcal{M}$, the input-output data generated during the exploration phase (see Section 5.5.1) could be used as a learning data-set. Further work is required to test these ideas.

The dynamic responses (including the natural dynamics) can be use to generate trajectories satisfying point constraints in the phase space of the system. Nevertheless, any set of orthonormal functions would also solve the interpolation problem; What is then, the advantage of using the dynamic responses? From the developmental robotics perspective, the responses set can be autonomously generated by a machine, while any other set of functions

would have to be pre-programmed reducing the autonomy of the agent. Furthermore, these responses can be generated from arbitrary purposeless inputs, e.g. step inputs chosen randomly or low-passed random signals. Even more, they can be generated following a procedure that minimizes its size and maximizes its generative power, as illustrated in Section 5.5.1. Additionally, physical changes of the machine are directly reflected in its dynamic responses and, *et ceteris paribus*, a simple comparison of the functions in this set will make variations of parameters evident, and perhaps help their quantification. This would be impossible if the set would have no relation to the physical substrate executing the motion. Among other possibilities, this could be exploited to drive task-dependent morphological changes that improve the performance of the system. Finally, the method illustrated so far allows us to blend the nonlinear properties of the system with a linear method (i.e. linear projections) to construct solutions without resorting to explicit linearization nor inversion of the equations modeling the system.

The current formulation of the methods does not include configuration limits explicitly (e.g. joint limits of the arm). The interpolated trajectories shown here are valid, i.e. they do not go beyond the limits, due to the lack of intricacy of the configuration space. In higher dimensions, especially when configuration space and task space are not mapped one-to-one (as in the 2DoF planar kinematic chain), this may not be the case anymore. Nevertheless, joint limits can be included by reformulating the interpolation as a constrained minimization problem. Another solution might be the creation of proto-tasks with a tree-topology, relating our method to tree based path planning algorithms(Shkolnik and Tedrake, 2009, 2011).

Altogether, the results in the second part of the thesis constitute the quantification of what hitherto was a conceptual notion: exploiting the natural dynamics of an agent to generate purposeful behavior.

6.1 Summary of contributions

The document contains the following main scientific contributions:

- Experimental and numerical quantification of the adaptation of morphology for three parametric robots (Chapter 2). Robotic counterpart of biological phenomenology reported in Ferris and Farley (1997); Ferris et al. (1998); Liao et al. (2003); Beal et al. (2006).
- Revision of the behavior of linear 1D hoppers (Chapter 3). Reviewing and complementing the results in Buchli et al. (2006); Buchli and Ijspeert (2008).
- Formal definition and direct application to several control problems of the notion of natural dynamics (Chapters 4-5).
- A new method for the autonomous generation of open loop controllers based on dynamic responses (DRD method) (Chapters 4-5).
- A developmental interpretation of the biomechanical hypothesis of synergies (Chapter 5).

Other contributions:

- Freely available programs implementing the NOFRF method (Chapter 2,`http://ailab.ifi.uzh.ch/images/stories/people/carbajal/NonLinearFrequencyResponse_1010.zip`). As reported in Lang and Billings (1997); Peng et al. (2007).

- Freely available programs implementing the DRD method (Chapter 4, https://files.ifi.uzh.ch/ailab/people/carbajal/DRD/drd.html).

During the course of the doctoral studies the following papers where published.
Used for the content of this document:

- Alessandro, C.; Carbajal, J.P.; d'Avella, A. (2012). Synthesis and Adaptation of Effective Motor Synergies for the Solution of Reaching Tasks. 12th International Conference on Adaptive Behaviour.
- Ziegler, M.; Hoffmann, M.; Carbajal, J.P.; Pfeifer, R. (2011), Varying body stiffness for aquatic locomotion, in 'Proc. IEEE Int. Conf. Robotics and Automation (ICRA)'.
- Carbajal, J.P.; Kuppuswamy, N. (2010). Magneto-mechanical actuation model for fin-based locomotion. In Design and Nature V: Comparing Design in Nature with Science and Engineering.
- Hoffmann, M.; Ziegler, M.; Carbajal, J.P. (2009). From Locomotion to Cognition. FET09, The European Future Technologies Conference and Exhibition.

Related papers with the same thematic:

- Salazar, H.R.M.; Carbajal, J.P.(2012) Can we design controllers for bipedal robots based on simple models (templates) of their dynamics? International Conference on Dynamic Walking
- Salazar, H.R.M.; Carbajal, J.P.(2011) Including the Passive Dynamics of a Compliant Leg in gait control, IEEE/RSJ International Conference on Intelligent Robots and Systems.
- Salazar, H.R.M.; Carbajal, J.P. (2011). From Walking to Running a Natural Transition in the SLIP Model Using the Hopping Gait. Int. conf. on Robotics and Biomimetics. IEEE-ROBIO.
- Salazar, H.R.M; Carbajal, J.P. (2011). Exploiting the passive dynamics of a compliant leg to develop gait transitions. Physical Review E 83, 066707.
- Kuppuswamy, N.; Carbajal, J.P. (2011). Learning a curvature dynamic model of an octopus-inspired soft robot arm using flexure sensors. FET11, The European Future Technologies Conference and Exhibition

Other publications:

- Carbajal, J.P.; Assaf, D.; Benker, E. (2011). Promoting Scientific Thinking with Robots. In 2nd International Conference on Robotics in Education (RIE 2011).
- Dermitzakis, K.; Carbajal, J.P.; Marden, J. H. (2011). Scaling laws in robotics. FET11, The European Future Technologies Conference and Exhibition.
- Castro, R.; Carbajal, J.P. (2010). Interacción con entornos dinámicos usando autómatas celulares (Interaction with dynamic environments using cellular automata). In Proceedings of the First Argentinian Workshop in Videogames.

Bibliography

Adolfsson, J. *A Study of Stability in AutoBalancing Systems using multiple Correction Masses*. Master thesis, KTH Royal Institute of Technology, 1997. URL http://www.mech.kth.se/thesis/1997/lic/lic_1997_jesper_adolfsson.pdf.

Agrawal, S. Inertia matrix singularity of planar series-chain manipulators. In *Proceedings. 1991 IEEE International Conference on Robotics and Automation*, pages 102–107. IEEE Comput. Soc. Press, 1991. ISBN 0-8186-2163-X. doi: 10.1109/ROBOT.1991.131561. URL http://ieeexplore.ieee.org/lpdocs/epic03/wrapper.htm?arnumber=131561.

Ahlborn, B. and Blake, R. W. Walking and running at resonance. *Zoology (Jena, Germany)*, 105(2):165–74, Jan. 2002. ISSN 0944-2006. doi: 10.1078/0944-2006-00057. URL http://www.ncbi.nlm.nih.gov/pubmed/16351865.

Ahlborn, B., Chapman, S., Stafford, R., and Harper, R. Experimental simulation of the thrust phases of fast-start swimming of fish. *J Exp Biol*, 200(17):2301–2312, 1997. URL http://jeb.biologists.org/cgi/content/abstract/200/17/2301.

Alben, S. On the swimming of a flexible body in a vortex street. *J. Fluid Mech.*, 635(-1): 27, Sept. 2009. ISSN 0022-1120. doi: 10.1017/S0022112009990619. URL http://www.journals.cambridge.org/abstract_S0022112009990619.

Alessandro, C. and Nori, F. Identification of synergies by optimization of trajectory tracking tasks. Submitted, 2012.

Alessandro, C., Carbajal, J. P., and Avella, A. Synthesis and Adaptation of Effective Motor Synergies for the Solution of Reaching Tasks. In Hallam, J., Balkenius, C., and Ziemke, T., editors, *12th International Conference on Adaptive Behaviour*, page 12, Odense, Denmark, 2012. Springer. URL http://arxiv.org/abs/1205.3668v1.

Alexander, R. M. Three Uses for Springs in Legged Locomotion. *The International Journal of Robotics Research*, 9(2):53–61, Apr. 1990. ISSN 0278-3649. doi: 10.1177/027836499000900205. URL http://ijr.sagepub.com/cgi/content/abstract/9/2/53.

Allen, J. and Smits, A. Energy harvesting eeL. *Journal of Fluids and Structures*, 15(3-4):629–640, Apr. 2001. ISSN 08899746. doi: 10.1006/jfls.2000.0355. URL http://www.sciencedirect.com/science/article/B6WJG-45818PJ-T/2/13abcc3c72ae071960a1f1fdec3da879http://linkinghub.elsevier.com/retrieve/pii/S0889974600903554.

Arnold, V. I. *Mathematical Methods of Classical Mechanics*, volume 60 of *Graduate texts in mathematics*. Springer, 1989. ISBN 9780387968902.

Beal, D. N., Hover, F. S., Triantafyllou, M. S., Liao, J. C., and Lauder, G. V. Passive propulsion in vortex wakes. *Journal of Fluid Mechanics*, 549(-1):385, Feb. 2006. ISSN 0022-1120. doi: 10.1017/S0022112005007925. URL http://www.journals.cambridge.org/abstract_S0022112005007925.

Bejan, A. and Marden, J. H. Unifying constructal theory for scale effects in running, swimming and flying. *The Journal of experimental biology*, 209(Pt 2):238–48, Jan. 2006. ISSN 0022-0949. doi: 10.1242/jeb.01974. URL http://www.ncbi.nlm.nih.gov/pubmed/16391346.

Benker, E. *Tunable Springs*. Bsc., Fachhochschule Nordwestschweiz, 2009. URL http://ailab.ifi.uzh.ch/images/stories/people/carbajal/BT_Emanuel_Benker_2009.pdf.

Bhat, S. P. and Bernstein, D. S. Second-Order Systems with Singular Mass Matrix and an Extension of Guyan Reduction. *SIAM Journal on Matrix Analysis and Applications*, 17 (3):649, 1996. ISSN 08954798. doi: 10.1137/S0895479894268269. URL http://link.aip.org/link/SJMAEL/v17/i3/p649/s1&Agg=doi.

Biewener, A. A. and Daley, M. A. Unsteady locomotion: integrating muscle function with whole body dynamics and neuromuscular control. *The Journal of experimental biology*, 210(Pt 17):2949–60, Sept. 2007. ISSN 0022-0949. doi: 10.1242/jeb.005801. URL http://www.pubmedcentral.nih.gov/articlerender.fcgi?artid=2651961&tool=pmcentrez&rendertype=abstract.

Bongard, J. C. How Evolution Shapes the Way Roboticists Think. *Procedia Computer Science*, 7:8–10, Jan. 2011. ISSN 18770509. doi: 10.1016/j.procs.2011.12.004. URL http://linkinghub.elsevier.com/retrieve/pii/S1877050911006697.

Brilliant, M. B. Theory of the analysis of nonlinear systems, 1958. URL http://dspace.mit.edu/bitstream/handle/1721.1/4476/RLE-TR-345-04739002.pdf?sequence=1.

Buchli, J. and Ijspeert, A. J. Self-organized adaptive legged locomotion in a compliant quadruped robot. *Autonomous Robots*, 25(4):331, 2008. doi: 10.1007/s10514-008-9099-2.

Buchli, J., Iida, F., and Ijspeert, A. J. Finding Resonance: Adaptive Frequency Oscillators for Dynamic Legged Locomotion. In *2006 IEEE/RSJ International Conference on Intelligent Robots and Systems*, pages 3903–3909. IEEE, Oct. 2006. ISBN 1-4244-0258-1. doi: 10.1109/IROS.2006.281802. URL http://ieeexplore.ieee.org/lpdocs/epic03/wrapper.htm?arnumber=4059016.

Buescu, J., Graça, D. S., and Zhong, N. Computability and Dynamical Systems. In Peixoto, M. M., Pinto, A. A., and Rand, D. A., editors, *Dynamics, Games and Science I*, volume 1 of *Springer Proceedings in Mathematics*, pages 169–181. Springer Berlin Heidelberg, 2011. ISBN 978-3-642-11456-4. URL http://dx.doi.org/10.1007/978-3-642-11456-4_11.

Burdet, E., Osu, R., Franklin, D. W., Milner, T. E., and Kawato, M. The central nervous system stabilizes unstable dynamics by learning optimal impedance. *Nature*, 414(6862):446–9, Nov. 2001. ISSN 0028-0836. doi: 10.1038/35106566. URL http://dx.doi.org/10.1038/35106566http://www.nature.com/nature/journal/v414/n6862/suppinfo/414446a0_S1.htmlhttp://www.ncbi.nlm.nih.gov/pubmed/11719805.

Bush, V. The differential analyzer. A new machine for solving differential equations. *Journal of the Franklin Institute*, 212(4):447–488, Oct. 1931. ISSN 00160032. doi: 10.1016/S0016-0032(31)90616-9. URL http://www.sciencedirect.com/science/

article/pii/S0016003231906169http://linkinghub.elsevier.com/retrieve/pii/S0016003231906169.

Candes, E., Romberg, J., and Tao, T. Robust uncertainty principles: exact signal reconstruction from highly incomplete frequency information. *IEEE Transactions on Information Theory*, 52(2):489–509, Feb. 2006. ISSN 0018-9448. doi: 10.1109/TIT.2005.862083. URL http://ieeexplore.ieee.org/xpl/freeabs_all.jsp?arnumber=1580791.

Canuto, C., Hussaini, Y., and Quarteroni, A. *Spectral Methods: Fundamentals in Single Domains*. Scientific Computation. Springer-Verlag, 2006. ISBN 9783540307266.

Cappellini, G., Ivanenko, Y. P., Poppele, R. E., and Lacquaniti, F. Motor patterns in human walking and running. *Journal of neurophysiology*, 95(6):3426–37, June 2006. ISSN 0022-3077. doi: 10.1152/jn.00081.2006. URL http://www.ncbi.nlm.nih.gov/pubmed/16554517.

Carbajal, J. P. and Kuppuswamy, N. Magneto-mechanical actuation model for fin-based locomotion. In Brebbia, C. A. and Carpi, A., editors, *Design and Nature V: Comparing Design in Nature with Science and Engineering*, pages 375–387, Ashurst Lodge, Southampton, UK, 2010. WIT Press.

Carbajal, J. P., Bayma, R., Ziegler, M., and Lang, Z.-Q. Modeling and frequency domain analysis of nonlinear compliant joints for a passive dynamic swimmer. *Arxiv - Preprint*, Aug. 2011. URL http://arxiv.org/abs/1108.3206.

Cavagna, G. a. and Legramandi, M. a. The bounce of the body in hopping, running and trotting: different machines with the same motor. *Proceedings. Biological sciences / The Royal Society*, 276(1677):4279–85, Dec. 2009. ISSN 1471-2954. doi: 10.1098/rspb.2009.1317. URL http://www.ncbi.nlm.nih.gov/pubmed/19759034.

Cheng, J.-Y., Pedley, T. J., and Altringham, J. D. A continuous dynamic beam model for swimming fish. *Philosophical Transactions of the Royal Society B: Biological Sciences*, 353 (1371):981–997, June 1998. ISSN 0962-8436. doi: 10.1098/rstb.1998.0262. URL http://rstb.royalsocietypublishing.org/cgi/doi/10.1098/rstb.1998.0262.

Cottone, F., Vocca, H., and Gammaitoni, L. Nonlinear Energy Harvesting. *Physical Review Letters*, 102(8):80601, Feb. 2009. ISSN 0031-9007. doi: 10.1103/PhysRevLett.102.080601. URL http://link.aps.org/doi/10.1103/PhysRevLett.102.080601.

Cottone, F., Mincigrucci, R., Neri, I., Orfei, F., Travasso, F., Vocca, H., and Gammaitoni, L. Nonlinear Kinetic Energy Harvesting. *Procedia Computer Science*, 7:190–191, Jan. 2011. ISSN 18770509. doi: 10.1016/j.procs.2011.09.048. URL http://linkinghub.elsevier.com/retrieve/pii/S1877050911006089.

Crawford, E. C. Mechanical aspects of panting in dogs. *Journal of applied physiology*, 17:249–51, Mar. 1962. ISSN 0021-8987. URL http://www.ncbi.nlm.nih.gov/pubmed/13882058.

D'Avella, A., Saltiel, P., and Bizzi, E. Combinations of muscle synergies in the construction of a natural motor behavior. *Nature neuroscience*, 6(3):300–8, Mar. 2003. ISSN 1097-6256. doi: 10.1038/nn1010. URL http://www.ncbi.nlm.nih.gov/pubmed/12563264.

D'Avella, A., Portone, A., Fernandez, L., and Lacquaniti, F. Control of fast-reaching movements by muscle synergy combinations. *The Journal of neuroscience : the official journal of the Society for Neuroscience*, 26(30):7791–810, July 2006. ISSN 1529-2401. doi: 10.1523/JNEUROSCI.0830-06.2006. URL http://www.ncbi.nlm.nih.gov/pubmed/16870725.

D'Avella, A., Fernandez, L., Portone, A., and Lacquaniti, F. Modulation of phasic and tonic muscle synergies with reaching direction and speed. *Journal of neurophysiology*, 100(3):1433–54, Sept. 2008. ISSN 0022-3077. doi: 10.1152/jn.01377.2007. URL http://www.ncbi.nlm.nih.gov/pubmed/18596190.

Deng, X. and Avadhanula, S. Biomimetic Micro Underwater Vehicle with Oscillating Fin Propulsion: System Design and Force Measurement. In *Proceedings of the 2005 IEEE International Conference on Robotics and Automation*, pages 3312–3317. IEEE, 2005. ISBN 0-7803-8914-X. doi: 10.1109/ROBOT.2005.1570621. URL http://ieeexplore.ieee.org/lpdocs/epic03/wrapper.htm?arnumber=1570621.

Desoer, C. A. and Vidyasagar, M. *Feedback Systems: Input-Output Properties*, volume 55 of *Classics in Applied Mathematics*. Society for Industrial and Applied Mathematics, unabridged edition, 2009. ISBN 9780898716702.

Deutsch, D. Quantum Theory, the Church-Turing Principle and the Universal Quantum Computer. *Proceedings of the Royal Society A: Mathematical, Physical and Engineering Sciences*, 400(1818):97–117, July 1985. ISSN 1364-5021. doi: 10.1098/rspa.1985.0070. URL http://rspa.royalsocietypublishing.org/cgi/doi/10.1098/rspa.1985.0070.

Dickinson, M. H., Farley, C. T., Full, R. J., Koehl, M. A. R., Kram, R., and Lehman, S. How Animals Move: An Integrative View. *Science*, 288(5463):100–106, Apr. 2000. ISSN 00368075. doi: 10.1126/science.288.5463.100. URL http://www.sciencemag.org/cgi/doi/10.1126/science.288.5463.100.

Dominici, N., Ivanenko, Y. P., Cappellini, G., D'Avella, A., Mondì, V., Cicchese, M., Fabiano, A., Silei, T., Di Paolo, A., Giannini, C., Poppele, R. E., and Lacquaniti, F. Locomotor primitives in newborn babies and their development. *Science (New York, N.Y.)*, 334 (6058):997–9, Nov. 2011. ISSN 1095-9203. doi: 10.1126/science.1210617. URL http://www.ncbi.nlm.nih.gov/pubmed/22096202.

Douglass, J. K., Wilkens, L., Pantazelou, E., and Moss, F. Noise enhancement of information transfer in crayfish mechanoreceptors by stochastic resonance. *Nature*, 365(6444):337–340, 1993. doi: 10.1038/365337a0.

Eldredge, J. D. A Reconciliation of Viscous and Inviscid Approaches to Computing Locomotion of Deforming Bodies. *Experimental Mechanics*, 2009. doi: 10.1007/s11340-009-9275-0.

Eldredge, J. D. and Pisani, D. Passive locomotion of a simple articulated fish-like system in the wake of an obstacle. *Journal of Fluid Mechanics*, 607, 2008. doi: 10.1017/S0022112008002218.

Ellner, S. P. and Guckenheimer, J. Building Dynamical Models. In *Dynamic Models in Biology*, chapter 9, pages 247–321. Princeton University Press, 2006.

Epps, B. P., Valdivia y Alvarado, P., Youcef-Toumi, K., and Techet, A. H. Swimming performance of a biomimetic compliant fish-like robot. *Experiments in Fluids*, 47(6):927–939, June 2009. ISSN 0723-4864. doi: 10.1007/s00348-009-0684-8. URL http://www.springerlink.com/index/10.1007/s00348-009-0684-8.

Farley, C. Leg stiffness and stride frequency in human running. *Journal of Biomechanics*, 29(2):181–186, Feb. 1996. ISSN 00219290. doi: 10.1016/0021-9290(95)00029-1. URL http://linkinghub.elsevier.com/retrieve/pii/0021929095000291.

Farley, C. T., Glasheen, J., and McMahon, T. A. Running springs: speed and animal size. *The Journal of experimental biology*, 185:71–86, Dec. 1993. ISSN 0022-0949. URL http://www.ncbi.nlm.nih.gov/pubmed/8294853.

Farley, C. T., Houdijk, H. H., Van Strien, C., and Louie, M. Mechanism of leg stiffness adjustment for hopping on surfaces of different stiffnesses. *Journal of applied physiology (Bethesda, Md. : 1985)*, 85(3):1044–55, Sept. 1998. ISSN 8750-7587. URL http://www.ncbi.nlm.nih.gov/pubmed/9729582.

Ferris, D. P. and Farley, C. T. Interaction of leg stiffness and surfaces stiffness during human hopping. *Journal of applied physiology (Bethesda, Md. : 1985)*, 82(1):15–22; discussion 13–4, Jan. 1997. ISSN 8750-7587. URL http://www.ncbi.nlm.nih.gov/pubmed/9029193.

Ferris, D. P., Louie, M., and Farley, C. T. Running in the real world: adjusting leg stiffness for different surfaces. *Proceedings. Biological sciences / The Royal Society*, 265(1400):989–94, June 1998. ISSN 0962-8452. doi: 10.1098/rspb.1998.0388. URL http://www.pubmedcentral.nih.gov/articlerender.fcgi?artid=1689165&tool=pmcentrez&rendertype=abstract.

Flash, T. and Hogan, N. The coordination of arm movements: an experimentally confirmed mathematical model. *The Journal of neuroscience : the official journal of the Society for Neuroscience*, 5(7):1688–703, July 1985. ISSN 0270-6474. URL http://www.ncbi.nlm.nih.gov/pubmed/4020415.

Funaro, D. *Polynomial approximation of differential equations*, volume 8 of *Lecture notes in physics: Monographs*. Springer-Verlag, Heidelberg, 1992. ISBN 9783540552307. URL http://cdm.unimo.it/home/matematica/funaro.daniele/bube.htm.

Gammaitoni, L., Marchesoni, F., and Santucci, S. Stochastic Resonance as a Bona Fide Resonance. *Phys. Rev. Lett.*, 74(7):1052–1055, Feb. 1995. doi: 10.1103/PhysRevLett.74.1052.

Geyer, H. *Simple models of legged locomotion based on compliant leg behavior*. Phd, Friedrich-Schiller-Universität Jena, 2005. URL http://www.cs.cmu.edu/~hgeyer/Publications/Geyer05PhDThesis.pdf.

Ghigliazza, R. and Holmes, P. Towards a neuromechanical model for insect locomotion: hybrid dynamical systems. *Regular and Chaotic Dynamics*, 10(2):193–225, 2005. ISSN 1560-3547. doi: 10.1070/RD2005v010n02ABEH000311. URL http://www.turpion.org/php/paper.phtml?journal_id=rd&paper_id=311.

Goge, D., Sinapius, M., Fullekrug, U., and Link, M. Detection and description of non-linear phenomena in experimental modal analysis via linearity plots. *International Journal of Non-Linear Mechanics*, 40(1):27–48, Jan. 2005. ISSN 00207462. doi: 10.1016/j.ijnonlinmec.2004.05.011. URL http://linkinghub.elsevier.com/retrieve/pii/S0020746204000630.

Goldstein, H., Poole, C. P., and Safko, J. L. *Classical Mechanics*. Addison-Wesley, San Francisco, 3 edition, 2002. ISBN 9780201657029.

Guckenheimer, J. and Johnson, S. Planar Hybrid Systems. *Hybrid Systems II*, pages 202–225, 1995. URL http://www.springerlink.com/content/f523813t15560671/.

Harper, K., Berkemeier, M., and Grace, S. Decreasing the energy costs of swimming robots through passive elastic elements. In *Proceedings of International Conference on Robotics and Automation*, volume 3, pages 1839–1844. Robotics and Automation, 1997. Proceedings., 1997 IEEE International Conference on, 1997. ISBN 0-7803-3612-7. doi: 10.1109/ROBOT.1997.619055. URL http://ieeexplore.ieee.org/lpdocs/epic03/wrapper.htm?arnumber=619055.

Hauert, S., Zufferey, J.-C., and Floreano, D. Reverse-engineering of artificially evolved controllers for swarms of robots. In *2009 IEEE Congress on Evolutionary Computation*, pages 55–61. IEEE, May 2009. ISBN 978-1-4244-2958-5. doi: 10.1109/CEC.2009.4982930. URL http://ieeexplore.ieee.org/lpdocs/epic03/wrapper.htm?arnumber=4982930.

Hauser, H., Ijspeert, A. J., Füchslin, R. M., Pfeifer, R., and Maass, W. Towards a theoretical foundation for morphological computation with compliant bodies. *Biological Cybernetics*, 105(5-6):355–370, 2012. doi: 10.1007/s00422-012-0471-0.

Hollerbach, J. M. and Flash, T. Dynamic interactions between limb segments during planar arm movement. *Biological Cybernetics*, 44(1):67–77, May 1982. ISSN 0340-1200. doi: 10.1007/BF00353957. URL http://www.springerlink.com/index/10.1007/BF00353957.

Holmes, P. Ninety plus thirty years of Nonlinear Dynamics: less is more and more is different. *I. J. Bifurcation and Chaos*, 15(9):2703–2716, 2005. doi: 10.1142/S0218127405013678. URL http://dx.doi.org/10.1142/S0218127405013678.

Holmes, P. and Rand, D. The bifurcations of duffing's equation: An application of catastrophe theory. *Journal of Sound and Vibration*, 44(2):237–253, Jan. 1976. ISSN 0022460X. doi: 10.1016/0022-460X(76)90771-9. URL http://linkinghub.elsevier.com/retrieve/pii/0022460X76907719.

Ivanenko, Y. P., Cappellini, G., Dominici, N., Poppele, R. E., and Lacquaniti, F. Coordination of locomotion with voluntary movements in humans. *The Journal of neuroscience : the official journal of the Society for Neuroscience*, 25(31):7238–53, Aug. 2005. ISSN 1529-2401. doi: 10.1523/JNEUROSCI.1327-05.2005. URL http://www.ncbi.nlm.nih.gov/pubmed/16079406.

J. C. Gibbings. *Dimensional Analysis*. Springer, 1st edition, 2011. ISBN 9781849963169. URL http://www.springer.com/mathematics/analysis/book/978-1-84996-316-9.

Johnson, C. *Numerical Solution of Partial Differential Equations by the Finite Element Method*. Dover books on mathematics. Dover Publications, 2009. ISBN 9780486469003.

Joint Committee for Guides in Metrology. Evaluation of measurement data – Guide to the expression of uncertainty in measurement. Technical Report September, Joint Committee for Guides in Metrology, 2008. URL http://www.bipm.org/utils/common/documents/jcgm/JCGM_100_2008_E.pdf.

Jürgen Appell, Espedito De Pascale, and Alfonso Vignoli. *Nonlinear spectral theory*, volume 10 of *De Gruyter series in nonlinear analysis and applications*. Walter de Gruyter, 2004. ISBN 3110181436, 9783110181432.

Kanso, E. Swimming due to transverse shape deformations. *Journal of Fluid Mechanics*, 631:127, July 2009. ISSN 0022-1120. doi: 10.1017/S0022112009006806. URL http://www.journals.cambridge.org/abstract_S0022112009006806.

Kanso, E. and Newton, P. K. Passive locomotion via normal-mode coupling in a submerged spring-mass system. *Journal of Fluid Mechanics*, 641:205, Dec. 2009. ISSN 0022-1120. doi: 10.1017/S0022112009992357. URL http://www.journals.cambridge.org/abstract_S0022112009992357.

Kawato, M. Internal models for motor control and trajectory planning. *Current Opinion in Neurobiology*, 9(6):718–727, Dec. 1999. ISSN 09594388. doi: 10.1016/S0959-4388(99)00028-8. URL http://www.sciencedirect.com/science/article/pii/S0959438899000288http://linkinghub.elsevier.com/retrieve/pii/S0959438899000288.

Kelly, S. *Fundamentals of Mechanical Vibrations*. McGraw-Hill International Editions. McGraw-Hill, 2000. ISBN 9780071163255.

Kerschen, G., Peeters, M., Golinval, J., and Vakakis, A. F. Nonlinear normal modes, Part I: A useful framework for the structural dynamicist. *Mechanical Systems and Signal Processing*, 23(1):170, 2009. doi: 10.1016/j.ymssp.2008.04.002.

Kokshenev, V. B. Key principle of the efficient running, swimming, and flying. *EPL (Europhysics Letters)*, 90(4):48005, May 2010. ISSN 0295-5075. doi: 10.1209/0295-5075/90/48005. URL http://stacks.iop.org/0295-5075/90/i=4/a=48005?key=crossref.188689086692d0a5e7eb4ec357e1f214.

Lang, Z.-Q. and Billings, S. A. Output frequencies of nonlinear systems. *International Journal of Control*, 67(5):713–730, 1997. ISSN 0020-7179. doi: 10.1080/002071797223965. URL http://www.informaworld.com/openurl?genre=article&doi=10.1080/002071797223965&magic=crossref||D404A21C5BB053405B1A640AFFD44AE3.

Lang, Z.-Q. and Billings, S. A. Energy transfer properties of non-linear systems in the frequency domain. *International Journal of Control*, 78(5):345–362, Mar. 2005. ISSN 0020-7179. doi: 10.1080/00207170500095759. URL http://www.informaworld.com/openurl?genre=article&doi=10.1080/00207170500095759&magic=crossref||D404A21C5BB053405B1A640AFFD44AE3.

Lang, Z.-Q., Billings, S. A., Yue, R., and Li, J. Output frequency response function of nonlinear Volterra systems. *Automatica*, 43:805 – 816, 2007. doi: 10.1016/j.automatica.2006.11.013.

Lauder, G. V., Anderson, E. J., Tangorra, J., and Madden, P. G. A. Fish biorobotics: kinematics and hydrodynamics of self-propulsion. *The Journal of experimental biology*, 210(Pt 16):2767–80, Aug. 2007. ISSN 0022-0949. doi: 10.1242/jeb.000265. URL http://www.ncbi.nlm.nih.gov/pubmed/17690224.

Liao, J. C. A review of fish swimming mechanics and behaviour in altered flows. *Philosophical transactions of the Royal Society of London. Series B, Biological sciences*, 362(1487):1973–93, Nov. 2007. ISSN 0962-8436. doi: 10.1098/rstb.2007.2082. URL http://www.pubmedcentral.nih.gov/articlerender.fcgi?artid=2442850&tool=pmcentrez&rendertype=abstract.

Liao, J. C., Beal, D. N., Lauder, G. V., and Triantafyllou, M. S. Fish exploiting vortices decrease muscle activity. *Science (New York, N.Y.)*, 302(5650):1566–9, Nov. 2003. ISSN 1095-9203. doi: 10.1126/science.1088295. URL http://www.ncbi.nlm.nih.gov/pubmed/14645849.

Ljung, L. *System identification: theory for the user*. Prentice Hall PTR, 2nd editio edition, 1999. ISBN 9780136566953. URL http://books.google.com/books?id=nHFoQgAACAAJ.

Luo, A. A quantitative stability and bifurcation analyses of the generalized duffing oscillator with strong nonlinearity. *Journal of the Franklin Institute*, 334(3):447–459, May 1997. ISSN 00160032. doi: 10.1016/S0016-0032(96)00089-0. URL http://linkinghub.elsevier.com/retrieve/pii/S0016003296000890.

Martinez Salazar, H. and Carbajal, J. P. Exploiting the passive dynamics of a compliant leg to develop gait transitions. *Physical Review E*, 83(6), June 2011a. ISSN 1539-3755. doi: 10.1103/PhysRevE.83.066707. URL http://link.aps.org/doi/10.1103/PhysRevE.83.066707.

Martinez Salazar, H. and Carbajal, J. P. From Walking to Running a Natural Transition in the SLIP Model Using the Hopping Gait. In *IEEE International Conference on Robotics and Biomimetics*, page 2163, 2011b.

Maxima.sourceforge.net. Maxima, a Computer Algebra System, 2011. URL http://maxima.sourceforge.net/.

McDonnell, M. D., Abbott, D., and Friston, K. J. What Is Stochastic Resonance? Definitions, Misconceptions, Debates, and Its Relevance to Biology. *PLoS Computational Biology*, 5 (5):e1000348, 2009. doi: 10.1371/journal.pcbi.1000348.

McGeer, T. Passive Dynamic Walking. *The International Journal of Robotics Research*, 9 (2):62–82, Apr. 1990. ISSN 0278-3649. doi: 10.1177/027836499000900206. URL http://ijr.sagepub.com/cgi/content/abstract/9/2/62.

McMillen, T. and Holmes, P. An elastic rod model for anguilliform swimming. *Journal of mathematical biology*, 53(5):843–86, Nov. 2006. ISSN 0303-6812. doi: 10.1007/s00285-006-0036-8. URL http://www.ncbi.nlm.nih.gov/pubmed/16972099.

Mead, J. Control of respiratory frequency. *Journal of applied physiology*, 15(3):325–336, 1960. URL http://jap.physiology.org/content/15/3/325.abstract.

Moritz, C. T. and Farley, C. T. Human hopping on damped surfaces: strategies for adjusting leg mechanics. *Proceedings. Biological sciences / The Royal Society*, 270(1525):1741–6, Aug. 2003. ISSN 0962-8452. doi: 10.1098/rspb.2003.2435. URL http://www.pubmedcentral.nih.gov/articlerender.fcgi?artid=1691428&tool=pmcentrez&rendertype=abstract.

Moss, F. Stochastic resonance and sensory information processing: a tutorial and review of application. *Clinical Neurophysiology*, 115(2):267, 2004. doi: 10.1016/j.clinph.2003.09.014.

Muceli, S., Boye, A. T. l., D'Avella, A., and Farina, D. Identifying representative synergy matrices for describing muscular activation patterns during multidirectional reaching in the horizontal plane. *Journal of neurophysiology*, 103(3):1532–42, Mar. 2010. ISSN 1522-1598. doi: 10.1152/jn.00559.2009. URL http://www.ncbi.nlm.nih.gov/pubmed/20071634.

Nassar, P. N., Jackson, a. C., and Carrier, D. R. Entraining the natural frequencies of running and breathing in guinea fowl (Numida meleagris). *The Journal of experimental biology*, 204(Pt 9):1641–51, May 2001. ISSN 0022-0949. URL http://www.ncbi.nlm.nih.gov/pubmed/11398753.

Neptune, R. R., Clark, D. J., and Kautz, S. A. Modular control of human walking: a simulation study. *Journal of biomechanics*, 42(9):1282–7, June 2009. ISSN 1873-2380. doi: 10.1016/j.jbiomech.2009.03.009. URL http://www.pubmedcentral.nih.gov/articlerender.fcgi?artid=2696580&tool=pmcentrez&rendertype=abstract.

Niiyama, R., Nagakubo, A., and Kuniyoshi, Y. Mowgli: A Bipedal Jumping and Landing Robot with an Artificial Musculoskeletal System. In *Proceedings 2007 IEEE International Conference on Robotics and Automation*, pages 2546–2551. IEEE, Apr. 2007. ISBN 1-4244-0602-1. doi: 10.1109/ROBOT.2007.363848. URL http://ieeexplore.ieee.org/lpdocs/epic03/wrapper.htm?arnumber=4209466.

Nori, F. *Symbolic Control with Biologically Inspired Motion Primitives*. PhD thesis, University of Genova, 2005. URL http://people.liralab.it/iron/Papers/NoriPhDThesis.pdf.

Octave community. GNU/Octave, 2011. URL www.gnu.org/software/octave/.

Ortega, R., Loria, A., Nicklasson, P. J., and Sira-Ramirez, H. *Passivity-based Control of Euler-Lagrange Systems*. Springer, New York, New York, USA, 1st editio edition, 1998. ISBN 978-1-84996-852-2. URL http://books.google.com/books?hl=en&lr=&id=GCVn0oRqP9YC&pgis=1.

Peng, Z., Lang, Z.-Q., and Billings, S. A. Resonances and resonant frequencies for a class of nonlinear systems. *Journal of Sound and Vibration*, 300(3-5):993–1014, Mar. 2007. ISSN 0022460X. doi: 10.1016/j.jsv.2006.09.012. URL http://linkinghub.elsevier.com/retrieve/pii/S0022460X06007267.

Pescheck, E. A new Galerkin-based approach for accurate non-linear normal modes through invariant manifolds. *Journal of Sound and Vibration*, 249(5):971–993, Jan. 2002. ISSN 0022460X. doi: 10.1006/jsvi.2001.3914. URL http://linkinghub.elsevier.com/retrieve/pii/S0022460X01939148.

Pfeifer, R. and Scheier, C. *Understanding Intelligence*. MIT Press 238 Main St., Suite 500, Cambridge, MA 02142-1046 USA journals-info@mit.edu, 1999. ISBN 978-0-262-16181-7.

Piiroinen, P. T. and Kuznetsov, Y. A. An event-driven method to simulate Filippov systems with accurate computing of sliding motions. *ACM Transactions on Mathematical Software*, 34(3):1–24, May 2008. ISSN 00983500. doi: 10.1145/1356052.1356054. URL http://portal.acm.org/citation.cfm?doid=1356052.1356054.

Potkonjak, V. Modelling and control of active systems with variable geometry . Part I : General approach and its application. *Mechanism and Machine Theory*, 35(2):179–195, 1999. ISSN 0094-114X. doi: 10.1016/S0094-114X(99)00010-5. URL http://dx.doi.org/10.1016/S0094-114X(99)00010-5.

Potkonjak, V. and Vukobratovic, M. Part II : Case study and numerical examples. *Mechanism and Machine Theory*, 35(2):197–220, 2000. ISSN 0094-114X. doi: 10.1016/S0094-114X(99)00011-7. URL http://dx.doi.org/10.1016/S0094-114X(99)00011-7.

Press, W. H. *Numerical recipes: the art of scientific computing*. Cambridge University Press, 3rd edition, 2007. ISBN 9780521880688. URL http://www.nr.com.

Raibert, M., Brown, H., Chepponis, M., Hastings, E., Koechling, J., and INST., C.-M. U. P. P. R. *Dynamically stable legged locomotion*. MIT Artificial Intelligence Laboratory, Cambridge, 1983. URL http://dspace.mit.edu/handle/1721.1/6820.

Richardson, W. J., Greene, C. R., Malme, C. I., and Thomson, D. H. *Marine Mammals and Noise*. Academic Press, London and San Diego, 1995.

Roberts, T. J. and Azizi, E. Flexible mechanisms: the diverse roles of biological springs in vertebrate movement. *The Journal of experimental biology*, 214(Pt 3):353–61, Feb. 2011. ISSN 1477-9145. doi: 10.1242/jeb.038588. URL http://jeb.biologists.org/cgi/doi/10.1242/jeb.038588http://www.pubmedcentral.nih.gov/articlerender.fcgi?artid=3020146&tool=pmcentrez&rendertype=abstract.

Roederer, J. G. On the concept of information and its role in nature. *Entropy*, 5(1):3–33, 2003. URL http://www.mdpi.com/1099-4300/5/1/3/.

Roederer, J. G. *Information and Its Role in Nature*. The Frontiers Collection. Springer, Berlin, Heidelberg, 2010. ISBN 9783642062001.

Roozenburg, N. F. M. and Eekels, J. *Product design: fundamentals and methods*. A Wiley series in product development. Wiley, 1995. ISBN 9780471943518.

Rosenberg, R. M. On nonlinear vibrations of systems with many degrees of freedom. In von Mises, R., Kuerti, G., and von Karman, T., editors, *Advances in Applied Mechanics*, page 155. Academic Press, 1966. ISBN 9780120020096.

Sastry, S. and Bodson, M. *Adaptive Control: Stability, Convergence and Robustness*. Prentice-Hall, 1994. ISBN 0-13-004326-5.

Schaal, S., Peters, J., Nakanishi, J., and Ijspeert, A. Learning Movement Primitives. In Dario, P. and Chatila, R., editors, *Robotics Research*, volume 15 of *Springer Tracts in Advanced Robotics*, pages 561–572. Springer Berlin / Heidelberg, 2005. ISBN 978-3-540-23214-8. URL http://dx.doi.org/10.1007/11008941_60.

Schetzen, M. *The Volterra and Wiener theories of nonlinear systems*. Wiley-Interscience, 1980. ISBN 9781575242835.

Schutte, A. and Udwadia, F. New Approach to the Modeling of Complex Multibody Dynamical Systems. *Journal of Applied Mechanics*, 78(2):021018, 2011. ISSN 00218936. doi: 10.1115/1.4002329. URL http://link.aip.org/link/JAMCAV/v78/i2/p021018/s1&Agg=doi.

Seyfarth, A., Geyer, H., Günther, M., and Blickhan, R. A movement criterion for running. *Journal of biomechanics*, 35(5):649–655, May 2002.

Shkolnik, A. and Tedrake, R. Path planning in 1000+ dimensions using a task-space Voronoi bias. In *2009 IEEE International Conference on Robotics and Automation*, pages 2061–2067. IEEE, May 2009. ISBN 978-1-4244-2788-8. doi: 10.1109/ROBOT.2009.5152638. URL http://ieeexplore.ieee.org/lpdocs/epic03/wrapper.htm?arnumber=5152638.

Shkolnik, A. and Tedrake, R. Sample-Based Planning with Volumes in Configuration Space. Available online via arxiv.org, Sept. 2011. URL http://arxiv.org/abs/1109.3145.

Shukla, R. K. and Eldredge, J. D. An inviscid model for vortex shedding from a deforming body. *Theoretical and Computational Fluid Dynamics*, 21(5):343, 2007. doi: 10.1007/s00162-007-0053-2.

Siegelmann, H. T. and Fishman, S. Analog computation with dynamical systems. *Physica D: Nonlinear Phenomena*, 120(1-2):214–235, Sept. 1998. ISSN 01672789. doi: 10.1016/S0167-2789(98)00057-8. URL http://linkinghub.elsevier.com/retrieve/pii/S0167278998000578.

Sims, K. Evolving 3D Morphology and Behavior by Competition. *Artificial Life*, 1(4):353–372, Jan. 1994a. ISSN 1064-5462. doi: 10.1162/artl.1994.1.4.353. URL http://www.mitpressjournals.org/doi/abs/10.1162/artl.1994.1.4.353.

Sims, K. Evolving virtual creatures. In *Proceedings of the 21st annual conference on Computer graphics and interactive techniques - SIGGRAPH '94*, pages 15–22, New York, New York, USA, 1994b. ACM Press. ISBN 0897916670. doi: 10.1145/192161.192167. URL http://portal.acm.org/citation.cfm?doid=192161.192167.

Spence, A. J., Revzen, S., Seipel, J., Mullens, C., and Full, R. J. Insects running on elastic surfaces. *The Journal of experimental biology*, 213(11):1907–20, June 2010. ISSN 1477-9145. doi: 10.1242/jeb.042515. URL http://www.ncbi.nlm.nih.gov/pubmed/20472778.

Strogatz, S. *Nonlinear dynamics and chaos: with applications to physics, biology, chemistry, and engineering*. Studies in nonlinearity. Westview Press, 1994. ISBN 9780738204536.

Thompson, C. M. and Raibert, M. H. Passive Dynamic Running. In Hayward, V. and Khatib, O., editors, *Experimental Robotics I*, pages 74–83. Springer-Verlag, Berlin/Heidelberg, June 1989. ISBN 3-540-52182-8. doi: 10.1007/BFb0042513. URL http://portal.acm.org/citation.cfm?id=645621.661423.

Thompson, W. Electrical Units of Measurement. In *Popular Lectures and Addresses, vol. 1*, page 73. The Institution of Civil Engineers, 1883.

Thurner, S., Hanel, R., and Klimek, P. Physics of evolution: Selection without fitness. *Physica A: Statistical Mechanics and its Applications*, 389(4):747–753, Feb. 2010. ISSN 03784371. doi: 10.1016/j.physa.2009.10.030. URL http://linkinghub.elsevier.com/retrieve/pii/S0378437109009005.

Todorov, E. A generalized iterative LQG method for locally-optimal feedback control of constrained nonlinear stochastic systems. In *Proceedings of the 2005, American Control Conference, 2005.*, pages 300–306. IEEE, 2005. ISBN 0-7803-9098-9. doi: 10.1109/ACC.2005.1469949. URL http://ieeexplore.ieee.org/lpdocs/epic03/wrapper.htm?arnumber=1469949.

Todorov, E. and Ghahramani, Z. Unsupervised learning of sensory-motor primitives. In *Proceedings of the 25th Annual International Conference of the IEEE Engineering in Medicine and Biology Society (IEEE Cat. No.03CH37439)*, pages 1750–1753. IEEE, 2003. ISBN 0-7803-7789-3. doi: 10.1109/IEMBS.2003.1279744. URL http://ieeexplore.ieee.org/lpdocs/epic03/wrapper.htm?arnumber=1279744.

Todorov, E. and Jordan, M. I. Smoothness Maximization Along a Predefined Path Accurately Predicts the Speed Profiles of Complex Arm Movements. *J Neurophysiol*, 80(2):696–714, 1998. URL http://jn.physiology.org/cgi/content/abstract/80/2/696.

Toffoli, T. What you always wanted to know about genetic algorithms but were afraid to hear. In *Perspectives on Adaptation in Natural and Artificial Systems*, pages 131–136. 2004. URL http://arxiv.org/abs/nlin/0007013.

Vakakis, A. F., Gendelman, O. V., Bergman, L. A., McFarland, D. M., Kerschen, G., and Lee, Y. S. *Nonlinear Targeted Energy Transfer in Mechanical and Structural Systems*, volume 156 of *Solid Mechanics and Its Applications*. Springer Netherlands, Dordrecht, 2009. ISBN 978-1-4020-9125-4. doi: 10.1007/978-1-4020-9130-8. URL http://www.springerlink.com/index/10.1007/978-1-4020-9130-8.

Vogel, S. Nature's Swell, But Is It Worth Copying? *MRS (Materials Research Society) BULLETIN*, 28:404—-408, 2003. URL http://stuff.mit.edu/afs/athena.mit.edu/course/3/3.225/refs/vogel_nature.pdf.

Vogel, S. *Glimpses of creatures in their physical worlds*. Princeton University Press, 2009. ISBN 9780691138060.

Vokoun, D., Beleggia, M., Heller, L., and Šittner, P. Magnetostatic interactions and forces between cylindrical permanent magnets. *Journal of Magnetism and Magnetic Materials*, 321(22):3758–3763, 2009. ISSN 0304-8853. doi: 10.1016/j.jmmm.2009.07.030. URL http://www.sciencedirect.com/science/article/pii/S030488530900746X.

Westervelt, E. R., Grizzle, J. W., Chevallereau, C., Choi, J. H., and Morris, B. *Feedback Control of Dynamic Bipedal Robot Locomotion*. Taylor & Francis LLC, first edition, 2007. ISBN 9781420053722.

Winter, D. A. *Biomechanics and Motor Control of Human Movement*. Wiley, 2009. ISBN 9780470398180.

Youden, W. *Experimentation and measurement*. Courier Dover, 1998. ISBN 9780486404516.

Zhechev, M. M. Equations of motion for singular systems of massed and massless bodies. *Proceedings of the Institution of Mechanical Engineers, Part K: Journal of Multi-body Dynamics*, 221(4):591–597, Jan. 2007. ISSN 1464-4193. doi: 10.1243/14644193JMBD87. URL http://pik.sagepub.com/lookup/doi/10.1243/14644193JMBD87.

Ziegler, M., Hoffmann, M., Carbajal, J. P., and Pfeifer, R. Varying Body Stiffness for Aquatic Locomotion. In *2011 IEEE International Conference on Robotics and Automation*, Shanghai, China, 2011.

Åström, K. J. and Wittenmark, B. *Adaptive control*. Addison-Wesley series in electrical engineering. Addison-Wesley, 2nd edition, 1994. ISBN 9780201558661. URL http://books.google.com/books?id=FJ4eAQAAIAAJ.